

s-Process in Low Metallicity Stars.

III. Individual analysis of CEMP-*s* and CEMP-*s/r* with AGB models.

S. Bisterzo^{1*}, R. Gallino^{1,2}, O. Straniero², S. Cristallo³ and F. Käppeler⁴

¹*Dipartimento di Fisica Generale, Università di Torino, Via P. Giuria 1, 10125 Torino, Italy*

²*INAF Osservatorio Astronomico di Collurania, via M. Maggini, 64100 Teramo, Italy*

³*Departamento de Física Teórica y del Cosmos, Universidad de Granada, Campus de Fuentenueva, 18071 Granada, Spain*

⁴*Karlsruhe Institute of Technology, Campus Nord, Institut für Kernphysik, D-76021 Karlsruhe, Germany*

Accepted 1988 December 15. Received 1988 December 14; in original form 1988 October 11

ABSTRACT

We provide an individual analysis of 94 carbon enhanced metal-poor stars showing an *s*-process enrichment (CEMP-*s*) collected from the literature. The *s*-process enhancement observed in these stars is ascribed to mass transfer by stellar winds in a binary system from a more massive companion evolving faster toward the asymptotic giant branch (AGB) phase. The theoretical AGB nucleosynthesis models have been presented in Paper I. Several CEMP-*s* stars show an enhancement in both *s* and *r*-process elements (CEMP-*s/r*). In order to explain the peculiar abundances observed in CEMP-*s/r* stars, we assume that the molecular cloud from which CEMP-*s* formed was previously enriched in *r*-elements by Supernovae pollution.

A general discussion and the method adopted in order to interpret the observations have been provided in Paper II. We present in this paper a detailed study of spectroscopic observations of individual stars. We consider all elements from carbon to bismuth, with particular attention to the three *s*-process peaks, ls (Y, Zr), hs (La, Nd, Sm) and Pb, and their ratios [hs/ls] and [Pb/hs]. The presence of an initial *r*-process contribution may be typically evaluated by the [La/Eu] ratio. We found possible agreements between theoretical predictions and spectroscopic data. In general, the observed [Na/Fe] (and [Mg/Fe]) provide information on the AGB initial mass, while [hs/ls] and [Pb/hs] are mainly indicators of the *s*-process efficiency. A range of ¹³C-pocket strengths is required to interpret the observations. However, major discrepancies between models and observations exist. We highlight star by star the agreements and the main problems encountered and, when possible, we suggest potential indications for further studies. These discrepancies provide starting points of debate for unsolved problems in which spectroscopic and theoretical studies may intervene.

Key words: Stars: AGB – Stars: carbon – Stars: Population II – nucleosynthesis

1 INTRODUCTION

This paper is the third of a series of papers dedicated to the analysis of carbon rich metal-poor stars showing a *slow* neutron capture process (*s*-process) enhancement (CEMP-*s*). The peculiar *s*-enrichment observed in these stars is currently explained by mass transfer through stellar winds from a more massive companion while suffering the ther-

mally pulsing asymptotic giant branch (TP-AGB) phase, then evolved toward a (now invisible) white dwarf. This is because CEMP-*s* are main-sequence or giant stars, far from the AGB phase. Then, the binary system scenario is the most plausible explanation for the *s*-process enhancement detected in these old, low-metallicity stars ([Fe/H] $\lesssim -2$) of low initial mass ($M < 0.9 M_{\odot}$). For a detailed discussion of *s*-process nucleosynthesis in AGB stars we refer to Busso et al. (1999), Herwig (2005), Straniero et al. (2006), Käppeler et al. (2011).

A complete description of the AGB models adopted here

* E-mail: bisterzo@ph.unito.it (AVR); sarabisterzo@gmail.com (ANO)

has been presented by Bisterzo et al. (2010a, hereafter Paper I) and Bisterzo et al. (2011, hereafter Paper II). Theoretical results are obtained with a post-process nucleosynthesis method (Gallino et al. 1998), based on full evolutionary FRANEC (Frascati Raphson-Newton Evolutionary Code, Chieffi & Straniero 1989) models, following the prescriptions by Straniero et al. (2003), as described in Paper I. AGB models with initial masses $M = 1.3, 1.4, 1.5, 2 M_{\odot}$, metallicities $-3.6 \leq [\text{Fe}/\text{H}] \lesssim -1.5$, and a range of ^{13}C -pockets are adopted. The ^{13}C -pocket is a thin ^{13}C -rich layer, which forms when few protons diffuse after a thermal instability, once the bottom of the convective envelope penetrates into the top layers of the radiative He-intershell (the zone between the H- and He-shells). This recurrent phenomenon is called third dredge-up (TDU). At H-shell re-ignition, protons are captured by the abundant ^{12}C and the ^{13}C -pocket is produced at the top of the He-intershell. Subsequently, when the temperature increases up to 1×10^8 K, neutrons are released in radiative conditions via the $^{13}\text{C}(\alpha, n)^{16}\text{O}$ reaction. This is the major neutron source in low mass AGB stars. The physical environments involved in the formation of the ^{13}C -pocket are still affected by large uncertainties. According to the description of our AGB models provided in Paper I, we assumed a range of ^{13}C -pocket strengths. This assumption is based on the spectroscopic observations of different stellar populations (MS, S, C(N), Ba stars, CEMP-*s* stars): for a given metallicity, they show a spread that may be reproduced by AGB models if a range of *s*-process efficiencies is assumed (Busso et al. 1995, 2001; Abia et al. 2001, 2002; Sneden et al. 2008; Käppeler et al. 2011). Starting from the case ST defined by Gallino et al. (1998) in order to reproduce the solar main *s*-process component (Arlandini et al. 1999), we multiply or divide the ^{13}C (and ^{14}N) abundance in the pocket by different factors: from a minimum fraction of ST, below which the *s*-process contribution becomes negligible¹, up to a maximum (ST $\times 2$), because further proton ingestion gives rise to ^{14}N instead of ^{13}C . Note that in our approximation, we did not account for a likely decrease in mass of the ^{13}C -pocket with the number of TDUs, as obtained by recent FRANEC models (see Cristallo et al. 2011, and references therein). They introduced a physical algorithm for the treatment of the transition region between the convective envelope and the radiative H-exhausted core, based on a non-diffusive mixing scheme (Straniero et al. 2006; Cristallo et al. 2009a). This allows the formation of a tiny ^{13}C -pocket, which decreases in mass with the number of TDUs. The interpretation of the *s*-process spread observed in different stars with new FRANEC models (Cristallo et al. 2011) is under investigation.

A second neutron source is driven in the convective thermal pulse by the partial activation of the $^{22}\text{Ne}(\alpha, n)^{25}\text{Mg}$ reaction.

When neutrons are released, both in the pocket and in the convective TP, a fraction is captured via the resonant reaction $^{14}\text{N}(n, p)^{14}\text{C}$. As discussed in Paper I, a complex chain

of proton captures occurs, affecting in particular the production of F (Lugaro et al. 2008; Abia et al. 2010; Gallino et al. 2010, and references therein).

Besides the formation of the ^{13}C -pocket, additional uncertainties that affect AGB models and *s*-process nucleosynthesis are the evaluation of the mass loss and the efficiency of the TDU. Mass loss plays a key role during the AGB phase, and it affects several stellar properties, as the efficiency of the TDU (in which the surface is enriched with freshly synthesised ^{12}C and *s*-process elements), the number of thermal pulses and, therefore, the duration of this evolutionary phase. In Paper I, we discussed these topics and their effects on our theoretical predictions.

With the recent discovery of peculiar stars showing both *s* and *r*-process enhancements (CEMP-*s/r*) incompatible with a pure *s*-process nucleosynthesis, a highly debated issue has begun. Indeed, the two processes are synthesised in different astrophysical conditions. Several hypotheses have been proposed in order to justify the presence of the products of both processes in the same star (e.g., Cohen et al. 2003; Jonsell et al. 2006; Lugaro et al. 2009, and references therein). Our working scenario, already presented by Sneden et al. (2008) and Bisterzo et al. (2009), has been discussed in detail in Paper II. Considering the large spread observed for [Eu/Fe] in field halo stars, we follow the hypothesis that the molecular cloud from which a given binary system formed was initially enriched in different proportions in *r*-process elements.

The astrophysical site and physical conditions of the *r*-process are not understood and several theoretical models have been advanced in order to estimate the *r* component. As discussed in Paper II, a good approximation of the *r*-process contribution to isotopes from Ba to Bi is evaluated with the residual method, $N_r = N_{\odot} - N_s$, starting from the solar main and strong *s*-process contributions. According to the spread observed for [Eu/Fe] in Galactic halo stars with $[\text{Fe}/\text{H}] \lesssim -2$ (e.g., Paper II, Fig. 2), where Eu is a typical *r*-process element, observations of CEMP-*s* and CEMP-*s/r* stars may be interpreted under the hypothesis of a range of initial *r*-enhancements ($[\text{r}/\text{Fe}]^{\text{ini}} \sim 0.0, 0.5, 1.0, 1.5, 2.0$, scaled to Eu). The [La/Eu] ratio provides a good indicator of the initial *r*-process contribution in these stars. Indeed, 70% of solar La is synthesised by the *s*-process, while less than 5% of solar Eu is produced by the *s*-process. On the basis of the initial *r*-enhancement adopted, we consider as CEMP-*s/r* those stars that need an $[\text{r}/\text{Fe}]^{\text{ini}}$ from 1.0 to 2.0, while CEMP-*s* are those stars that require an $[\text{r}/\text{Fe}]^{\text{ini}} < 1$. If not differently specified, CEMP-*s* stars are interpreted by assuming an $[\text{r}/\text{Fe}]^{\text{ini}} = 0.5$, in agreement with the average of [Eu/Fe] observed in field halo stars (Paper II, Section 3).

The goal of this paper is to provide a first step toward our understanding of these puzzling CEMP-*s* and CEMP-*s/r* stars, through a comparison between the AGB models presented in Paper I and the spectroscopic observations of each individual star. This analysis is of fundamental importance in order to account for the uncertainties, number of lines, resolution spectra obtained by different authors. This highlights possible agreements or discrepancies between theory and observations and suggests starting points for future investigations.

A general discussion of the sample considered here has been provided in Paper II, in which we pre-

¹ Note that the minimum choice of the ^{13}C -pocket depends on the metallicity. Indeed, the *s*-process efficiency increases by decreasing the metallicity because of the lower number of iron seeds (see Paper I).

sented an extensive analysis of the sample of a hundred of CEMP-*s* stars collected from the literature (Aoki et al. 2002a,c,d, 2006, 2007, 2008; Barbuy et al. 2005; Barklem et al. 2005; Behara et al. 2010; Cohen et al. 2003, 2006; Goswami et al. 2006; Goswami & Aoki 2010; Ivans et al. 2005; Ishigaki et al. 2010; Israelian et al. 2001; Jonsell et al. 2006; Johnson & Bolte 2002, 2004; Junqueira & Pereira 2001; Lucatello et al. 2003, 2011; Lucatello 2004; Masseron et al. 2006, 2010; Pereira & Drake 2009; Preston & Sneden 2001; Roederer et al. 2008, 2010a; Schuler et al. 2008; Sneden et al. 2003b; Thompson et al. 2008; Tsangarides 2005; Van Eck et al. 2003; Zhang et al. 2009).

At halo metallicities, major constraints on the AGB initial mass are provided by the observed [Na/Fe] (and [Mg/Fe]) and, in some cases, by [hs/ls] (see Paper II). As described in Paper I, the predicted [Na/Fe], [Mg/Fe] and [ls/Fe] mainly depend on the number of TDUs. Indeed, by decreasing the metallicity, an increasing amount of primary ^{22}Ne in the advanced thermal pulses is produced starting from primary ^{12}C (via $^{14}\text{N}(\alpha, \gamma)^{18}\text{F}(\beta^+\nu)^{18}\text{O}$ and $^{18}\text{O}(\alpha, \gamma)^{22}\text{Ne}$; see e.g., Mowlavi et al. 1999; Gallino et al. 2006). In our models, ^{23}Na is mainly synthesised via neutron capture on the abundant ^{22}Ne during the thermal pulses (Paper I). Starting from ^{23}Na , Mg is also produced during the advanced TPs, via the reactions $^{23}\text{Na}(n, \gamma)^{24}\text{Mg}$, $^{22}\text{Ne}(\alpha, n)^{25}\text{Mg}$ and $^{22}\text{Ne}(\alpha, \gamma)^{26}\text{Mg}$ (Mowlavi et al. 1999; Gallino et al. 2006; Husti et al. 2007). Gorieli & Mowlavi (2000) firstly suggested an additional important source of Na. It derives from their choice of the proton profile in the pocket: they considered an exponentially decreasing proton profile, starting from the envelope abundance ($X(H) \sim 0.7$) down to $\sim 10^{-6}$. A similar range of H abundance has been introduced by new FRANEC (Cristallo et al. 2009a, their Fig. 13). In the outer layer of the pocket, when ^{12}C get destroyed by the very high hydrogen fraction introduced in the pocket, and ^{22}Ne becomes more abundant than ^{12}C , proton capture on ^{22}Ne feeds ^{23}Na at a temperature close to 40 MK. Instead, in our prescriptions, we adopted an H profile limited to the range $X(H) < 1.8 \times 10^{-3}$, as described by Gallino et al. (1998) (their Fig. 1), which excludes the region in which a large amount of protons reaches the He-intershell. Consequently, we do not have in the pocket the ^{14}N -rich and ^{23}Na -rich regions. However, we have accounted for the contribution to ^{23}Na by ^{22}Ne that comes from the ashes of the H-burning shell. As anticipated above, during the TP almost all ^{14}N left by H-burning is converted to primary ^{22}Ne . This primary ^{22}Ne , which is mixed with the envelope by subsequent TDU episodes, also affects the final ^{23}Na production. Indeed, in the interpulse phase the H-burning shell advances in mass. By adopting the reaction rates by NACRE, about 20% of ^{22}Ne is converted to ^{23}Na via $^{22}\text{Ne}(p, \gamma)^{23}\text{Na}$ during the H-shell. This implies an increase of the [Na/Fe] on the surface by ~ 0.1 dex.

As well as ^{23}Na , the large amount of primary ^{22}Ne also produces Sr, Y and Zr via the $^{22}\text{Ne}(\alpha, n)^{25}\text{Mg}$ neutron source. This results in an increase of the predicted [ls/Fe] with the AGB initial mass. Note that, by decreasing the metallicity, the reduced abundance of the major seed ^{56}Fe , together with large amount of primary ^{22}Ne , highlights the effect of the $^{22}\text{Ne}(n, \gamma)$ reaction, which acts as efficient seed, besides as neutron poison (see Gallino et al. 2006;

Section 6).

The two *s*-process indicators [hs/ls] and [Pb/hs] provide information about the choice of the ^{13}C -pocket². A dilution factor *dil* (defined as the logarithm of the mass of the convective envelope of the observed star, M_{\star}^{obs} , over the mass transferred from the AGB to the companion, $M_{\text{AGB}}^{\text{trans}}$) is adopted in order to simulate the mixing occurring in the envelope after the mass transfer from the AGB. The [hs/Fe] ratio gives the first assessment of the dilution of the C and *s*-rich material transferred from the AGB. For subgiants/giants having suffered the first dredge-up (FDU, a large mixing involving about 80% of the mass of the star), *dil* $\gtrsim 1$ dex is needed. The method adopted to interpret the spectroscopic observations has been described in Paper II for three stars taken as example: the CEMP-*s* giant HD 196944, the main-sequence CEMP-*s/r* HE 0338-3945, and a CEMP-*s* HE 1135+0139 for which no lead is measured. We extend this analysis here to 94 CEMP-*s* and CEMP-*s/r* stars following the classification adopted in Paper II, in agreement with the *s*- and *r*-process enhancements observed:

- CEMP-*s*II stars show high *s*-process enhancement with [hs/Fe] $\gtrsim 1.5$ (Section 2.1);
- CEMP-*s*I stars show mild *s*-process enhancement with [hs/Fe] < 1.5 (Section 2.2);
- CEMP-*s*II/*r* are high *s*-process enhanced stars, also showing an *r*-process contribution not compatible with a pure AGB nucleosynthesis ([hs/Fe] $\gtrsim 1.5$; $0.0 \lesssim [\text{La}/\text{Eu}] \lesssim 0.4$). Similarly to the *s*-process enhancement, we may distinguish two subgroups among CEMP-*s*II/*r* stars, according to the initial *r*-process enhancement (Section 3):
 - CEMP-*s*II/*r*II with $1.5 \lesssim [\text{r}/\text{Fe}]^{\text{ini}} \leq 2.0$
 - CEMP-*s*II/*r*I with $[\text{r}/\text{Fe}]^{\text{ini}} \sim 1.0$.

One would expect a further class of stars with both mild *s*- and *r*-process contributions, the CEMP-*s*I/*r*I. None of the stars of the sample belongs to this group probably because these stars cannot be distinguished from Galactic halo stars due to their low initial *r*-enhancement.

Moreover, we consider in a separate category those stars without Eu detection, because a possible initial *r*-process enrichment can not be excluded: among them, we separate CEMP-*s*II/– (Section 4.1) and CEMP-*s*I/– (Section 4.2) stars.

At the beginning of each Section we list the name of the stars analysed in alphabetical order, with a distinction between main-sequence/turnoff subgiant stars before the FDU and subgiants/giants having suffered the FDU. Stars with a large number of observations (collected in Table 2 and 10 of Paper II) are analysed in Sections 2, 3, and 4. Stars with a limited number of *s*-process observations (Table 3 and 11 of Paper II) are discussed in Appendix A. A summary of the results is given in Section 7. For convenience, we report in Tables 1 and 2 a list of the stars studied here, with their references, metallicity, classification provided in Paper II, the number of the Figure associated to the theoretical interpretation.

The initial chemical composition described in Paper I, Section 2.1 is adopted. We assume initial negative Cr and

² As in Paper II, we define ls = <Y,Zr>, hs = <La,Nd,Sm>.

Table 1. Summary of the CEMP-*s* and CEMP-*s/r* stars analysed in this paper. References are Aoki et al. (2002a,c,d, 2006, 2007, 2008), A02a, A02c, A02d, A06, A07, A08; Barbuy et al. (2005), BB05; Barklem et al. (2005), B05; Beers et al. (2007), Beers07; Behara et al. (2010), B10; Cohen et al. (2003, 2006), C03, C06; Drake & Pereira (2008), DP08; Goswami et al. (2006), G06; Goswami & Aoki (2010), GA10; Ivans et al. (2005), I05; Ishigaki et al. (2010), I10; Israelian et al. (2001), I01; Jonsell et al. (2005, 2006), J05,J06; Johnson & Bolte (2002, 2004), JB02, JB04; Johnson et al. (2007), J07; Junqueira & Pereira (2001), JP01; Lai et al. (2007), Lai07; Lai et al. (2004), Lai04; Lucatello (2004), L04; Lucatello et al. (2011), L11; Masseron et al. (2006,2010), M06, M10; Pereira & Drake (2009), P09; Preston & Sneden (2001), PS01; Roederer et al. (2008, 2010), R08, R10; Schuler et al. (2007, 2008), Sch07, Sch08; Thompson et al. (2008), T08; Tsangarides (2005), T05; Van Eck et al. (2003), VE03; Zhang et al. (2009), Z09. Following Section 1, in column 4 we distinguish between CEMP-*sI* (*sI*), CEMP-*sII* (*sII*), CEMP-*sI/rI* (*sI/rI*) and CEMP-*sII/rII* (*sII/rII*) stars. Labels *sI*– of *sII*– refer to CEMP-*sI* and CEMP-*sII* without Eu detection. In column 5, label ‘*ms*’ means main-sequence, ‘*TO*’ turnoff, ‘*SG*’ subgiant and ‘*G*’ giant. The number of the Figure and the page number associated to the theoretical interpretation are listed in column 6.

Star (1)	Ref. (2)	[Fe/H] (3)	Type (4)	Phase (5)	Page, Fig. (6)
BD +04°2466	P09,I10,Z09	-1.92,-2.10	<i>sI</i> –	G	p. 26, Fig. 45
BS 16080–175	T05	-1.86	<i>sII</i>	<i>ms</i> /TO	p. 8, Fig. 5
BS 17436–058	T05	-1.90	<i>sI</i>	G	p. 13, Fig. 16
CS 22183–015	A07,C06	-2.75	<i>sII/rII</i>	SG	p. 21, Fig. 32
CS 22880–074	A07,A02c,d	-1.93	<i>sI</i>	SG	p. 8, Fig. 7
CS 22881–036	PS01	-2.06	<i>sII</i>	<i>ms</i> /TO	p. 5, Fig. 1
CS 22887–048	T05	-1.70	<i>sII/rI</i>	<i>ms</i> /TO	p. 23, Fig. 36
CS 22898–027	A07,A02c,d	-2.26	<i>sII/rII</i>	<i>ms</i> /TO	p. 13, Fig. 17
CS 22942–019	A02c,d,PS01,Sch08,M10,L11	-2.64	<i>sI</i>	G	p. 9, Fig. 9
CS 22948–27	BB05,A07,L11	-2.47	<i>sII/rII</i>	G	p. 18, Fig. 27
CS 22964–161A/B	T08	-2.39	<i>sI</i>	<i>ms</i> /TO	p. 8, Fig. 6
CS 29497–030	I05	-2.57	<i>sII/rII</i>	<i>ms</i>	p. 14, Fig. 18
CS 29497–34	BB05,A07,L11	-2.90	<i>sII/rII</i>	G	p. 19, Fig. 28
CS 29513–032	R10	-2.08	<i>sI</i>	SG	p. 9, Fig. 8
CS 29526–110	A07,A02c,d,A08	-2.38,-2.06	<i>sII/rII</i>	<i>ms</i> /TO	p. 16, Fig. 23
CS 29528–028	A07	-2.86	<i>sII</i> –	<i>ms</i>	p. 24, Fig. 37
CS 30301–015	A07,A02c,d	-2.64	<i>sI</i>	G	p. 10, Fig. 10
CS 30322–023	M06,A07,M10,L11	-3.50,-3.25	<i>sI</i>	G	p. 11, Fig. 11
CS 31062–012	I01,A07,A02c,d,A08	-2.55	<i>sII/rII</i>	<i>ms</i>	p. 17, Fig. 24
CS 31062–050	JB04,A07,A06,A02c,d	-2.42	<i>sII/rII</i>	SG	p. 18, Fig. 26
HD 26	VE03,M10	-1.25,-1.02	<i>sII</i>	G	p. 29, Fig. 49
HD 5223	G06,L11	-2.06	<i>sII</i> –	G	p. 24, Fig. 41
HD 187861	VE03,M10,L11	-2.30,-2.36	<i>sII/rI</i>	G	p. 20, Fig. 29
HD 189711	VE03	-1.80	<i>sI</i> –	G	p. 27, Fig. A1
HD 196944	A07,A02c,d,VE03,M10	-2.25	<i>sI</i>	G	p. 11, Fig. 12
HD 198269	VE03	-2.20	<i>sI</i> –	G	p. 27, Fig. 46
HD 201626	VE03	-2.10	<i>sII</i> –	G	p. 24, Fig. 40
HD 206983	M10, JP01	-0.99,-1.43	<i>sI</i>	G	p. 29, Fig. 50
HD 209621	GA10	-1.93	<i>sII/rI</i>	G	p. 22, Fig. 35
HD 224959	VE03,M10	-2.20	<i>sII/rII</i>	G	p. 20, Fig. 30
HE 0143–0441	C06	-2.31	<i>sII/rI</i>	<i>ms</i> /TO	p. 21, Fig. 33
HE 0202–2204	B05	-1.98	<i>sI</i>	G	p. 11, Fig. 13
HE 0212–0557	C06	-2.27	<i>sII</i> –	G	p. 25, Fig. 42
HE 0231–4016	B05	-2.08	<i>sI</i> –	SG	p. 26, Fig. 43
HE 0336+0113	C06	-2.68	<i>sII</i>	SG	p. 6, Fig. 2
HE 0338–3945	J06	-2.42	<i>sII/rII</i>	<i>ms</i> /TO	p. 14, Fig. 19
HE 0430–4404	B05	-2.07	<i>sI</i> –	<i>ms</i>	p. 41, Fig. A3
HE 1031–0020	C06	-2.86	<i>sI</i> –	G	p. 28, Fig. 47
HE 1105+0027	B05	-2.42	<i>sII/rII</i>	<i>ms</i> /TO	p. 15, Fig. 20
HE 1135+0139	B05	-2.33	<i>sI</i>	G	p. 12, Fig. 14
HE 1152–0355	G06,L11	-1.27	<i>sI</i> –	G	p. 30, Fig. 51
HE 1305+0007	G06,L11	-2.03	<i>sII/rII</i>	G	p. 16, Fig. 22
HE 1430–1123	B05	-2.71	<i>sII</i> –	SG	p. 24, Fig. 38
HE 1434–1442	C06	-2.39	<i>sI</i> –	SG	p. 28, Fig. 48
HE 1509–0806	C06	-2.91	<i>sII</i> –	G	p. 7, Fig. 3
HE 2148–1247	C03	-2.30	<i>sII/rII</i>	<i>ms</i> /TO	p. 15, Fig. 21
HE 2150–0825	B05	-1.98	<i>sI</i> –	SG	p. 41, Fig. A4
HE 2158–0348	C06	-2.70	<i>sII</i>	G	p. 8, Fig. 4
HE 2232–0603	C06	-1.85	<i>sI</i> –	SG	p. 26, Fig. 44
HKII 17435–00532	R08	-2.23	<i>sI</i>	G	p. 12, Fig. 15
LP 625–44	A02,A06	-2.70	<i>sII/rII</i>	G	p. 20, Fig. 31
V Ari	VE03	-2.40	<i>sI</i> –	G	p. 40, Fig. A2
SDSS 0126+06	A08	-3.11	<i>sII</i> –	<i>ms</i>	p. 24, Fig. 39
SDSSJ 0912+0216	B10	-2.50	<i>sII/rI</i>	<i>ms</i>	p. 22, Fig. 34
SDSSJ 1349–0229	B10	-3.00	<i>sII/rII</i>	<i>ms</i>	p. 17, Fig. 25

Mn abundances ($[\text{Cr}/\text{Fe}] = -0.2$; $[\text{Mn}/\text{Fe}] = -0.4$), in agreement with the average of unevolved halo stars (Cayrel et al. 2004; François et al. 2004). Note that Bergemann & Gehren (2008) found that the observed Mn may increase up to $[\text{Mn}/\text{Fe}] \sim -0.1$ due to NLTE corrections. Concerning Cu, we assume an initial solar-scaled value if no observations are provided. Actually, because AGBs marginally produce

Cu, a better choice would be $[\text{Cu}/\text{Fe}]^{\text{ini}} \sim -0.7$, which represents the average ratio observed in unevolved halo stars (Bisterzo et al. 2004; Romano & Matteucci 2007). We accounted for this effect when discussing the four CEMP-*s* stars for which Cu has been detected (HE 0338–3945 discussed in Paper II, Section 5.2, CS 30322–023, CS 31062–050 and HD 206983).

Table 2. The same as Table 1, but for the CEMP-*s* and CEMP-*s/r* stars with a limited number of spectroscopic observations. A discussion of these stars is provided in Appendix A. References are the same as Table 1. Additional references are Lucatello et al. (2003), L03 and Sneden et al. (2003b), S03. In column 5, label 'ms' means main-sequence, 'TO' turnoff, 'SG' subgiant, 'G' giant and 'HB' horizontal branch. The page number and, when provided, the Figure associated to the theoretical interpretation are given in column 6.

Star (1)	Ref. (2)	[Fe/H] (3)	Type (4)	Phase (5)	Page, Fig. (6)
CS 22891–171	M10	-2.25	sII/rII	G	p. 45, Fig. A9
CS 22956–28	M10,S03	-2.33,-2.08	sI/–	ms/TO	p. 47, Fig. A13
CS 22960–053	A07	-3.14	sI/–	G	p. 48
CS 22967–07	L04	-1.81	sII(/–)	ms	p. 42
CS 29495–42	L04	-1.88	sI	SG	p. 43
CS 29503–010	A07	-1.06	s(II)/–	ms	p. 30
CS 29509–027	S03	-2.02	sI/–	ms	p. 47
CS 30315–91	L04	-1.68	sI/–	SG	p. 43
CS 30323–107	L04	-1.75	sII(/–)	ms	p. 42
CS 30338–089	A07,L04	-2.45,-1.75	sII(/rII)	G	p. 45
G 18–24	I10	-1.62	sI/–	ms	p. 48
HE 0012–1441	C06	-2.52	sI/–	SG	p. 47
HE 0024–2523	L03	-2.70	sII(/–)	ms	p. 42, Fig. A5
HE 0131–3953	B05	-2.71	sII/rII	TO/SG	p. 44, Fig. A8
HE 0206–1916	A07	-2.09	sII/–	SG	p. 46
HE 0400–2030	A07	-1.73	sII/–	SG	p. 46
HE 0441–0652	A07	-2.47	sI/–	G	p. 48
HE 0507–1653	A07	-1.38	sII/–	G	p. 30
HE 1001–0243	M10	-2.88	sI	G	p. 43, Fig. A6
HE 1005–1439	A07	-3.17	sI/–	G	p. 48
HE 1157–0518	A07	-2.34	sII/–	G	p. 46
HE 1305+0132	Sch08	-1.92	sI/–	G/HB	p. 48
HE 1319–1935	A07	-1.74	sII/–	G	p. 46
HE 1410–0004	C06	-3.02	sI/–	SG	p. 47
HE 1419–1324	M10	-3.05	sI	G	p. 43, Fig. A7
HE 1429–0551	A07	-2.47	sII/–	G	p. 46
HE 1443+0113	C06	-2.07	sI/–	G	p. 47
HE 1447+0102	A07	-2.47	sII/–	G	p. 46
HE 1523–1155	A07	-2.15	sII/–	G	p. 46
HE 1528–0409	A07	-2.61	sII/–	G	p. 46
HE 2221–0453	A07	-2.22	sII/–	G	p. 46
HE 2227–4044	B05	-2.32	sI/–	SG	p. 48
HE 2228–0706	A07	-2.41	sII/–	G	p. 46
HE 2240–0412	B05	-2.20	sI/–	SG	p. 48
HE 2330–0555	A07	-2.78	sI/–	G	p. 48
SDSS 0817+26	A08	-3.16	(sI/–)	ms	p. 48
SDSS 0924+40	A08	-2.51	sII/–	ms	p. 45, Fig. A10
SDSS 1707+58	A08	-2.52	sII/–	ms	p. 45, Fig. A11
SDSS 2047+00	A08	-2.05	sII/–	ms	p. 45, Fig. A12

The comparison between theoretical predictions and observations may help to establish the efficiency of non-convective mixing occurring in the envelope of the observed star during their main-sequence phase (e.g., thermohaline, gravitational settlings, radiative levitation, see Richard et al. 2002; Vauclair 2004; Stancliffe et al. 2007; Stancliffe & Glebbeek 2008; Stancliffe et al. 2009; Thompson et al. 2008; Theado & Vauclair 2010). For stars on the red giant branch, having undergone the FDU, all mixing processes occurred during the main-sequence phase are erased.

2 CEMP-*s* STARS

In this Section we provide an individual analysis of CEMP-*s*II and CEMP-*s*I stars (with Eu measured). As anticipated

in Section 1, CEMP-*s* are generally interpreted with an initial *r*-process enhancement $[r/Fe]^{ini} = 0.5$, on the basis of an average of the $[Eu/Fe]$ observed in halo field stars (see Paper II, Fig. 2). Different $[r/Fe]^{ini}$ from -1.0 to 0.7 are adopted for some peculiar stars, as discussed below.

2.1 CEMP-*s*II stars

There are six stars with an *s*-process enhancement higher than $[hs/Fe] \gtrsim 1.5$. One star having not suffered the FDU, CS 22881–036 by Preston & Sneden (2001), and a second star with uncertain occurrence of the FDU, HE 0336+0113 by Cohen et al. (2006), (see discussion in Paper II, Section 2); two giants, HE 1509–0806 and HE 2158–0348 by Cohen et al. (2006). Note that the low Eu upper limit detected for HE 1509–0806 excludes a high initial *r*-process enhancement, and classifies this star as a CEMP-*s*II. In addi-

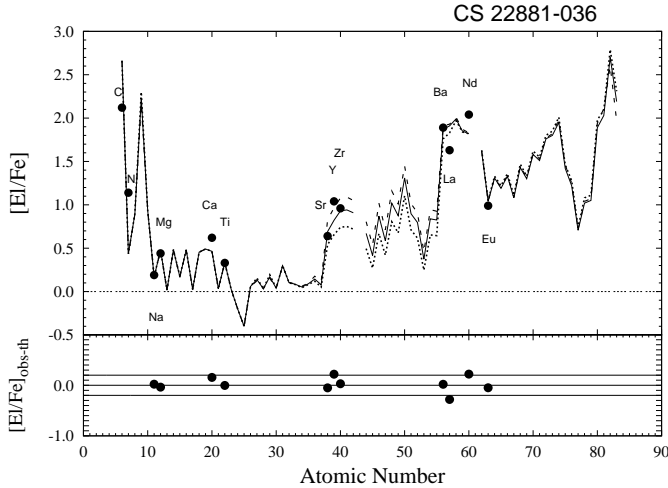


Figure 1. Spectroscopic $[\text{El}/\text{Fe}]$ observations of the main-sequence/turnoff star CS 22881-036 ($[\text{Fe}/\text{H}] = -2.06$; $T_{\text{eff}} = 6200$ K; $\log g = 4.0$) compared with AGB models of $M_{\text{ini}}^{\text{AGB}} = 1.3 M_{\odot}$, ST/6 (dotted line), ST/8 (solid line) and ST/9 (dashed line), no dilution. Observations are from Preston & Sneden (2001). This star shows $[\text{hs}/\text{ls}] = 0.76$. No error bars are provided by the authors for single species (see text). Here and in the following Figures, the lower panel displays the difference between observations and the AGB model represented with solid line ($[\text{El}/\text{Fe}]_{\text{obs-th}}$). C and N are not included because they may be affected by deep-mixing (see text). The range between the two lines corresponds to a typical model uncertainty of 0.2 dex. An initial r -process enrichment of $[\text{r}/\text{Fe}]^{\text{ini}} = 0.5$ is adopted. Here and in the following Figures, both theoretical and spectroscopic abundances have been normalised to the solar photospheric values by Lodders, Palme & Gail (2009). This explains possible discrepancies with respect to the observations listed in Paper II (Tables 2 and 3), in which we adopted the normalisations provided by the different authors.

tion, we describe in this Section the CEMP-*s*II subgiant BS 16080-175, for which spectroscopic data have been analysed by Tsangarides (2005) (PhD Thesis). HD 26 (Van Eck et al. 2003; Masseron et al. 2010), which shows a higher metallicity ($[\text{Fe}/\text{H}] = -1$), is discussed separately in Section 5.

2.1.1 CS 22881-036 (Fig. 1)

This turnoff star with $[\text{Fe}/\text{H}] = -2.06$, $T_{\text{eff}} = 6200$ K and $\log g = 4.0$, was studied by Preston & Sneden (2001). After the first radial velocity study by Preston & Sneden (2000), Preston et al. (2009) find variations over a period of 16 years, with $P = 378$ days.

Following the method explained in Paper II (Section 5), the choice of the ^{13}C -pocket is made according to the observed s -process indicator $[\text{hs}/\text{ls}] = 0.76$. Preston & Sneden (2001) suggest typical uncertainties of 0.2 – 0.3 dex for species with many transitions. No lead is detected in this star. In Fig. 1, we show possible solutions with AGB models of $M_{\text{ini}}^{\text{AGB}} = 1.3 M_{\odot}$, cases ST/6, ST/8 and ST/9, and no dilution. Here and in the following Figures the name of the star, its metallicity, the literature of the spectroscopic data, and the characteristics of the AGB models adopted (i.e. initial mass, ^{13}C -pocket, dilution factor and initial r -process enhancement) are given in the caption. In the lower panel the differences between observations and AGB predictions $[\text{El}/\text{Fe}]_{\text{obs-th}}$ are

represented. The two lines placed at ± 0.2 dex are to indicate possible uncertainties of the model or of the initial abundances of light elements.

As discussed in Paper II, Section 5, the $[\text{C}/\text{Fe}]$, $[\text{N}/\text{Fe}]$ and $^{12}\text{C}/^{13}\text{C}$ ratios measured in CEMP-*s* stars are largely overestimated by AGB models. Indeed, AGB models predict a large amount of ^{12}C in the envelope already after the first thermal pulses with TDU (Paper I). The occurrence of extra-mixing like the cool bottom processing (CBP) have been hypothesised in order to interpret observations in AGB stars and pre-solar grains of AGB origin (Nollett et al. 2003; Domínguez et al. 2004a,b; Wasserburg et al. 2006; Zinner et al. 2006; Cristallo et al. 2007; Busso et al. 2010). Several physical processes may concur in this mixing (e.g., rotation, magnetic fields, thermohaline mixing), and their efficiency is difficult to estimate. An additional deep mixing may reduce the $^{12}\text{C}/^{13}\text{C}$ ratio and increase ^{14}N in low-mass low-metallicity AGB stars ($[\text{Fe}/\text{H}] \lesssim -2.5$): during the first fully developed TP, an ingestion of protons from the envelope down to the convective He-intershell occurs (Hollowell et al. 1990; Iwamoto et al. 2004; Campbell & Lattanzio 2008; Cristallo et al. 2009b; Campbell, Lugaro, Karakas 2010). This leads to efficient proton captures on CNO isotopes, with a large production of ^{13}C and, at lower level, of ^{14}N . This episode may also modify the s -process pattern. There is a maximum mass (which increases with decreasing the metallicity) below which AGB models undergo proton ingestion. The assumption of an initial enhanced distribution (e.g., of α -elements compatible with observations of metal-poor stars) would further decrease this mass limit (Straniero et al. 2011). Further studies on this topic are desirable. For these reasons, C and N are not included in the lower panel of Fig. 1 and in the following Figures. We refer to Paper II for a general discussion about C and N. We are planning to reconsider this topic in a forthcoming study. However, we underline that high uncertainties affect the spectroscopic determination of C and N, because of NLTE or 3D model corrections (Asplund 2005; Collet et al. 2007; Grevesse et al. 2007; Asplund et al. 2009; Caffau et al. 2009; Frebel & Norris 2011).

The AGB models displayed in Fig. 1 predict $[\text{Pb}/\text{Fe}]_{\text{th}} \sim 2.7$. The uncertainty estimated for the $[\text{hs}/\text{Fe}]$ ratio could decrease the lead prediction down to $[\text{Pb}/\text{Fe}]_{\text{th}} \sim 1.4$ (case ST/18). Pb detection is highly desirable in this star. In agreement with the average of field halo stars (for which a $[\text{Eu}/\text{Fe}]$ ratio about 0.5 is observed), we adopt an initial r -process enrichment $[\text{r}/\text{Fe}]^{\text{ini}} = 0.5$. Note that the solution without initial r -enhancement ($[\text{r}/\text{Fe}]^{\text{ini}} = 0$) would decrease the predicted $[\text{Eu}/\text{Fe}]$ by about 0.1 dex, still in agreement with the observation. The s -elements can be matched by AGB models with higher initial mass ($M_{\text{ini}}^{\text{AGB}} \sim 1.5 - 2 M_{\odot}$), but the estimated $[\text{Na}/\text{Fe}]$ is too high. The most plausible interpretations are found with $M_{\text{ini}}^{\text{AGB}} = 1.3 M_{\odot}$ and $\text{dil} = 0.0 - 0.3$ dex. The range of dilution accounts for the spread observed in the hs elements: indeed, with a slightly lower ^{13}C -pocket efficiency and $\text{dil} = 0.3$ dex, we may still interpret the two s -peaks. This indicates that mixing during the main-sequence phase were not efficient in this CEMP-*s*. In order to estimate plausible variations of the dilution resulting from the uncertainties of the ^{13}C -pocket, we test the effect on the abundances of a variation of the mass involved in the pocket. We recall that in our models, the mass of the

pocket is $5 \times 10^{-4} M_{\odot}$, that is about 1/20 of the typical mass involved in a thermal pulse. A mass of the pocket of the order of 1/10 of the mass involved in the thermal pulse can be considered as an extreme case. This would increase the $[\text{El}/\text{Fe}]$ of the *s*-process elements of about 0.3 dex. Therefore, we found that the uncertainty of the mass of the ^{13}C -pocket only marginally affects the dilution (up to ~ 0.2 dex, given that the previous example is an extreme case). AGB models with low initial mass undergo a limited number of thermal pulses. In these models, the $[\text{El}/\text{Fe}]$ abundances predicted in the envelope after two subsequent TDUs differ by ~ 0.2 dex, corresponding to an increase of the initial mass of about $+0.025 M_{\odot}$. This is not the case of AGB models with initial mass $M > 1.4 M_{\odot}$, for which negligible differences are observed in the *s*-process distribution after the 12th TDU (see Paper I, Fig. 4, top panel). Summing up, for lower AGB initial masses, the dilution may increase up to ~ 0.4 dex, owing to a plausible increase of the mass of the pocket, or to an additional TDU. This value may be considered in agreement with a moderate mixing.

2.1.2 HE 0336+0113 (Fig. 2)

HE 0336+0113 was analysed by Cohen et al. (2006), who found $[\text{Fe}/\text{H}] = -2.7$, $T_{\text{eff}} = 5700 (\pm \sim 150)$ K and $\log g = 3.5 (\pm \sim 0.4)$. As anticipated in Paper II (Section 2), the onset of the FDU for subgiants may involve marginal mixing of the accreted AGB wind material with the original envelope of the observed star, unless efficient thermohaline mixing is at play. The high Mg observed ($[\text{Mg}/\text{Fe}] \sim 1$ dex) can be interpreted only by AGB models with initial masses higher than $1.3 M_{\odot}$. A high $[\text{Na}/\text{Fe}]$ is predicted. Observations of Na lines are highly desirable. Among ls elements, Zr is not detected, and among hs elements no Sm is measured, making the $[\text{hs}/\text{ls}]$ ratio very uncertain. The low upper limit detected for Pb ($[\text{Pb}/\text{hs}] \leq 0.2$) indicates low ^{13}C -pocket efficiencies. In case of very low ^{13}C -pocket choices, the predicted $[\text{hs}/\text{Fe}]$ does not exceed ~ 2 dex, in agreement with a low dilution. In Fig. 2, we show solutions with $M_{\text{ini}}^{\text{AGB}} = 1.4$ and $2 M_{\odot}$, cases close to ST/50, and $\text{dil} = 0.0 - 0.3$ dex. The low dilution suggests that the envelope did not reach yet its maximum penetration during the FDU episode. For these stars we can not properly quantify the efficiency of mixing during the main-sequence phase (see Section 2.1.1). We adopt an initial *r*-process enrichment $[\text{r}/\text{Fe}]^{\text{ini}} = 0.5$ in agreement with the average of field halo stars to obtain $[\text{Eu}/\text{Fe}]_{\text{th}}^{\text{s+r}} = 1.03$. A similar value within 0.1 dex is predicted by a model without initial *r*-process enhancement. C and N are very uncertain for this star and no systematic errors are provided by Cohen et al. (2006). Solutions with $M_{\text{ini}}^{\text{AGB}} = 1.5 M_{\odot}$ give even worse interpretations for C, N and Mg.

2.1.3 HE 1509-0806 (Fig. 3)

This is one of the coolest giants studied by Cohen et al. (2006) ($[\text{Fe}/\text{H}] = -2.91$; $T_{\text{eff}} = 5185$ K; $\log g = 2.5$). HE 1509-0806 already suffered the FDU and theoretical interpretations with negligible dilutions would not account for this large mixing involving about 80% of the convective envelope of the observed star (see Paper II). AGB models with low initial mass undergo a limited number of thermal pulses

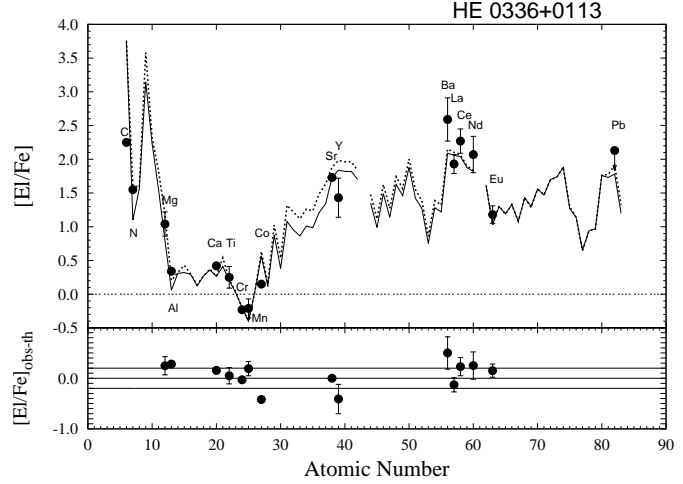


Figure 2. Spectroscopic $[\text{El}/\text{Fe}]$ abundances of the subgiant HE 0336+0113 ($[\text{Fe}/\text{H}] = -2.68$; $T_{\text{eff}} = 5700$ K; $\log g = 3.5$, uncertain FDU, see text) compared with AGB models of $M_{\text{ini}}^{\text{AGB}} = 1.4 M_{\odot}$, ST/55, no dilution (solid line), or $M_{\text{ini}}^{\text{AGB}} = 2 M_{\odot}$, ST/45 and $\text{dil} = 0.3$ dex (dotted line). Observations are from Cohen et al. (2006). This star shows $[\text{hs}/\text{ls}] \sim 0.2$ and $[\text{Pb}/\text{hs}] \leq 0.2$. No Zr and Sm are detected and the observed $[\text{hs}/\text{ls}]$ ratio is very uncertain. The differences $[\text{El}/\text{Fe}]_{\text{obs-th}}$ refer to a model for $M_{\text{ini}}^{\text{AGB}} = 1.4 M_{\odot}$ (solid line). An initial *r*-process enrichment of $[\text{r}/\text{Fe}]^{\text{ini}} = 0.5$ is adopted.

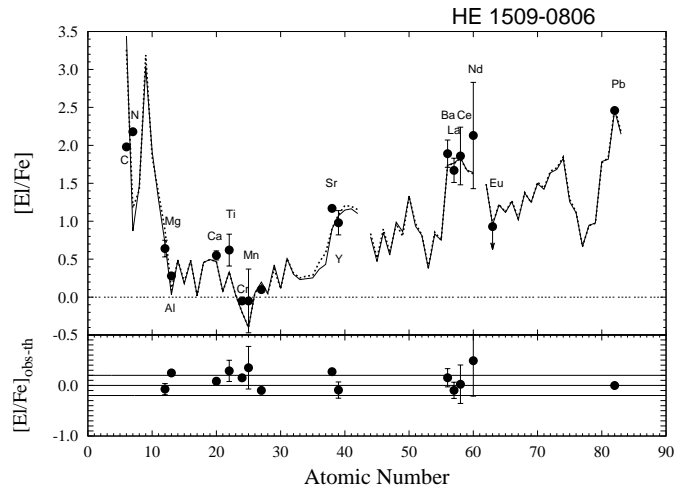


Figure 3. Spectroscopic $[\text{El}/\text{Fe}]$ abundances of the giant HE 1509-0806 ($[\text{Fe}/\text{H}] = -2.91$; $T_{\text{eff}} = 5185$ K; $\log g = 2.5$) compared with AGB models of $M_{\text{ini}}^{\text{AGB}} = 1.4 M_{\odot}$ (pulse 8th), ST/18, $\text{dil} = 0.7$ dex (solid line), or $M_{\text{ini}}^{\text{AGB}} = 2 M_{\odot}$, ST/12 and $\text{dil} = 1.2$ dex (dotted line). Observations are from Cohen et al. (2006). Cohen et al. (2006) observed $[\text{hs}/\text{ls}] = 0.70$ and $[\text{Pb}/\text{hs}] = 0.83$. The differences $[\text{El}/\text{Fe}]_{\text{obs-th}}$ refer to a model for $M_{\text{ini}}^{\text{AGB}} = 1.4 M_{\odot}$ (solid line). An initial *r*-process enrichment of $[\text{r}/\text{Fe}]^{\text{ini}} = 0.5$ is adopted.

with TDU (e.g., n3, n4, n5 for $M_{\text{ini}}^{\text{AGB}} \sim 1.2 - 1.3 M_{\odot}$ models) and, consequently, the $[\text{El}/\text{Fe}]$ distribution predicted in the envelope is low. Therefore, low dilutions must be applied, in contrast with a giant after the FDU. By increasing the AGB initial mass, plausible interpretations are found, as shown in Fig. 3, with $M_{\text{ini}}^{\text{AGB}} = 1.4$ and $2 M_{\odot}$ models, cases ST/18 and ST/12, $\text{dil} = 0.7 - 1.2$ dex, respectively. Both models may equally interpret the spectroscopic abundances

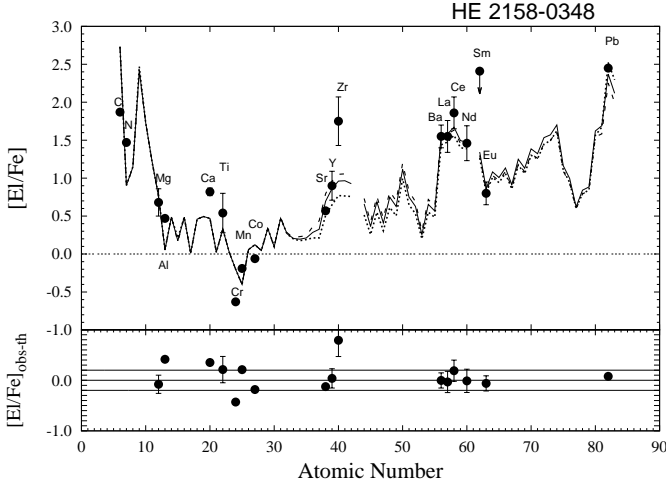


Figure 4. Spectroscopic $[El/Fe]$ abundances of the giant HE 2158–0348 ($[Fe/H] = -2.70$; $T_{\text{eff}} = 5215$ K; $\log g = 2.5$) compared with AGB models of $M_{\text{ini}}^{\text{AGB}} = 1.5 M_{\odot}$, cases ST/3 (dotted line), ST/5 (solid line), ST/6 (dashed line), and $dil = 1.4$ dex. Observations are from Cohen et al. (2006). This star shows $[hs/ls] = 0.25$ and $[Pb/hs] = 1.13$. $[Zr/Fe]$ (two lines) is about 0.8 dex higher than $[Y/Fe]$ (three lines), which agrees with AGB models (see text). An initial r -process enrichment of $[r/Fe]_{\text{ini}} = 0.5$ is adopted.

($[hs/ls] = 0.70$ and $[Pb/hs] = 0.83$). Nd is highly uncertain and no Sm lines have been detected. $[Mg/Fe]$ is slightly overestimated by a $M_{\text{ini}}^{\text{AGB}} = 1.5 M_{\odot}$ model. The low Eu upper limit permits to exclude high initial r -process enhancements: $0 \leq [r/Fe]_{\text{ini}} \leq 0.5$ dex may equally interpret the observations.

2.1.4 HE 2158–0348 (Fig. 4)

Similarly to HE 1509–0806, AGB models of low initial mass are excluded for this CEMP-sII giant ($[Fe/H] = -2.70$; $T_{\text{eff}} = 5215$ K and $\log g = 2.5$; Cohen et al. 2006), because a low dilution does not agree with a star having suffered the FDU. Significant differences among the ls elements are observed, $[Zr/Y] \sim 0.8$ dex (two lines are detected for Zr and three lines for Y). As displayed in Fig. 4 for AGB models with $M_{\text{ini}}^{\text{AGB}} = 1.5 M_{\odot}$ (ST/3, ST/5 and ST/6) and $dil = 1.4$ dex, we predict $[Zr/Y]_{\text{th}} \sim 0$ and $[hs/ls]_{\text{th}} \sim 0.56$. A similar result is provided by a $M_{\text{ini}}^{\text{AGB}} = 2 M_{\odot}$ model (case ST/9). $[Zr/Fe]$ is 0.8 dex higher than the AGB prediction. The observed $[Zr/Fe]$ may be interpreted by decreasing the choice of the ^{13}C -pocket, but $[Pb/Fe]_{\text{th}}$ would be about 1 dex lower than observed.

2.1.5 BS 16080–175 (Fig. 5)

The main-sequence/turnoff star BS 16080–175 was studied by Tsangarides (2005), with $[Fe/H] = -1.86$, $T_{\text{eff}} = 6240$ K and $\log g = 3.7$. The s -process indicators show $[hs/ls] = 0.4$ and $[Pb/hs] = 1.0$. Note that only Ba and La are detected among the hs elements. In Fig. 5, we show possible theoretical interpretations with $M_{\text{ini}}^{\text{AGB}} = 1.5 M_{\odot}$ models, two s -process efficiencies (ST/3 and ST/5) and a large dilution ($dil \sim 1.2$ dex). Similar solutions can be obtained with $M_{\text{ini}}^{\text{AGB}} = 1.35$ and $2 M_{\odot}$ models ($dil = 0.6$ and 1.2 dex; cases ST/9

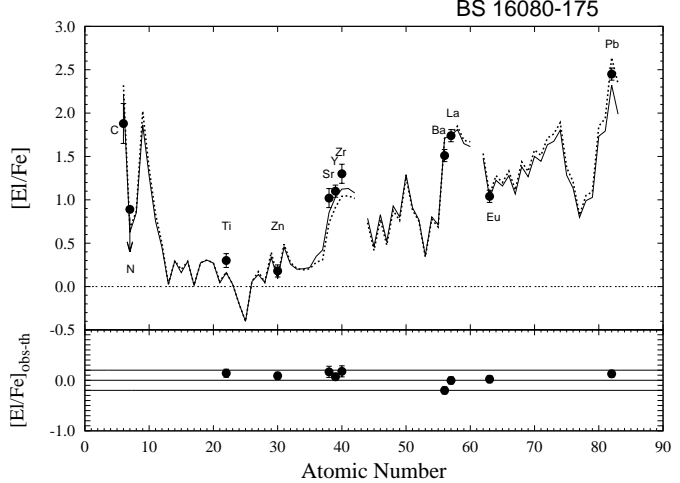


Figure 5. Spectroscopic $[El/Fe]$ abundances of the main-sequence/turnoff star BS 16080–175 ($[Fe/H] = -1.86$; $T_{\text{eff}} = 6240$ K; $\log g = 3.7$) compared with AGB models of $M_{\text{ini}}^{\text{AGB}} = 1.5 M_{\odot}$, cases ST/3 and ST/5 with $dil = 1.2 - 1.3$ dex, dashed and solid lines, respectively. Observations are from Tsangarides (2005), ($[hs/ls] = 0.42$ and $[Pb/hs] = 0.98$). A similar solution is obtained by $M_{\text{ini}}^{\text{AGB}} = 2 M_{\odot}$. An initial r -process enrichment $[r/Fe]_{\text{ini}} = 0.7$ is adopted.

and ST/6, respectively). An r -process enhancement $[r/Fe]_{\text{ini}} = 0.7$ is adopted in order to interpret the observed $[La/Eu] = 0.7$. AGB models with $M_{\text{ini}}^{\text{AGB}} = 1.3 M_{\odot}$ do not reproduce both the $[hs/ls]$ and $[Pb/hs]$ observed: a case ST/6 and $dil = 0.4$ dex predicts a low first s -process peak ($[ls/Fe]_{\text{th}} = 0.6$), while a case ST/15 predicts $[Pb/hs]_{\text{th}} \sim 0$, about 1 dex lower than observed. This excludes interpretations with $M_{\text{ini}}^{\text{AGB}} = 1.3 M_{\odot}$ models and low dilutions, suggesting the occurrence of mixing during the main-sequence phase. Measurement of Na and Mg are highly desirable.

2.2 CEMP-sI

Twelve stars show mild s -process enhancement. The turnoff star CS 22964–161 by Thompson et al. (2008); two stars for which the occurrence of the FDU is uncertain, CS 22880–074 by Aoki et al. (2002c,d, 2007) and CS 29513–032 by Roederer et al. (2010a); seven giants, CS 22942–019 by Aoki et al. (2002c,d); Preston & Sneden (2001), CS 30301–015 by Aoki et al. (2002c,d, 2007), CS 30322–023 by Masseron et al. (2006); Aoki et al. (2007), HD 196944 by Aoki et al. (2002c,d, 2007); Masseron et al. (2010) (already discussed in Paper II, Section 5), HE 0202–2204 and HE 1135+0139 by Barklem et al. (2005) (already discussed in Paper II, Section 5), HK II 17435–00532 by Roederer et al. (2008). In addition, we described in this Section a further CEMP-sI giant, BS 17436–058, for which spectroscopic data have been analysed by Tsangarides (2005) (PhD Thesis). Similarly to HD 26, the giant HD 206983 studied by Junqueira & Pereira (2001) and Masseron et al. (2010) has metallicity $[Fe/H] \sim -1$ and will be discussed in Section 5.

2.2.1 CS 22964–161 (Fig. 6)

This main-sequence/turnoff star is a double-lined spectroscopic binary ($[Fe/H] = -2.39$; $T_{\text{eff}} = 6050$ and 5950 K,

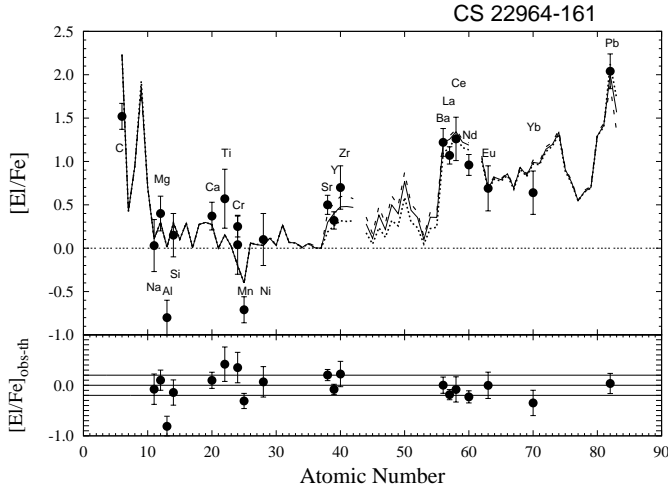


Figure 6. Spectroscopic $[El/Fe]$ abundances of main-sequence/turnoff star CS 22964-161 ($[Fe/H] = -2.39$; $T_{\text{eff}} = 6050$ K; $\log g = 3.7$) compared with AGB models of $M_{\text{ini}}^{\text{AGB}} = 1.3 M_{\odot}$, cases ST/9 (dotted line), ST/12 (solid line), ST/15 (dashed line), and $dil = 0.9$ dex. Observations are from Thompson et al. (2008). This star shows $[hs/ls] = 0.65$ and $[Pb/hs] = 1.15$. A solution with $dil \sim 0.4$ dex may be obtained with a $M_{\text{ini}}^{\text{AGB}} \sim 1.2 M_{\odot}$ model at the 3rd pulse (case ST/15). An initial r -process enrichment of $[r/Fe]^{\text{ini}} = 0.5$ is adopted.

$\log g = 3.7$ and 4.1 , for primary and secondary, respectively, Thompson et al. 2008), with enhanced lithium ($\log \epsilon$ (Li) = 2.0 ± 0.2). The abundances of the secondary star are more uncertain, but an s -process enhancement is observed in both stars, with $[Pb/Fe] \sim 2$ dex. Theoretical interpretations with AGB models have been widely discussed by Thompson et al. (2008). Satisfactory solutions for the three s -process peaks are found with $1.3 \leq M/M_{\odot} \leq 2$. The close to solar $[Na/Fe]$ agrees with AGB models of initial mass $M = 1.3 M_{\odot}$, cases ST/9, ST/12, ST/15, and $dil = 0.9$ dex, as displayed in Fig. 6. A large dilution is applied in order to interpret the mild s -process enhancement observed ($[ls/Fe] \sim 0.5$ and $[hs/Fe] \sim 1$). However, theoretical interpretations with lower dilution ($dil \sim 0.4$ dex) may be obtained by AGB models with $M_{\text{ini}}^{\text{AGB}} \sim 1.2 M_{\odot}$ at the 3rd pulse (case ST/15). Thompson et al. (2008) conclude that only moderate thermohaline mixing could occur in this star. Indeed, gravitational settling, which involved the star in the first 3 – 4 Gyr before the mass accretion of the AGB, offsets the thermohaline efficiency, producing a mean molecular weight (μ) barrier below the convective zone, which confined the thermohaline convection (see also Richard et al. 2002). This is sustained by the high Li observed ($\log \epsilon$ (Li) = $+2.09 \pm 0.20$), which otherwise would be depleted, because of the higher temperature reached in the inner layers of the star. However, these computations do not include radiative levitation, hence they do not represent the conclusive step of investigations of mixing on the secondary star.

2.2.2 CS 22880-074 (Fig. 7)

This subgiant ($[Fe/H] = -1.93$, $T_{\text{eff}} = 5850$ K and $\log g = 3.8$) was analysed by Aoki et al. (2002c,d). CS 22880-074 lies in the region of the HR diagram in which the occurrence of the FDU is uncertain. We remind that in

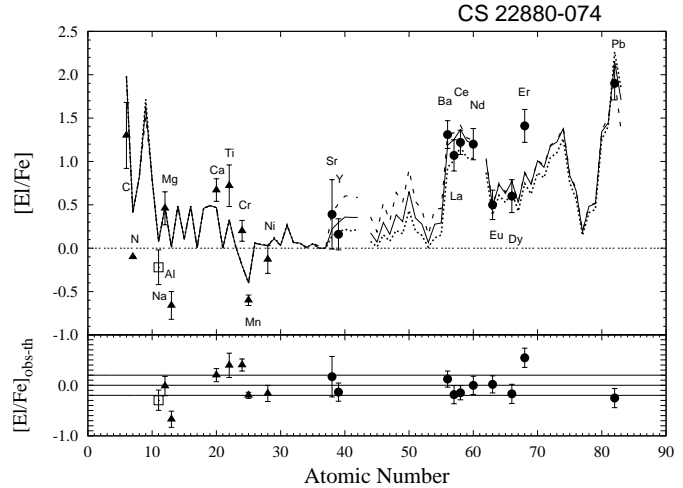


Figure 7. Spectroscopic $[El/Fe]$ abundances of the subgiant CS 22880-074 ($[Fe/H] = -1.93$; $T_{\text{eff}} = 5850$ K; $\log g = 3.8$, uncertain FDU, see text) compared with AGB models of $M_{\text{ini}}^{\text{AGB}} = 1.3 M_{\odot}$, cases ST/5 (dotted line), ST/6 (solid line), ST/9 (dashed line), and $dil = 0.9$ dex. Observations are from Aoki et al. (2002c), (filled triangles), Aoki et al. (2002d), (filled circles), Aoki et al. (2007), (empty square). Aoki et al. (2002d) detected $[hs/ls] = 0.84$ and $[Pb/hs] = 0.80$. Aoki et al. (2002c) highlight the unreliability of N in this star. An initial $[r/Fe]^{\text{ini}} = 0.0$ is adopted. The observed $[Er/Fe]$ is about 0.5 dex higher than AGB models (see text).

very metal-poor stars Na may be affected by strong uncertainties due to non-local thermodynamic equilibrium (NLTE) corrections (Andrievsky et al. 2007; Aoki et al. 2007; Barbuy et al. 2005 and references therein). For this star, the NLTE correction for the Na I D lines decreases the $[Na/Fe]$ abundance by 0.7 dex (Aoki et al. 2007). We show in Fig. 7 theoretical interpretations using $M_{\text{ini}}^{\text{AGB}} = 1.3 M_{\odot}$ models (cases ST/5, ST/6 and ST/9, in agreement with the observed $[hs/ls] = 0.84$ and $[Pb/hs] = 0.80$). Due to the mild s -enhancement, a large dilution is needed (0.9 dex). With an AGB model of lower initial mass, $M_{\text{ini}}^{\text{AGB}} = 1.2 M_{\odot}$ at the 3rd pulse, a similar result is obtained with $dil = 0.4$ dex. Dilutions of the order of 0.4 – 0.9 dex suggest that internal mixing occurred in this star (e.g., FDU or thermohaline, gravitational settling; see Section 1). Lower dilutions may only be obtained by AGB models suffering a lower number of TDUs (simulated with a $M_{\text{ini}}^{\text{AGB}} \sim 1.2 M_{\odot}$ model at the 2nd pulse). These solutions slightly overestimated the observed subsolar $[Na/Fe]$. Models with $M_{\text{ini}}^{\text{AGB}} = 1.5 - 2 M_{\odot}$ ($dil \sim 2$ dex) predict higher Na and Y ($[Na/Fe]_{\text{th}} \sim 0.3$; $[Y/Fe]_{\text{th}} \sim 0.4$). AGB models disagree with the negative $[N/Fe]$ observed: Aoki et al. (2002c) underline that N is unreliable in this star. Only one line is detected for the three r -process elements Eu, Dy and Er. The observed $[Eu,Dy/Fe]$ are about 0.9 dex lower than $[Er/Fe]$ and suggest no initial r -process enhancement. Note that the $[Er/Fe]$ measured is even higher than $[hs/Fe]$. Further investigations on the r -elements would be desirable.

No radial velocity variations were registered over a time of 16 years (Preston & Sneden 2001; Aoki et al. 2002c; Preston et al. 2009).

2.2.3 CS 29513-032 (Fig. 8)

This subgiant with $[\text{Fe}/\text{H}] = -2.08$, $T_{\text{eff}} = 5810$ K and $\log g = 3.3$, has been recently studied by Roederer et al. (2010a). The occurrence of the FDU is uncertain in this star. It is a member of a stellar stream identified by Helmi et al. (1999), probably originating from the disruption of a former Milky Way satellite galaxy. Roederer et al. (2010a) studied twelve of these stars, but only CS 29513-032 is *s*-process enhanced. The authors firstly have hypothesised a contribution from an AGB companion. Despite the presence of a definite, albeit moderate, *s*-process signature, CS 29513-032 shows $[\text{C}/\text{Fe}] = 0.63 (\pm 0.2 \text{ dex})$, lower than usually observed in CEMP-*s* stars. Actually, some authors consider CEMP those stars with $[\text{C}/\text{Fe}] \geq 1$, according to the definition of Beers & Christlieb (2005); we include among CEMP all objects with $[\text{C}/\text{Fe}] \gtrsim 0.5$. For this mild *s*-rich star a very large dilution is necessary in order to interpret the observations ($[\text{ls}/\text{Fe}] \sim 0$, $[\text{hs}/\text{Fe}] \sim 0.5$, $[\text{Pb}/\text{Fe}] \sim 1.6$) even for AGB models with low initial mass: already at the 5th TDU (with $M_{\text{ini}}^{\text{AGB}} = 1.3 M_{\odot}$) a dilution of 1.4 dex is needed. Lower dilutions may be obtained at the 2nd TDU ($M_{\text{ini}}^{\text{AGB}} \sim 1.2 M_{\odot}$; $dil = 0.3 \text{ dex}$). This may imply that efficient mixing have taken place in this subgiant (e.g., FDU or thermohaline, gravitational settling; see Section 1). The low observed $[\text{Na}/\text{Fe}]$ accounts for NLTE corrections. Owing to the large dilution applied, a low $[\text{Na}/\text{Fe}]$ is also predicted by models with $M_{\text{ini}}^{\text{AGB}} = 1.5$ and $2 M_{\odot}$. For this star, Na and can not provide constraints on the AGB initial mass and all AGB models in the range $1.3 \lesssim M/M_{\odot} \leq 2$ may equally fit the observations. In Fig. 8, two solutions are shown, $M_{\text{ini}}^{\text{AGB}} = 1.3$ and $1.5 M_{\odot}$ models, cases ST/9 and ST/3, $dil = 1.4$ and 2.4 dex , respectively. We adopt a negative initial $[\text{Y}/\text{Fe}]^{\text{ini}} = -0.5$, which is compatible with the spread of $[\text{Y}/\text{Fe}]$ observed in field halo stars (e.g., François et al. 2007), in order to interpret the subsolar $[\text{Y}/\text{Fe}]$ observed. Under this assumption, a model of $M_{\text{ini}}^{\text{AGB}} = 1.5 M_{\odot}$ that requires a large dilution, provides $[\text{Y}/\text{Fe}]_{\text{th}} = -0.12$. $[\text{La}/\text{Fe}]$ (4 lines detected) is overestimated by both models. A similar solution is obtained for a $M_{\text{ini}}^{\text{AGB}} = 2 M_{\odot}$ model (case ST/5 and $dil = 2.5 \text{ dex}$).

No radial velocity variations have been detected in a span of three months (Roederer et al. 2010a) and further investigations are desirable.

2.2.4 CS 22942-019 (\equiv HE 0054-2542), (Fig. 9)

The giant CS 22942-019 is a long period binary ($P = 2800$ d; 3616 d; Preston & Sneden 2001; Lucatello et al. 2009) with $[\text{Fe}/\text{H}] = -2.43$, $T_{\text{eff}} = 5100$ K and $\log g = 2.5$. Spectroscopic observations of several elements have been investigated by different authors: Aoki et al. (2002c,d); Schuler et al. (2008); Masseron et al. (2010); Lucatello et al. (2011). A high $[\text{Na}/\text{Fe}]$ was detected by Preston & Sneden (2001), $[\text{Na}/\text{Fe}] = 1.44$. However, Preston & Sneden (2001) do not consider NLTE corrections that could reduce the observed $[\text{Na}/\text{Fe}]$. The low upper limit measured for lead ($[\text{Pb}/\text{Fe}] \leq 1.6$; $[\text{Pb}/\text{hs}] \lesssim 0.3$) is interpreted by an AGB model of initial mass $M = 2 M_{\odot}$, as shown in Fig. 9. The low $[\text{Pb}/\text{Fe}]$ upper limit is interpreted by a case ST/50. Together with HE 0336+0113 (Section 2.1.2), CS 22942-019 is one of the stars with the low-

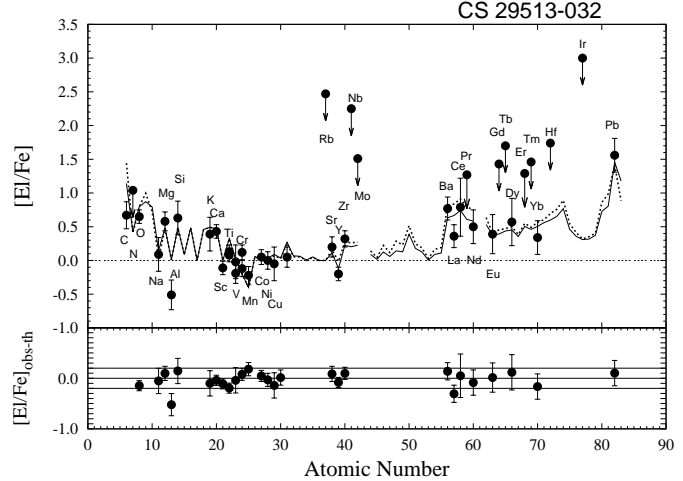


Figure 8. Spectroscopic $[\text{El}/\text{Fe}]$ abundances of the subgiant CS 29513-032 ($[\text{Fe}/\text{H}] = -2.08$; $T_{\text{eff}} = 5810$ K; $\log g = 3.3$, uncertain FDU) compared with $M_{\text{ini}}^{\text{AGB}} = 1.3$ or $1.5 M_{\odot}$ models, cases ST/9 or ST/3 and $dil = 1.4$ or 2.4 dex , (dotted or solid lines, respectively). Observations are from Roederer et al. (2010a), who detected $[\text{hs}/\text{ls}] = 0.45$ and $[\text{Pb}/\text{hs}] = 1.29$. In order to interpret the negative $[\text{Y}/\text{Fe}]$ value, we assume $[\text{Y}/\text{Fe}]^{\text{ini}} = -0.5$ (see text). Solar-scaled initial abundances for Sr and Zr are adopted. The observed $[\text{La}/\text{Fe}]$ is slightly overestimated by both models. The differences $[\text{El}/\text{Fe}]_{\text{obs-th}}$ represented in the lower panel refer to the $M_{\text{ini}}^{\text{AGB}} = 1.5 M_{\odot}$ model (solid line). An initial *r*-process enrichment of $[\text{r}/\text{Fe}]^{\text{ini}} = 0.3$ is adopted.

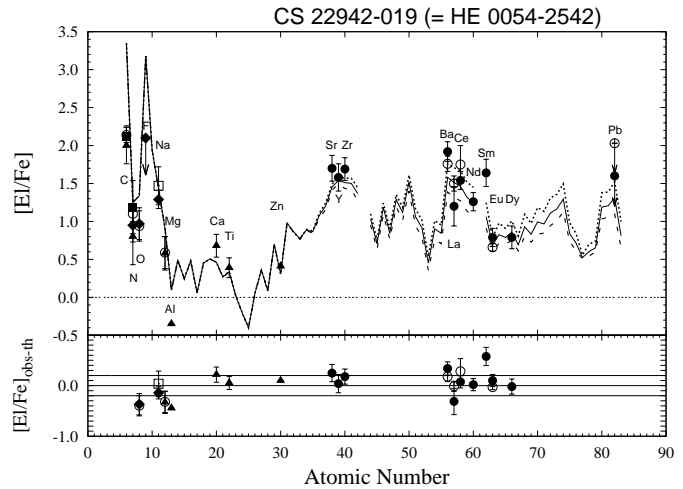


Figure 9. Spectroscopic $[\text{El}/\text{Fe}]$ abundances of the giant CS 22942-019 ($[\text{Fe}/\text{H}] = -2.43$; $T_{\text{eff}} = 5100$ K; $\log g = 2.5$) compared with AGB models of $M_{\text{ini}}^{\text{AGB}} = 2 M_{\odot}$, cases ST/45 (dotted line), ST/50 (solid line), ST/60 (dashed line), and $dil = 0.7 \text{ dex}$. Observations are from Aoki et al. (2002c) (filled triangles), Aoki et al. (2002d) (filled circles), Preston & Sneden (2001) (empty square), Schuler et al. (2008) (filled squares), Masseron et al. (2010) (empty circles), Lucatello et al. (2011) (filled diamonds). This star shows $[\text{hs}/\text{ls}] = -0.36$, while an upper limit is observed for Pb. The spread observed among the *hs* elements is discussed in the text. An initial *r*-process enrichment of $[\text{r}/\text{Fe}]^{\text{ini}} = 0.5$ is adopted.

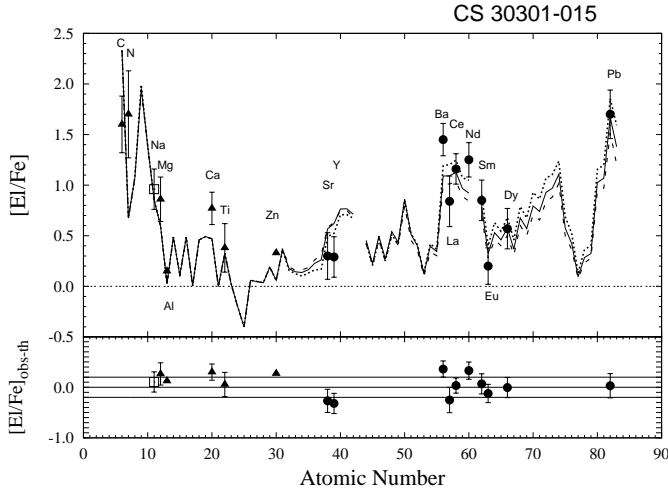


Figure 10. Spectroscopic $[El/Fe]$ abundances of the giant CS 30301-015 ($[Fe/H] = -2.64$; $T_{\text{eff}} = 4750$ K; $\log g = 0.8$) compared with AGB models of $M_{\text{ini}}^{\text{AGB}} = 1.5 M_{\odot}$, cases ST/6 (dotted line), ST/9 (solid line), ST/12 (dashed line), and $dil = 1.8$ dex. Observations are from Aoki et al. (2002c) (filled triangles), Aoki et al. (2002d) (filled circles), Aoki et al. (2007) (empty squares). Aoki et al. (2002d) detected $[hs/lc] = 0.45$ and $[Pb/hs] = 0.72$. An initial $[r/Fe]_{\text{ini}} = 0$ is adopted.

est ^{13}C -pocket choice, because of the decreasing behaviour of $[ls/Fe] > [hs/Fe] > [Pb/Fe]$ (see also Section 7). The observed $[hs/Fe]$ shows a spread of about 0.6 dex. AGB models with low ^{13}C -pockets predict a slightly decrease, by increasing the atomic number, of the abundances from Ba to Sm. The observed Ba and Sm are overestimated by models. We consider Ce and Nd (6 and 7 lines detected, respectively) more reliable than La and Sm (2 and 1 lines, respectively)³. A dilution of 0.7 dex is applied. AGB models with lower initial mass ($M_{\text{ini}}^{\text{AGB}} \leq 1.5 M_{\odot}$) would need $dil \leq 0.5$ dex, which disagrees with the large mixing occurring in a giant. An upper limit for fluorine is detected by Lucatello et al. (2011) ($[F/Fe] < 2.1$). AGB models predict higher $[F/Fe]$ abundance (almost at the same order than $[C/Fe]$, see Paper I). Further spectroscopic investigations are desirable in order to constrain theoretical predictions.

2.2.5 CS 30301-015 (Fig. 10)

The spectra of cool giants are highly contaminated by molecular bands. This is the case of CS 30301-015, showing $[Fe/H] = -2.64$, $T_{\text{eff}} = 4750$ K and $\log g = 0.8$ (Aoki et al. 2002c,d, 2007). The CN molecular bands are too strong for a reliable N abundance determination. The high $[Na/Fe]$ and $[Mg/Fe]$ observed by Aoki et al. (2007) ($[Na/Fe] = 1.09$ and $[Mg/Fe] = 0.80$) exclude interpretations with $M_{\text{ini}}^{\text{AGB}} \leq 1.3 M_{\odot}$ models. By increasing the number of TDUs, solutions with $M_{\text{ini}}^{\text{AGB}} = 1.5 M_{\odot}$ (ST/6, ST/9 and ST/12) and $dil = 1.8$ dex are shown in Fig. 10. The spread observed among the hs elements does not agree with AGB predictions. Aoki et al. (2002c) detected 13 lines for Ce, 4 for Ba,

³ The number of lines are taken from Aoki et al. (2002c,d). The observational data by Masseron et al. (2010) reported in Fig. 9 will be discussed by the authors in Masseron et al., in preparation

and 3 for La, Nd and Sm. Solutions with $M_{\text{ini}}^{\text{AGB}} = 2 M_{\odot}$ are excluded because they would underestimate the observed $[Na/Fe]$ and $[Mg/Fe]$ by about 0.4 dex. As highlighted by Aoki et al. (2002c), N is very uncertain in this star.

2.2.6 CS 30322-023 (Fig. 11)

The giant CS 30322-023 is the most metal-poor star of the sample ($[Fe/H] = -3.5$, -3.39 Masseron et al. 2006, 2010; $[Fe/H] = -3.25$ Aoki et al. 2007). Due to its low surface gravity ($T_{\text{eff}} = 4100$ K; $\log g = -0.3$)⁴, the hypothesis of an intrinsic AGB star at the beginning of its TP-AGB phase was advanced by Masseron et al. (2006). Aoki et al. (2007) measured $T_{\text{eff}} = 4300 \pm 100$ K and $\log g = 1.0 \pm 0.3$ dex, supporting instead the binary scenario.

CS 30322-023 shows a low carbon enhancement with respect to other CEMP-*s* stars ($[C/Fe] \sim 0.6$), together with a very strong nitrogen overabundance ($[N/Fe] \sim 2.5 - 2.8$). While negative $[Sr/Fe]$ and $[Y/Fe]$ are detected, the observed $[Zr/Fe]$ is slightly higher than solar, as other stars classified CEMP-*no/s* by Sivarani et al. (2006), CS 29528-041 and CS 31080-095, and possibly SDSS J1036+1212 (Behara et al. 2010), (see Paper II, Section 1). Cui, Zhang & Zhang (2007) hypothesised an AGB donor with initial mass in the range $2 \leq M/M_{\odot} \leq 4$, due to the high $[N/C]$ ratio⁵. IMS stars with $[Fe/H] \lesssim -2.3$, undergo an extremely deep TDU, in which the envelope reaches almost the bottom of the He inter-shell (Sugimoto 1971; Iben 1973; Karakas & Lattanzio 2003; Ventura & D'Antona 2005), possibly modifying the structure and the evolution of the star. Nucleosynthesis models including hot TDU are under study.

In Fig. 11, we present possible interpretations with AGB models of $M_{\text{ini}}^{\text{AGB}} = 1.5 M_{\odot}$ (cases ST/2, ST/3, ST/5) and a very large dilution ($dil = 2.5$ dex). Similar solutions are obtained with $M_{\text{ini}}^{\text{AGB}} = 1.4 - 2 M_{\odot}$ models and $dil = 1.7$ to 3 dex. The observed $[Na/Fe] = 1.04$ is underestimated by AGB models of lower initial mass ($M_{\text{ini}}^{\text{AGB}} = 1.3 M_{\odot}$).⁶ A low upper limit is detected for $[F/Fe]$ by Lucatello et al. (2011) ($[F/Fe] < 0.6$). AGB models predict larger fluorine abundance (see Paper I; Section 2.2.4).

As introduced in Section 1, we assume an initial $[Cu/Fe]_{\text{ini}} = -0.7$ according to the average of metal-poor Galactic stars. At halo metallicity, a spread is also observed for $[Sr/Fe]$ and $[Y/Fe]$ in unevolved Galactic stars (François et al. 2007), and we adopt initial $[Sr,Y/Fe]_{\text{ini}} = -1$. $[Eu/Fe]$ observations in unevolved stars show a large spread for $[Fe/H] \leq -2.0$, from $[Eu/Fe] \sim -1$ to $+2$ dex (Paper II, Fig. 2). The Eu detected in CS 30322-023 is negative ($[Eu/Fe] =$

⁴ The uncertainties of the atmospheric parameters ($\Delta T_{\text{eff}} = 250$ K and $\Delta \log g = 1.0$ dex) is due to the use of LTE instead of NLTE atmospheric models. In fact, the gravities of metal-poor giants derived from LTE iron-line analysis are most probably underestimated by 0.5 up to 1 dex (Thévenin & Idiart 1999; Israelian et al. 2001, 2004; Korn et al. 2003).

⁵ The condition $M_{\text{ini}}^{\text{AGB}} > 2 M_{\odot}$ comes from the hypothesis of the Hot Bottom Burning process in order to explain $[N/Fe] > [C/Fe]$, while the condition $M_{\text{ini}}^{\text{AGB}} < 4 M_{\odot}$ was adopted by the authors to justify the absence of an *r*-process overabundance, for which the AGB companion cannot evolve as Type 1.5 Supernova.

⁶ Note that the observed Na accounts for NLTE and 3D corrections (Aoki et al. 2007).

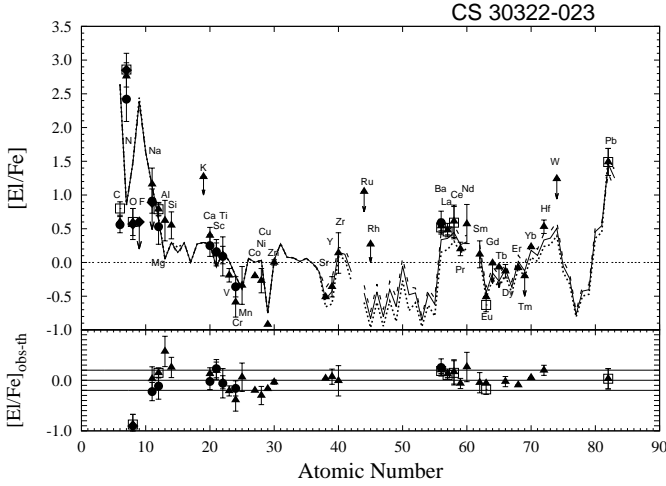


Figure 11. Spectroscopic $[El/Fe]$ abundances of the giant CS 30322-023 ($[Fe/H] \sim -3.4$, $T_{\text{eff}} = 4100$ K, $\log g = -0.3$ Masseron et al. 2006, 2010; $[Fe/H] = -3.25$, $T_{\text{eff}} = 4300$ K, $\log g = 1.0$ Aoki et al. 2007) compared with AGB models of $M_{\text{ini}}^{\text{AGB}} = 1.5 M_{\odot}$, cases ST/2 (dotted line), ST/3 (solid line), ST/5 (dashed line), and $dil = 2.5$ dex. Observations are from Masseron et al. (2006) (filled triangles), Masseron et al. (2010) (empty squares), Aoki et al. (2007) (filled circles), Lucatello et al. (2011) (filled diamonds). This star shows $[hs/lr] = 0.66$ and $[Pb/hs] = 0.96$. We assumed $[Sr, Y/Fe]_{\text{ini}} = -1$ in order to interpret the observed negative values. An $[r/Fe]_{\text{ini}} = -1$ is adopted.

-0.6), requiring a negative initial r -process composition of the molecular cloud ($[r/Fe]_{\text{ini}} = -1$). A $dil = 2.5$ dex means that the mass transferred from the AGB is 300 times lower than the mass of the convective envelope of the secondary star; then, the s -process contribution is very low, and negative values for $[Sr, Y/Fe]$, as well as for r -process elements as $[Eu, Gd, Tb, Dy/Fe]$ are obtained. Otherwise, for $dil \sim 1$ dex the negative initial $[El/Fe]$ abundances are overcome by the s -process contribution.

Because of the peculiarity of this star, caution in the interpretation of the spectroscopic data is suggested. In fact, due to the very low metallicity, the AGB nucleosynthesis may differ from the canonical scenario due to the occurrence of a proton ingestion episode (see Section 2.1.1).

2.2.7 HD 196944 (Fig. 12)

This CEMP-sI giant (Aoki et al. 2002c,d, 2007 and Van Eck et al. 2003; $[Fe/H] = -2.25$, $T_{\text{eff}} = 5250$ K and $\log g = 1.8$) has been analysed in Paper II, Section 5. An AGB model of initial mass $M = 1.5 M_{\odot}$, case ST/5, $dil \sim 2.0$ dex and no initial r -process enhancement provides a plausible theoretical interpretation for this star (Fig. 12). The observed $[Na/Fe]$ constrains the AGB initial mass, while the s -process elements ($[hs/lr] = 0.3$; $[Pb/hs] = 1.0$) may be equally interpreted by $M_{\text{ini}}^{\text{AGB}} = 1.3$ and $2 M_{\odot}$ models.

2.2.8 HE 0202-2204 (Fig. 13)

The giant HE 0202-2204 ($[Fe/H] = -1.98$, $T_{\text{eff}} = 5280$ K and $\log g = 1.65$) was studied by Barklem et al. (2005). In Fig. 13, we show two AGB models in agreement with the observed $[hs/lr] = 0.67$: $M_{\text{ini}}^{\text{AGB}} = 1.3$ and $2 M_{\odot}$, cases ST/9

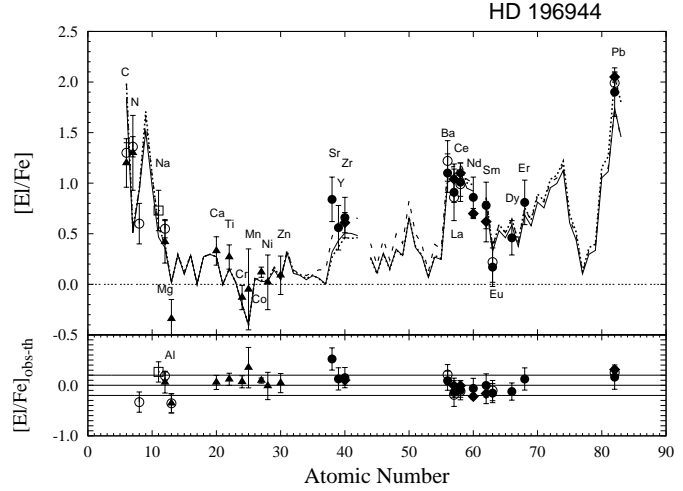


Figure 12. Spectroscopic $[El/Fe]$ abundances of the giant HD 196944 ($[Fe/H] = -2.25$; $T_{\text{eff}} = 5250$ K; $\log g = 1.8$) compared with AGB models of $M_{\text{ini}}^{\text{AGB}} = 1.5 M_{\odot}$, cases ST/3 (dotted line), ST/5 (solid line) and ST/6 (dashed line), $dil = 2.0$ dex ($[hs/lr]_{\text{obs}} = 0.3$; $[Pb/hs]_{\text{obs}} = 1.0$). Observations are from Aoki et al. (2002c) (filled circles), Aoki et al. (2002d) (filled triangles), Aoki et al. (2007) (empty square), Van Eck et al. (2003) (filled diamonds), Masseron et al. (2010) (empty circles). No initial r -process enhancement is adopted. This star was discussed in Paper II as representative of the CEMP-s stars (see Fig. 12), and it is reported here for completeness.

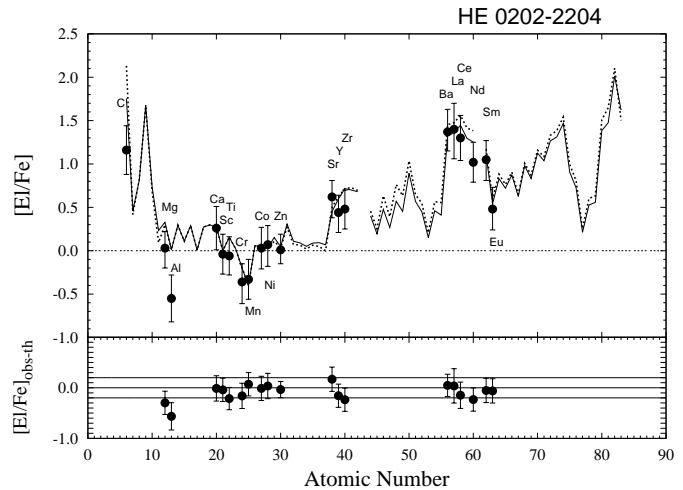


Figure 13. Spectroscopic $[El/Fe]$ abundances of the giant HE 0202-2204 ($[Fe/H] = -1.98$; $T_{\text{eff}} = 5280$ K; $\log g = 1.65$) compared with AGB models of $M_{\text{ini}}^{\text{AGB}} = 1.3$ or $2 M_{\odot}$, cases ST/9 or ST/6, $dil = 0.7$ or 1.7 dex, (dotted or solid lines, respectively; $[hs/lr]_{\text{obs}} = 0.67$). Observations are from Barklem et al. (2005). The $[La/Eu]_{\text{obs}}$ is better interpreted by a pure s -process distribution ($[r/Fe]_{\text{ini}} = 0.0$, as shown here); however, the initial r -process enhancement $[r/Fe]_{\text{ini}} = 0.5$ generally adopted in this paper for CEMP-s stars agrees within the errors with the observations. These models predict $[Pb/Fe]_{\text{th}} \sim 2$. The differences $[El/Fe]_{\text{obs-th}}$ displayed in the lower panel represent the $M_{\text{ini}}^{\text{AGB}} = 2 M_{\odot}$ model. No initial r -process enhancement is adopted.

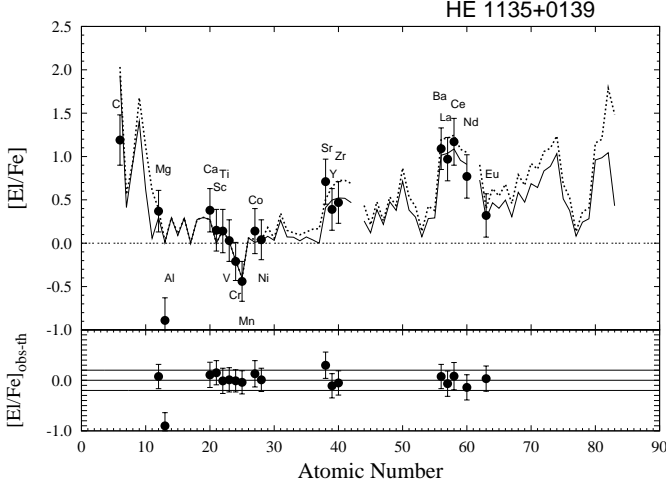


Figure 14. Spectroscopic $[\text{El}/\text{Fe}]$ abundances of the giant HE 1135+0139 ($[\text{Fe}/\text{H}] = -2.33$; $T_{\text{eff}} = 5487$ K; $\log g = 1.8$) compared with AGB models of $M_{\text{ini}}^{\text{AGB}} = 1.3 M_{\odot}$, case ST/24 and $dil = 1.2$ dex (solid line) and $M_{\text{ini}}^{\text{AGB}} = 1.5 M_{\odot}$, case ST/6 and $dil = 1.8$ dex (dotted line). Observations are from Barklem et al. (2005), who found $[\text{hs}/\text{ls}] = 0.48$. We predict $[\text{Pb}/\text{Fe}]_{\text{th}} \sim 1.0 - 1.8$. No initial r -process enrichment is assumed. The differences $[\text{El}/\text{Fe}]_{\text{obs-th}}$ displayed in the lower panel refer to the AGB model represented with solid line. This star was discussed in Paper II as representative of those CEMP- s stars without Pb detection (see Fig. 14), and it is reported here for completeness.

and ST/6 (solid and dashed lines, respectively). Both cases are in agreement with a giant having suffered the FDU because of the high dilutions applied ($dil = 0.7 - 1.7$ dex). These models predict $[\text{Pb}/\text{Fe}]_{\text{th}} \sim 2$. With higher s -process efficiencies (case ST) and $M_{\text{ini}}^{\text{AGB}} = 1.5 M_{\odot}$ ($dil = 0.9$ dex), the estimated Pb is very high ($[\text{Pb}/\text{Fe}]_{\text{th}} \sim 3.2$): this solution is discarded because $[\text{Mg}/\text{Fe}]$ would be largely overestimated ($[\text{Mg}/\text{Fe}]_{\text{th}} = 0.7$). No initial r -process enhancement is adopted in Fig. 13, but an $[\text{r}/\text{Fe}]^{\text{ini}} = 0.5$, generally assumed for CEMP- s stars, still agrees within the $[\text{La}/\text{Eu}]$ uncertainty.

2.2.9 HE 1135+0139 (Fig. 14)

This giant, with $[\text{Fe}/\text{H}] = -2.33$, $T_{\text{eff}} = 5487$ K and $\log g = 1.8$ (Barklem et al. 2005), has been analysed in Paper II, Section 5. Two possible theoretical interpretations were shown: $M_{\text{ini}}^{\text{AGB}} = 1.3 M_{\odot}$, case ST/24 and $dil = 1.2$ dex and $M_{\text{ini}}^{\text{AGB}} = 1.5 M_{\odot}$, case ST/6 and $dil = 1.8$ dex (Fig. 14). Similar solutions are obtained with $M_{\text{ini}}^{\text{AGB}} = 2 M_{\odot}$. The high dilutions applied agree with a giant having suffered the FDU. We predict $[\text{Pb}/\text{Fe}]_{\text{th}} \sim 1.0 - 1.8$.

2.2.10 HK II 17435-00532 (Fig. 15)

A complete analysis of this mild s -process giant was provided by Roederer et al. (2008) ($[\text{Fe}/\text{H}] = -2.23$, $T_{\text{eff}} = 5200$ K and $\log g = 2.15$). They found an unexpected high amount of lithium. So far HK II 17435-00532 does not seem to be member of a binary system. Further radial velocity measurements are required because the observation was done over a time span of about 180 days, which does not permit to discover very long periods.

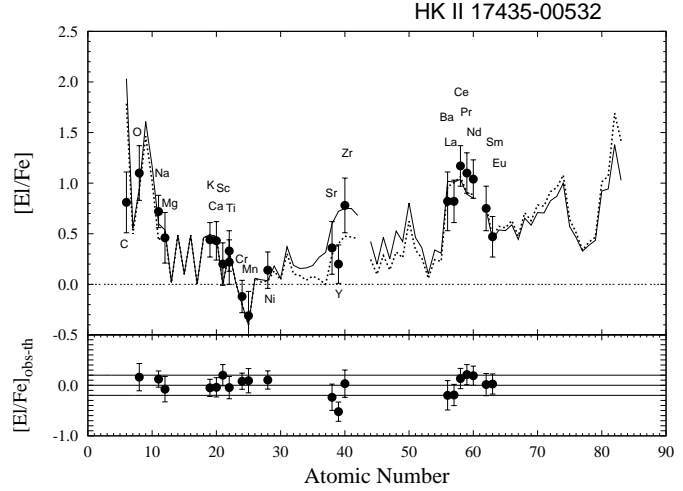


Figure 15. Spectroscopic $[\text{El}/\text{Fe}]$ abundances of the giant HK II 17435-00532 ($[\text{Fe}/\text{H}] = -2.23$; $T_{\text{eff}} = 5200$ K; $\log g = 2.15$) compared with $M_{\text{ini}}^{\text{AGB}} = 1.5 M_{\odot}$ models, cases ST/5 and ST/12, $dil = 2.1$ and 1.8 dex (dashed and solid lines, respectively). Observations are from Roederer et al. (2008), who detected $[\text{hs}/\text{ls}] = 0.55$. We predict $[\text{Pb}/\text{Fe}]_{\text{th}} \sim 1.4 - 1.7$. The differences $[\text{El}/\text{Fe}]_{\text{obs-th}}$ displayed in the lower panel refer to case ST/12, represented with solid line. An $[\text{r}/\text{Fe}]^{\text{ini}} = 0.3$ is adopted.

Theoretical interpretations with AGB models have been widely discussed by Roederer et al. (2008). In Fig. 15, we show solutions with $M_{\text{ini}}^{\text{AGB}} = 1.5 M_{\odot}$ models. The solid line represents the case ST/12 and $dil = 1.8$ dex examined by Roederer et al. (2008), in agreement with the observed $[\text{hs}/\text{ls}] = 0.55$. No lead is detected. $[\text{Y}/\text{Fe}]_{\text{obs}}$ is 0.5 dex lower than the AGB prediction. We present here an additional interpretation with a $M_{\text{ini}}^{\text{AGB}} = 1.5 M_{\odot}$ model, case ST/5 and $dil = 2.1$ dex (dashed line). This case agrees better with the observed $[\text{Y}/\text{Fe}]$, but predicts a low $[\text{Na}/\text{Fe}]$ (about 0.3 dex). Even by decreasing $[\text{Na}/\text{Fe}]$ of about 0.1 dex owing to NLTE corrections (Roederer et al. 2008), $[\text{Na}/\text{Fe}]$ would be slightly higher than the value predicted by the dashed line. We estimate $[\text{Pb}/\text{Fe}]_{\text{th}} \sim 1.4 - 1.7$. AGB solutions with lower initial mass (e.g., $M_{\text{ini}}^{\text{AGB}} = 1.3 M_{\odot}$) are discarded, because $[\text{Na}/\text{Fe}]$ would be underestimated by such models ($[\text{Na}/\text{Fe}]_{\text{th}} \sim 0$). This star requires a low r -process enrichment ($[\text{r}/\text{Fe}]^{\text{ini}} = 0.3$).

2.2.11 BS 17436-058 (Fig. 16)

BS 17436-058 is a giant with $[\text{Fe}/\text{H}] = -1.9$, $T_{\text{eff}} = 5390$ K and $\log g = 2.2$ (Tsangarides 2005). AGB models with an initial mass from 1.3 to $2 M_{\odot}$ ($dil = 0.7 - 1.6$ dex) may equally interpret the observations. Measurement of Na and Mg are highly desirable. In Fig. 16, we show three possible solutions: $M_{\text{ini}}^{\text{AGB}} = 1.3 M_{\odot}$, ST/12, $dil = 0.7$ dex, $M_{\text{ini}}^{\text{AGB}} = 1.4 M_{\odot}$, ST/9, $dil = 1.2$ dex, $M_{\text{ini}}^{\text{AGB}} = 1.5 M_{\odot}$, ST/5, $dil = 1.6$ dex, all in agreement with the two s -process indicators $[\text{hs}/\text{ls}] = 0.60$ and $[\text{Pb}/\text{hs}] = 0.76$. The observed $[\text{La}/\text{Eu}]$ is interpreted with an r -process enhancement $[\text{r}/\text{Fe}]^{\text{ini}} = 0.7$. Note that an $[\text{r}/\text{Fe}]^{\text{ini}} = 0.5$, generally adopted for CEMP- s stars, still agrees within the uncertainties. No velocity variations are detected; this does not necessarily disprove the presence of a companion, since this star could have an or-

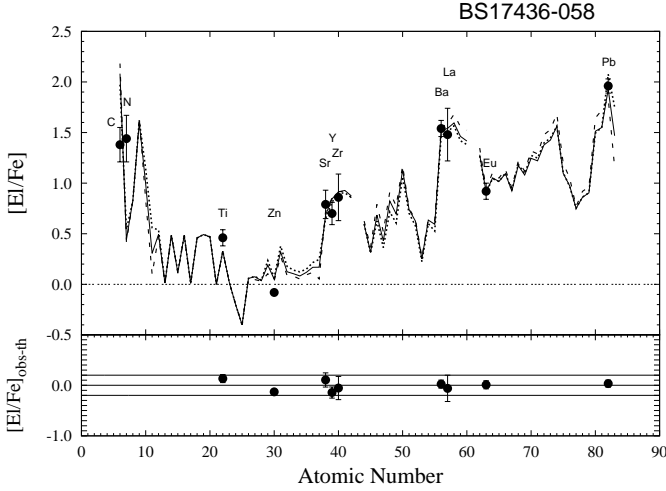


Figure 16. Spectroscopic $[El/Fe]$ abundances of the giant BS 17436-058 ($[Fe/H] = -1.9$; $T_{\text{eff}} = 5390$ K; $\log g = 2.2$) compared with three AGB stellar models: $M_{\text{ini}}^{\text{AGB}} = 1.3 M_{\odot}$, ST/12, $dil = 0.7$ dex (dashed line), $M_{\text{ini}}^{\text{AGB}} = 1.4 M_{\odot}$, ST/9, $dil = 1.2$ dex (solid line), $M_{\text{ini}}^{\text{AGB}} = 1.5 M_{\odot}$, ST/5, with $dil = 1.6$ dex (dotted line). Observations are from Tsangarides (2005), who detected $[hs/lis] = 0.60$ and $[Pb/hs] = 0.76$. The differences $[El/Fe]_{\text{obs-th}}$ displayed in lower panel refer to a model for $M_{\text{ini}}^{\text{AGB}} = 1.4 M_{\odot}$ (solid line). An $[r/Fe]_{\text{ini}} = 0.7$ is adopted (see text).

bital axis inclination which does not permit observations of velocity variations (Tsangarides 2005).

3 CEMP-S/R STARS

This Section is dedicated to CEMP-sII/r stars, divided in two smaller groups following their r -process enhancement: CEMP-sII/rII with $[r/Fe]_{\text{ini}}$ included between ~ 1.5 and 2 (Section 3.1 and 3.2) and CEMP-sII/rI with $[r/Fe]_{\text{ini}} = 1.0$ (Section 3.3).

3.1 CEMP-sII/rII with $[r/Fe]_{\text{ini}} \sim 2$

We discuss in this Section six stars showing very high s - and r -process enhancements ($[hs/Fe] \sim [Eu/Fe] \sim 2$) interpreted with an initial r -enrichment of the molecular cloud $[r/Fe]_{\text{ini}} \sim 2$. Five are main-sequence/turnoff stars, CS 22898-027 by Aoki et al. (2002c,d, 2007) with $[La/Eu] = 0.25$, CS 29497-030 by Ivans et al. (2005) with $[La/Eu] = 0.23$, HE 0338-3945 by Jonsell et al. (2006) with $[La/Eu] = 0.34$ (discussed in Paper II, Section 5), HE 1105+0027 by Barklem et al. (2005) with $[La/Eu] = 0.29$, HE 2148-1247 by Cohen et al. (2003) with $[La/Eu] = 0.40$; one is a giant HE 1305+0007 by Goswami et al. (2006) with $[La/Eu] = 0.59$ (and very high $[La/Fe] = 2.56$).

3.1.1 CS 22898-027 (Fig. 17)

This turnoff star ($[Fe/H] = -2.26$; $T_{\text{eff}} = 6250$ K and $\log g = 3.7$, before the occurrence of the FDU) has been analysed by Preston & Sneden (2001), Aoki et al. (2002c,d), and Aoki et al. (2007). No radial velocity variations are found for this star (Preston & Sneden 2001; Aoki et al. 2002c; Tsangarides 2005; Preston et al. 2009).

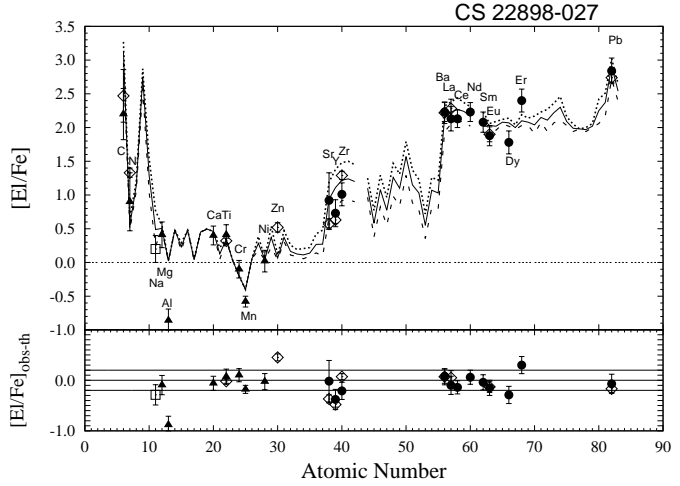


Figure 17. Spectroscopic $[El/Fe]$ abundances of the turnoff/subgiant CS 22898-027 ($[Fe/H] = -2.26$; $T_{\text{eff}} = 6250$ K; $\log g = 3.7$, before the FDU) compared with AGB models of $M_{\text{ini}}^{\text{AGB}} \sim 1.3 M_{\odot}$, case ST/12 and no dilution. Observations are from Aoki et al. (2002c) (filled triangles), Aoki et al. (2002d) (filled circles), Aoki et al. (2007) (empty square), Tsangarides (2005) (empty diamonds). Aoki et al. (2002c) detected $[hs/lis] = 1.30$ and $[Pb/hs] = 0.67$. Three thermal pulses are represented, pulses 4 (dashed line), 5 (solid line) and 6 (dotted line), corresponding to an increase of the AGB initial mass of $\Delta M \sim 0.025 M_{\odot}$ (see text). An initial r -process enrichment $[r/Fe]_{\text{ini}} = 2.0$ is assumed ($[La/Eu]_{s+r} = 0.2$; $[La/Eu]_s = 0.9$).

A theoretical interpretation of the spectroscopic abundances was presented by Sneden, Cowan & Gallino (2008). In Fig. 17, we provide similar solutions with updated models. The observed $[Na/Fe]$ is low while the second s -peak is high ($[hs/Fe] \lesssim 2$), as in several main-sequence stars. This agrees with a $M_{\text{ini}}^{\text{AGB}} \sim 1.3 M_{\odot}$ model, ST/12 and no dilution. Three thermal pulses with TDU are shown. They represent a plausible decrease (n4) or increase (n6) in mass of about $0.025 M_{\odot}$ for $M_{\text{ini}}^{\text{AGB}} \sim 1.3 M_{\odot}$ models (see Section 2.1.1). An additional TDU corresponds to an increase of the abundances of ~ 0.2 dex. The model with 4 TDUs seems to better interpret the low $[Na/Fe]$ and $[Y/Fe]$ observed. However, only one line has been detected for Na, while 2 lines for Y (as for Sr and Zr), and both elements agree with theoretical predictions within an uncertainty of 0.2 dex. An initial r -enrichment $[r/Fe]_{\text{ini}} = 2.0$ is adopted in order to interpret the average among Eu, Dy and Er (3, 2 and 4 lines, respectively). By increasing the number of TDUs ($M_{\text{ini}}^{\text{AGB}} = 1.5$ or $2 M_{\odot}$; case ST/4.5; $dil \sim 1$ dex), the observed $[Na/Fe]$ and $[ls/Fe]$ would be overestimated by AGB models. This excludes the possibility that the star underwent efficient mixing during its main-sequence phase.

3.1.2 CS 29497-030 (Fig. 18)

Preston & Sneden (2000) investigated a sample of 62 blue metal-poor (BMP) stars, including the main-sequence star CS 29497-030, arguing that half are binaries. This is the case of CS 29497-030, a BMP star subject to different studies (Sneden et al. 2003b; Sivarani et al. 2004; Ivans et al. 2005). Sneden et al. (2003b) confirm the binary scenario.

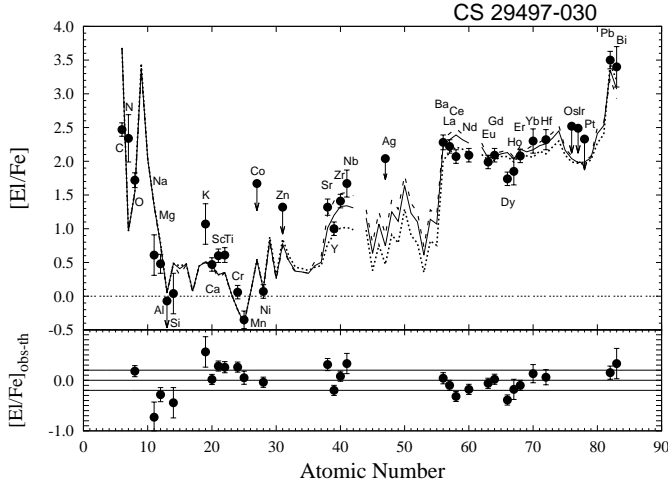


Figure 18. Spectroscopic $[El/Fe]$ abundances of the main-sequence star CS 29497-030 ($[Fe/H] = -2.57$; $T_{\text{eff}} = 7000$ K; $\log g = 4.1$) compared with AGB models of $M_{\text{ini}}^{\text{AGB}} = 1.35 M_{\odot}$ (pulse 7, see Sections 2.1.1 and 3.1.1), cases ST/6 (dotted line), ST/9 (solid line), ST/12 (dashed line), and no dilution. Observations are from Ivans et al. (2005), who found $[hs/ls] = 1.02$ and $[Pb/hs] = 1.46$. Note that the values represented for O, Na, Al, and K do not account for NLTE corrections. An initial r -process enrichment $[r/Fe]_{\text{ini}} = 2$ is assumed ($[La/Eu]_{s+r} = 0.3$; $[La/Eu]_s = 0.9$).

For this analysis, we consider only the most recent observations provided by Ivans et al. (2005) ($[Fe/H] = -2.57$; $T_{\text{eff}} = 7000$ K and $\log g = 4.1$). Theoretical AGB interpretations have been presented by Ivans et al. (2005), Bisterzo et al. (2008b) and Käppeler et al. (2011). In Fig. 18, solutions with $M_{\text{ini}}^{\text{AGB}} \sim 1.35 M_{\odot}$ models (at the seventh TDU, $n = 7$), cases ST/6, ST/9 and ST/12, and no dilution interpret the observed $[hs/ls] = 1.02$ and $[Pb/hs] = 1.46$. CS 29497-030 has the highest lead observed so far, $[Pb/Fe] = 3.65$. For the first time in metal-poor stars Bi is detected, with a high overabundance, in agreement with AGB predictions at these low metallicities: stars with a huge amount of lead are also expected to exhibit a high s -process abundance of bismuth. In fact, despite the solar bismuth is mainly produced by the r -process ($\sim 80\%$), at $[Fe/H] \sim -2.6$ and for a given ^{13}C -pocket, the number of neutrons per iron seed is ~ 400 times higher than solar, directly feeding the third s -process peak (Paper I). Also Nb was detected in this star supporting the binary scenario ($[Zr/Nb] \sim 0$; Ivans et al. 2005, see also Paper I). $[Na/Fe]$ is overestimated by AGB models in Fig. 18. We recall that Na may have a large uncertainty (of 0.6 dex or more) due to poorly understood NLTE effects on Na line formation and for 3D atmospheric models. By increasing the AGB initial mass, and therefore the number of TDUs, a dilution factor must be applied in order to reproduce the observed values, but both Na and Mg would be highly overestimated by theoretical models (Bisterzo et al. 2008b). Interpretations with negligible dilutions are compatible with moderate mixing during the main-sequence phase. An initial r -enrichment of 2 dex is assumed. Note that only an upper limit has been detected for Ag and at present we do not adopt initial r -process contributions for isotopes lower than Ba (see Paper II, Section 3). The low $[Y/Fe]$ observed does not agree with AGB predictions. The hypothesis of

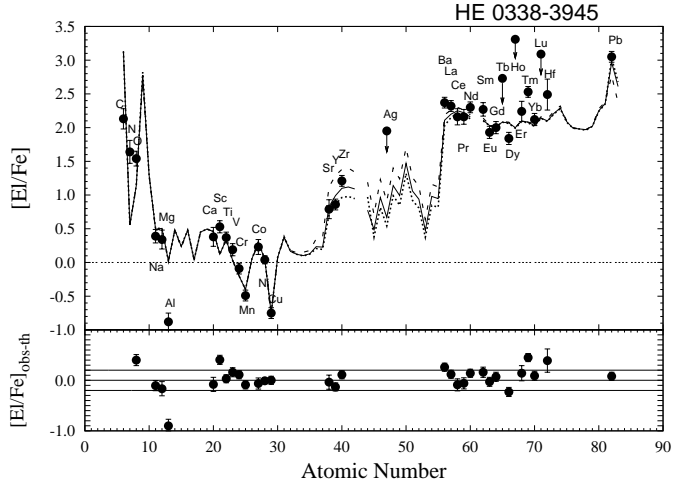


Figure 19. Spectroscopic $[El/Fe]$ abundances of the main-sequence star HE 0338-3945 ($[Fe/H] = -2.42$; $T_{\text{eff}} = 6160$ K; $\log g = 4.1$) compared with AGB models of $M_{\text{ini}}^{\text{AGB}} = 1.3 M_{\odot}$ cases ST/9 (dotted line), ST/11 (solid line), ST/15 (dashed line), and no dilution. Observations are from Jonsell et al. (2006), who found $[hs/ls] = 1.24$ and $[Pb/hs] = 0.81$. An initial r -process enrichment $[r/Fe]_{\text{ini}} = 2.0$ is assumed ($[La/Eu]_{s+r} = 0.12$; $[La/Eu]_s = 0.87$). We assumed an initial $[Cu/Fe] = -0.7$, in agreement with unevolved halo stars at this metallicity (see Section 1). This star was discussed in Paper II as representative of the CEMP- s/r stars (see Fig. 15), and is reported here for completeness.

an initial subsolar $[Y/Fe]$ does not change sensibly the final $[Y/Fe]$ prediction, because of the high s -process contribution to Y together with no dilution (Ivans et al. 2005).

3.1.3 HE 0338-3945 (Fig. 19)

This main-sequence star, with $[Fe/H] = -2.42$, $T_{\text{eff}} = 6160$ K and $\log g = 4.1$, has been widely discussed in Paper II, Section 5. An AGB model of initial mass $M = 1.3 M_{\odot}$, case ST/11, no dilution and $[r/Fe]_{\text{ini}} = 2.0$ provides a plausible theoretical interpretation for the observed $[hs/ls] = 1.24$, $[Pb/hs] = 0.81$ and $[La/Eu] = 0.34$ (Fig. 19). Solutions with no dilution suggest that only negligible or moderate mixing occurred in this star. The main constraints about the AGB initial mass are provided by the low $[Na/Fe]$ and $[ls/Fe]$ observed. Among the heavy elements, Ba, Dy and Hf lie within 0.2 dex of AGB model uncertainty, while the observed $[Tm/Fe]$ is 0.4 dex larger than AGB predictions. The four Tm lines analysed in this star have oscillator strengths from Kurucz (1995), which, according to Sneden et al. (1996), are rescaled laboratory data from Corliss & Bozman (1962). Tm should be reconsidered with the high-quality gf -values published by Wickliffe & Lawler (1997). A negative $[Cu/Fe]$ is observed, in agreement with unevolved halo stars (see Section 1).

3.1.4 HE 1105+0027 (Fig. 20)

HE 1105+0027 lies close to the turnoff ($[Fe/H] = -2.42$; $T_{\text{eff}} = 6132$ K and $\log g = 3.45$; Barklem et al. 2005). Two possible theoretical interpretations for HE 1105+0027 are shown in Fig. 20, with $M_{\text{ini}}^{\text{AGB}} = 1.3 M_{\odot}$, case ST/9 and no dilution, and $M_{\text{ini}}^{\text{AGB}} = 2 M_{\odot}$, case ST/3 and $dil = 0.6$ dex.

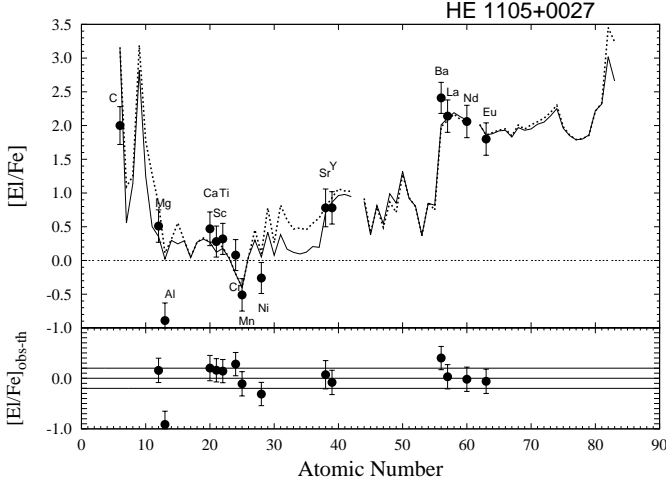


Figure 20. Spectroscopic $[El/Fe]$ abundances of the main-sequence/turnoff star HE 1105+0027 ($[Fe/H] = -2.42$; $T_{\text{eff}} = 6132$ K; $\log g = 3.45$) compared with AGB models of $M_{\text{ini}}^{\text{AGB}} = 1.3 M_{\odot}$ (ST/9 and no dilution; solid line) or $M_{\text{ini}}^{\text{AGB}} = 2 M_{\odot}$ (ST/3 and $dil = 0.6$ dex; dotted line). Observations are from Barklem et al. (2005), who found $[hs/ls] = 1.15$. For lead we predict $[Pb/Fe]_{\text{th}} \sim 3$. The differences $[El/Fe]_{\text{obs-th}}$ displayed in the lower panel refer to the $M_{\text{ini}}^{\text{AGB}} = 1.3 M_{\odot}$ model, represented by the solid line. An initial r -process enrichment $[r/Fe]_{\text{ini}} = 1.8$ is assumed.

A Na measurement is highly desirable. $[Mg/Fe]$ (0.5 ± 0.24) agrees within the errors with both AGB models, even if the solution with a lower number of TDUs better interprets the observations. $[Ba/Fe]_{\text{obs}}$ (with 2 lines detected) is underestimated by models. La (6 lines) and Nd (9 lines) are considered more reliable ($[hs/ls] = 1.15$). We predict $[Pb/Fe]_{\text{th}} \sim 3$. An r -process enrichment of $[r/Fe]_{\text{ini}} = 1.8$ dex is adopted.

3.1.5 HE 2148–1247 (Fig. 21)

The main-sequence star HE 2148–1247 ($[Fe/H] = -2.3$, $T_{\text{eff}} = 6380$ K and $\log g = 3.9$) was the first showing high enhancements in both s and r -process elements (Cohen et al. 2003), with $[Eu/Fe] = 2$, $[La/Eu] = 0.4$, $[hs/Eu] = 0.26$. Cohen et al. (2003) classify this star as a small-amplitude long-period binary.

In Fig. 21, we show theoretical interpretations with $M_{\text{ini}}^{\text{AGB}} \sim 1.35 M_{\odot}$ models (cases ST/8, ST/9, and ST/12) and no dilution. Note the difference between the observed $[Y/Fe]$ and $[Zr/Fe]$ (~ 0.6 dex; 5 and 3 lines detected, respectively), which disagrees with AGB predictions. Similar solutions may be obtained by $M_{\text{ini}}^{\text{AGB}} = 2 M_{\odot}$ models with $dil = 0.7$ dex and case ST/6. At present, the theoretical interpretations shown in Fig. 21 seem to better agree with the observed $[Mg/Fe]$ and $[ls/Fe]$, sustaining the hypothesis of negligible or moderate mixing. However, we may not exclude solutions with $M_{\text{ini}}^{\text{AGB}} = 2 M_{\odot}$, which predicts $[Mg/Fe]_{\text{th}} = 0.8$ and $[ls/Fe]_{\text{th}} = 1.4$. AGB models with $M_{\text{ini}}^{\text{AGB}} = 1.5 M_{\odot}$ ($dil = 0.5$ dex; case ST/3), are in accord with $[hs/ls]_{\text{obs}} = 1.21$ and $[Pb/hs]_{\text{obs}} = 0.84$, but $[Mg/Fe]_{\text{th}} = 1.16$ would be about 0.5 dex higher than observed. A Na detection would help to assess the AGB initial mass. An initial r -process enrichment of $[r/Fe]_{\text{ini}} = 2.0$ is adopted.

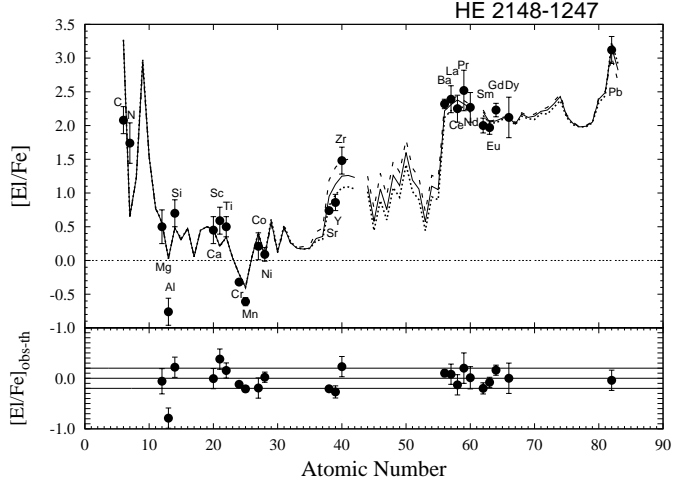


Figure 21. Spectroscopic $[El/Fe]$ abundances of the main-sequence star HE 2148–1247 ($[Fe/H] = -2.3$; $T_{\text{eff}} = 6380$ K; $\log g = 3.9$) compared with AGB models of $M_{\text{ini}}^{\text{AGB}} \sim 1.35 M_{\odot}$ (pulse 6, see Sections 2.1.1 and 3.1.1), cases ST/8 (dotted line), ST/9 (solid line), ST/12 (dashed line), and no dilution. Observations are from Cohen et al. (2003), who detected $[hs/ls] = 1.21$ and $[Pb/hs] = 0.84$. An initial r -process enrichment of $[r/Fe]_{\text{ini}} = 2.0$ is adopted ($[La/Eu]_{s+r} = 0.26$; $[La/Eu]_s = 0.86$).

3.1.6 HE 1305+0007 (Fig. 22)

The giant HE 1305+0007 shows $[Fe/H] = -2.03$, $T_{\text{eff}} = 4750$ K and $\log g = 2.0$ (Goswami et al. 2006). The spectrum is dominated by molecular absorption lines of CH, CN, C_2 . Note the large spread covered by the ls elements, with $[Zr/Fe]$ about 1.4 dex higher than $[Y/Fe]$ ⁷. Instead, AGB models predict $[Zr/Y]$ and $[La/Nd] \sim 0$. The second s -peak is very enhanced ($[hs/Fe] \sim 2.5$), similar to $[Zr/Fe]$ and $[Pb/Fe]$ ($[Pb/hs] \sim 0$). By considering $[ls/Fe] \sim [Zr/Fe]$, possible theoretical interpretations are displayed in Fig. 22, with $M_{\text{ini}}^{\text{AGB}} = 2 M_{\odot}$ models and low s -process efficiencies (cases ST/12, ST/18 and ST/24). The dilution adopted ($dil = 0.4$ dex) is low for a giant having suffered the FDU; moreover, this solution overestimates the observed $[Na/Fe]$ by about 1 dex. The sodium abundance is calculated from the resonance doublet (Na I D lines at 5890 and 5896 Å: Goswami et al. 2006) found $[Na/Fe] = +0.26$, based on the Na I D₂ line, and an overabundance $[Na/Fe] = +0.43$, based on the Na I D₁ line. We show both values in the Figure. Also the observed $[Mg/Fe]$ is ~ 0.5 dex lower than predicted. However, we must exclude AGB models with lower initial mass that need even lower dilutions or do not reach the high $[hs/Fe]$ observed. By excluding the observed Zr from the ls elements, the $[hs/ls]$ ratio would increase. AGB models with $[hs/ls]_{\text{th}} \geq 0.5$ would predict $[Pb/Fe]_{\text{th}} \gtrsim 3$ at $[Fe/H] = -2$ (see Paper I, Figs. 15 and 16, middle panels). Note that the Pb line at 4057 Å is strongly affected by molecular absorption lines. The interpretation for this giant remains a problem, for Na, Mg, the ls elements and for the low dilution applied. Beers et al. (2007) detected at low resolution C and

⁷ A similar behaviour has been also observed in the other two cold giants studied by Goswami et al. (2006): HD 5223 for ls -peak with $[Zr/Y] \sim 1$ (Section 4.1) and HE 1152–0355 for hs -peak with $[La/Nd] \sim 1.3$ (Section 4.2).

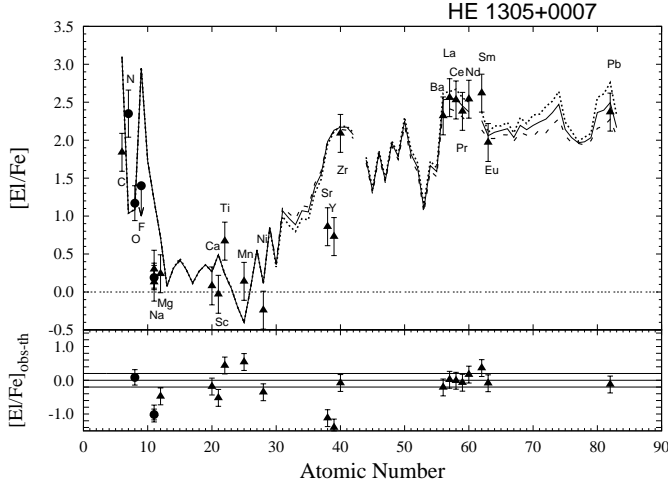


Figure 22. Spectroscopic $[El/Fe]$ abundances of the giant HE 1305+0007 ($[Fe/H] = -2.03$; $T_{\text{eff}} = 4750$ K; $\log g = 2.0$) compared with AGB models of $M_{\text{ini}}^{\text{AGB}} = 2 M_{\odot}$, cases ST/12 (dotted line), ST/15 (solid line), ST/18 (dashed line), and $dil = 0.4$ dex. Observations are from Goswami et al. (2006) (filled triangles) and Lucatello et al. (2011) (filled circles). Typical error bars of ± 0.3 dex are shown for data by Goswami et al. (2006), in agreement with the maximum fitting errors estimated by the authors. This star shows $[hs/ls] = 1.17$ and $[Pb/hs] = -0.21$. Note that AGB models can not predict $[Zr/Y] \sim 1.3$: we consider $[ls/Fe]_{\text{th}} \sim [Zr/Fe]_{\text{th}} \sim 2$, overestimating the observed $[Sr/Fe]$ and $[Y/Fe]$ by about 1 dex. Both the $[Na/Fe]$ abundance calculated from the resonance doublet Na I D lines are shown. $[N/Fe]$, $[O/Fe]$, $[F/Fe]$ by Lucatello et al. (2011) have been evaluated by adopting lower atmospheric parameters and metallicity than Goswami et al. (2006) ($\Delta[Fe/H] = 0.5$, $\Delta \log g = 1$). An $[r/Fe]_{\text{ini}} = 2.0$ is adopted.

N in this giant: they found $[C/Fe] = 2.4 \pm 0.35$ (0.6 dex higher than Goswami et al. 2006) and $[N/Fe] = 1.90 \pm 0.46$. Beers et al. (2007) adopt $[Fe/H] = -2.5$ and $\log g = 1.0$, about 0.5 and 1 dex lower than Goswami et al. (2006). Recently Lucatello et al. (2011) derive N, O, $^{12}\text{C}/^{13}\text{C}$ and an upper limit for F ($[F/Fe] < 1.4$) based on high-resolution spectra ($R = 50\,000$), by adopting the atmospheric parameters by Beers et al. (2007). AGB models predict too large $[C/Fe]$ and $[F/Fe]$ (see Paper I; Section 2.2.4). Further investigations are desirable.

3.2 CEMP-sII/rII with $[r/Fe]_{\text{ini}} \sim 1.5$

This class includes ten stars showing very high *s*-process enhancement ($[hs/Fe] \sim 2$) and an initial *r*-enrichment $[r/Fe]_{\text{ini}} \sim 1.5$.

Three are main-sequence stars, CS 29526-110, CS 31062-012 by Aoki et al. (2002c,d, 2007), and SDSS J1349-0229 by Behara et al. (2010). One star is a subgiant having not suffered the FDU, CS 31062-050 by Johnson & Bolte (2004) and Aoki et al. (2007). Five stars are giants, CS 22948-27 and CS 29497-34 by Barbuy et al. (2005) and Aoki et al. (2007), HD 187861 and HD 224959 by Van Eck et al. (2003) and Masseron et al. (2010), LP 625-44 by Aoki et al. (2002a,d, 2006). For the last star CS 22183-015, discrepant atmospheric parameters have been estimated by different authors (Johnson & Bolte 2002; Cohen et al. 2006), and the occurrence of the FDU remains uncertain.

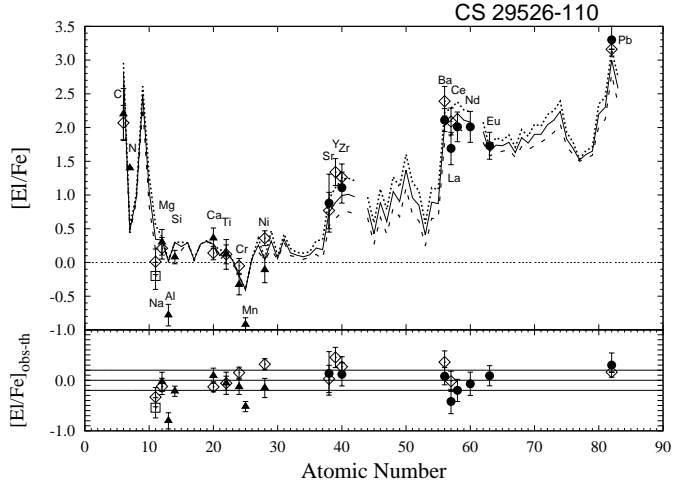


Figure 23. Spectroscopic $[El/Fe]$ abundances of the main-sequence star CS 29526-110 ($[Fe/H] = -2.06$; $T_{\text{eff}} = 6800$ K; $\log g = 4.1$, Aoki et al. 2008) compared with AGB models of $M_{\text{ini}}^{\text{AGB}} \sim 1.3 M_{\odot}$, case ST/6, and no dilution. Three thermal pulses are displayed, pulse 4 (dashed line), 5 (solid line) and 6 (dotted line), (Sections 2.1.1 and 3.1.1). Observations are from Aoki et al. (2002c) (filled triangles), Aoki et al. (2002d) (filled circles), Aoki et al. (2007) (empty square), Aoki et al. (2008) (empty diamonds). This star shows $[hs/ls] = 0.88$ and $[Pb/hs] = 1.42$. An initial *r*-process enrichment of $[r/Fe]_{\text{ini}} = 1.5$ is adopted.

3.2.1 CS 29526-110 (Fig. 23)

The main-sequence star CS 29526-110 was subject to different studies (Aoki et al. 2002c,d, 2007, 2008). It is a single-lined binary (Aoki et al. 2002d; Tsangarides 2005), although its period remains unknown. Different effective temperatures are estimated from V-K and B-V ($T_{\text{eff}}(B-V) = 6500$ K; $T_{\text{eff}}(V-K) = 6800$ K). We report the most recent values by Aoki et al. (2008) ($T_{\text{eff}} = 6800 \pm 150$ K; $\log g = 4.1 \pm 0.3$), with $[Fe/H] = -2.06$, about 0.3 dex higher than previous studies. Nitrogen is difficult to detect because the spectra are contaminated by CN molecular bands, and the value provided by Aoki et al. (2002d) is very uncertain. The solution which interprets the observed *s* indicators $[hs/ls] = 0.88$ and $[Pb/hs] = 1.42$ is shown in Fig. 23 and corresponds to $M_{\text{ini}}^{\text{AGB}} \sim 1.3 M_{\odot}$, case ST/6 and no dilution. Three thermal pulses are represented (pulses 4, 5 and 6). The most recent $[Ba/Fe]$ measurement (~ 0.3 dex higher than that measured by Aoki et al. 2002c) is based on two new red lines which are suitable for abundance determination, as well as the two very strong resonance lines previously considered (Aoki et al. 2008). The solution shown in Fig. 23 corresponding to the 6th TDU seems to better interpret the recent *s*-process measurements by Aoki et al. (2008), but predicts $[Na/Fe]$ about 0.5 dex higher than observed (the $[Na/Fe]$ estimated by Aoki et al. 2007 includes NLTE corrections). By adopting $M_{\text{ini}}^{\text{AGB}} \geq 1.4 M_{\odot}$ (and larger dilution), both the observed $[Na/Fe]$ and $[Mg/Fe]$ would be overestimated by AGB models. The lack of interpretations with dilution agrees with the occurrence of negligible or moderate mixing in this star. The $[La/Eu]$ ratio indicates an initial *r*-process enrichment $[r/Fe]_{\text{ini}} = 1.5$.

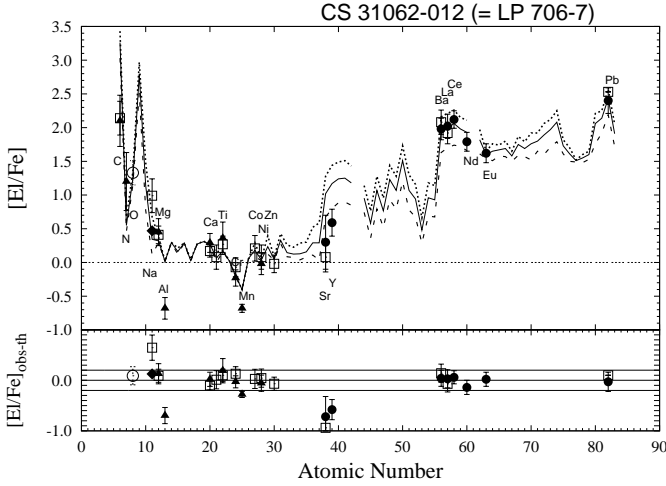


Figure 24. Spectroscopic $[El/Fe]$ abundances of the main-sequence star CS 31062-012 ($[Fe/H] = -2.55$; $T_{\text{eff}} = 6250$ K; $\log g = 4.5$) compared with AGB models of $M_{\text{ini}}^{\text{AGB}} \sim 1.3 M_{\odot}$, case ST/30, and no dilution. Three thermal pulses with TDU are displayed: pulse 3 (dashed line), 4 (solid line) and 5 (dotted line), (see Sections 2.1.1 and 3.1.1). Observations are from Israelian et al. (2001) (empty circle), Aoki et al. (2002c) (filled triangles), Aoki et al. (2002d) (filled circles), Aoki et al. (2007) (filled diamond), Aoki et al. (2008) (empty squares). This star shows $[hs/Y]_{\text{obs}} \sim 1.5$ and $[Pb/hs] = 0.48$. See text for discussion about Sr and Y. An initial r -process enrichment of $[r/Fe]_{\text{ini}} = 1.5$ is adopted.

3.2.2 CS 31062-012 (\equiv LP 706-7), (Fig. 24)

The main-sequence star CS 31062-012 ($[Fe/H] = -2.55$; $T_{\text{eff}} = 6250$ K; $\log g = 4.5$) has been analysed by Norris et al. (1997), Aoki et al. (2001), Israelian et al. (2001), Aoki et al. (2002c,d, 2007, 2008). CS 31062-012 does not show significant radial velocity variations (Norris et al. 1997; Aoki et al. 2002c), even with the extended period of 6000 days of observation (Aoki et al. 2008). Despite that, the high $[hs/Fe]$ (~ 2) and the detection of $[Pb/Fe] = 2.4$, implies a significant contribution from an AGB companion. Spectroscopic data are interpreted with AGB models of $M_{\text{ini}}^{\text{AGB}} = 1.3 M_{\odot}$, case ST/30 and no dilution (Fig. 24). Because of the high $[hs/ls]$ observed (~ 1.5 dex), the first s -peak is about 0.5 dex lower than theoretical predictions. No improvement may be obtained under the hypothesis of an initial $[Sr, Y/Fe]_{\text{ini}} = -1$, compatible with the spread observed in field stars (e.g., François et al. 2007), because the s -process contribution prevails if no dilution is applied. Moreover, with an initial r -process enhancement of $[r/Fe]_{\text{ini}} = 1.5$, the $[hs/ls]$ ratio does not increase appreciably (Paper II). However, only 2 lines for Sr and 1 line for Y have been detected. The Na measured in 2007 is lower with respect to the value detected in 2008, due to NLTE corrections ($\Delta[Na/Fe]_{\text{LTE-NLTE}} = 0.7$ dex, see Aoki et al. 2007, Table 13). Interpretations with $M_{\text{ini}}^{\text{AGB}} \geq 1.4 M_{\odot}$ models, which predict even higher $[Na/Fe]$ and $[ls/Fe]$, are excluded. This discards solutions with large dilutions, in agreement with the occurrence of negligible or moderate mixing during the main-sequence phase.

3.2.3 SDSS J1349-0229 (Fig. 25)

SDSS J1349-0229 is a main-sequence/turnoff star recently studied by Behara et al. (2010) ($[Fe/H] = -3.0$; $T_{\text{eff}} = 6200$ K; $\log g = 4.0$). It shows evidence for highly enhanced neutron capture elements, from both s - and r -process contributions. In Fig. 25, we display a solution with $M_{\text{ini}}^{\text{AGB}} \sim 1.35 M_{\odot}$ model (case ST/15 and no dilution). A large spread of the order of 1 dex is detected among the hs elements (e.g., $[Pr/La] = 1.13$). An average among Ba, La, Ce, Pr and Nd is chosen in Fig. 25 as representative of the hs peak. However, we underline the large discrepancy affecting the elements of the second s -peak and the s -process indicators $[hs/ls] = 0.57$ and $[Pb/hs] = 1.09$. We weight the initial r -enhancement on the observed $[Eu/Fe]$, because the other r -elements (Gd, Tb, Dy and Er) are generally affected by larger uncertainties. An initial r -process enrichment of $[r/Fe]_{\text{ini}} = 1.5$ is adopted. However, we underline the enhancement observed in the r -elements as Gd, Tb, Dy and Er with respect to Eu (e.g., $[Er/Eu] \sim 1$). Note that about 60% of solar Hf is produced by the s -process (Arlandini et al. 1999, Paper II), but the observed $[Hf/Fe]$ is very uncertain and no error bars are provided by the authors. This star shows high Na and Mg ($[Na/Fe] = 1.5$ and $[Mg/Fe] = 0.6$). At $[Fe/H] = -3$, a theoretical $[Na/Fe] \sim 1.5$ is predicted by AGB models already at the 6th TDU, as shown in Fig. 25 (see Paper I). The observed $[Na/Fe]$ accounts for the NLTE corrections from Gratton et al. (1999), using the Na D resonance lines at 588.995 and 589.592 nm. Behara et al. (2010) performed 3D model atmospheres calculations to determine the abundances of C and N, which decrease the values in Fig. 25 by 0.73 and 0.93 dex, respectively: the final values estimated from the CH lines are $[C/Fe]_{3D} = 2.09$ and $[N/Fe]_{3D} = 0.67$. This low $[N/Fe]$ is not interpreted by the AGB model shown in Fig. 25, which predicts $[N/Fe]_{\text{th}} = 1.11$. AGB models with $M_{\text{ini}}^{\text{AGB}} = 1.3$ or $1.5 M_{\odot}$ (cases ST/15 and ST/3) would predict an $[Na/Fe]$ lower or higher than observed, respectively. However, both N and Na are affected by large uncertainties in CEMP- s stars. The present study suggests that no efficient mixing had occurred in this star.

Further investigations are strongly desirable for this star. Indeed, serious problems are found in the theoretical interpretation with AGB models of both hs and r -process elements.

3.2.4 CS 31062-050 (Fig. 26)

The subgiant CS 31062-050 was examined by Aoki et al. (2002c,d, 2006, 2007) and Johnson & Bolte (2004), ($[Fe/H] = -2.42$; $T_{\text{eff}} = 5600$ K; $\log g = 3.0$). The occurrence of the FDU is uncertain for this star. Many elements have been observed, among them Os and Ir lines were detected by Aoki et al. (2006) for the first time in CEMP- s stars. Moreover, Aoki et al. (2003) and Tsangarides (2005) found radial velocity variations, confirming the binary scenario. Ba is higher than the other hs elements, even if the result of Johnson & Bolte (2004) is reduced by 0.2 dex according to Aoki et al. (2006), who used two weaker lines, which are less sensitive to hyperfine splitting. CS 31062-050 has been discussed in detail in the review by Käppeler et al. (2011). The low $[Na/Fe]$ (which accounts for NLTE corrections) agrees with a $M_{\text{ini}}^{\text{AGB}} = 1.3 M_{\odot}$ model with $dil = 0.2$ dex (Fig. 26), according to a star before the FDU and in

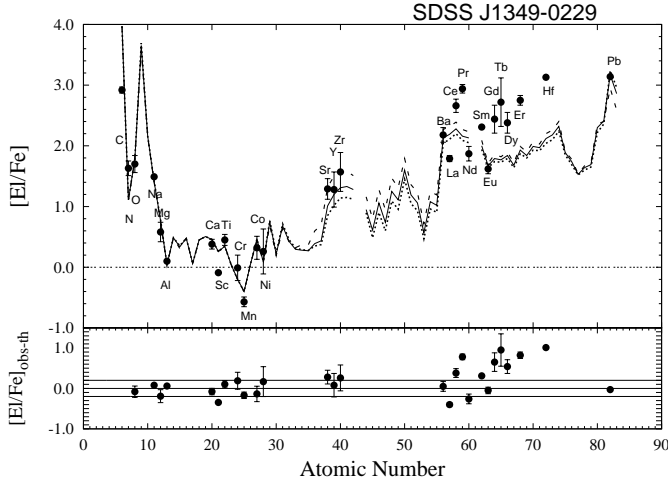


Figure 25. Spectroscopic $[El/Fe]$ abundances of the main-sequence star SDSS J1349-0229 ($[Fe/H] = -3.0$; $T_{\text{eff}} = 6200$ K; $\log g = 4.0$) compared with AGB model of $M_{\text{ini}}^{\text{AGB}} = 1.35 M_{\odot}$ (pulse 6th; see Sections 2.1.1 and 3.1.1), cases ST/12 (dotted line), ST/15 (solid line), ST/24 (dashed line), and no dilution. Observations are from Behara et al. (2010), who found $[hs/ls] = 0.57$ and $[Pb/hs] = 1.09$. See text for discussion about the spread shown by elements from Ba to Hf. $[C/Fe]$ and $[N/Fe]$ derived by CH and NH bands are displayed. 3D model atmospheres calculations reduce the observed $[C/Fe]$ and $[N/Fe]$ by 0.73 and 0.93 dex, respectively (see text). An initial r -process enrichment of $[r/Fe]_{\text{ini}} = 1.5$ is adopted.

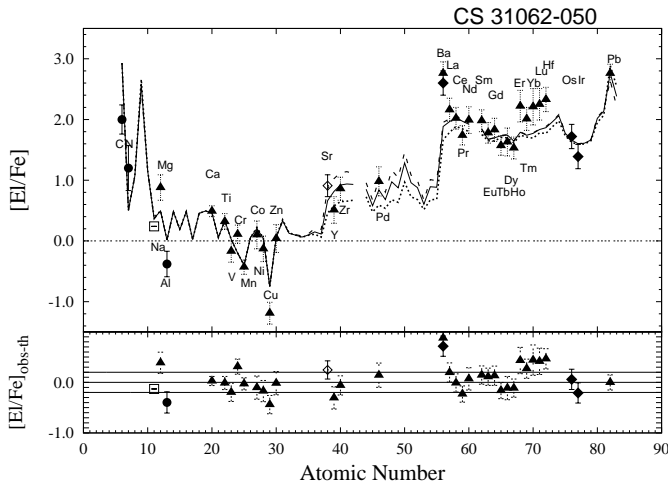


Figure 26. Spectroscopic $[El/Fe]$ abundances of the subgiant CS 31062-050 ($[Fe/H] = -2.42$; $T_{\text{eff}} = 5600$ K; $\log g = 3.0$, uncertain FDU) compared with AGB models of $M_{\text{ini}}^{\text{AGB}} = 1.3 M_{\odot}$, cases ST/8 (dotted line), ST/12 (solid line), ST/15 (dashed line), and $dil = 0.2$ dex. Observations are from Aoki et al. (2002c) (filled circles), Aoki et al. (2002d) (empty diamond), Aoki et al. (2006) (filled diamonds), Aoki et al. (2007) (empty square), Johnson & Bolte (2004) (filled triangles). This star shows $[hs/ls] = 1.40$ and $[Pb/hs] = 0.79$. The low $[Na/Fe]$ observed agrees with a star having not suffered the FDU episode. An initial r -process enhancement $[r/Fe]_{\text{ini}} = 1.6$ is adopted. In order to interpret the low $[Pd/Fe]$ observed, we adopt an initial r -process enhancement $[light-r/Fe]_{\text{ini}} = 0.5$ for the elements from Mo to Cs (see text).

agreement with moderate mixing during the main-sequence phase. This solution predicts a $[Mg/Fe]$ about 0.4 dex lower than observed. AGB models with $M_{\text{ini}}^{\text{AGB}} = 1.5$ and $2 M_{\odot}$ (case ST/3 and $dil = 1.1$ dex) provide similar solutions for the s -process distribution ($[hs/ls] = 1.40$; $[Pb/hs] = 0.79$), but the predicted $[Na/Fe]$ is about 1 dex higher than observed. Despite only one line was detected for Na, which is affected by a high uncertainty because of the severe contamination from interstellar Na absorption, Aoki et al. (2007) excluded $[Na/Fe]$ observations higher than 0.8 dex. Os and Ir, whose r -process fractions in the solar system material are 88% and 98%, respectively (see Paper II), are an important confirmation of the r -process enhancement. The initial r -process enrichment $[r/Fe]_{\text{ini}} = 1.6$ accounts for the observed low $[Ir/Fe]$ with correspondingly lower estimates for $[Er, Tm, Yb, Lu/Fe]$. The observed $[Hf/Fe]$ is higher than our theoretical prediction. We recall that Hf is mainly produced by the s -process (about 60% of solar Hf, Paper II). Therefore, larger initial r -process enhancements would not affect the $[Hf/Fe]$ prediction. This is the only star among CEMP- s and CEMP- s/r with a measurement among the light- r -elements from Mo to Cs: $[Pd/Fe] = 0.98$ (Johnson & Bolte 2004). About 50% of solar Pd is produced by the s -process (see Paper II, Table 5), while 50% of solar Pd is ascribed to the r -process. An $[r/Fe]_{\text{ini}} = 1.6$ would provide $[Pd/Fe]_{\text{th}} = 1.4$, about 0.4 dex higher than observed. Lower initial light- r -enhancements are assumed in order to interpret Pd, $[light-r/Fe]_{\text{ini}} = 0.5 - 1.0$, corresponding to $[Pd/Fe]_{\text{th}} = 0.8 - 1.0$, respectively. In Fig. 26, a $[light-r/Fe]_{\text{ini}} = 0.5$ is shown for elements from Mo to Cs. The exact site of nucleosynthesis of the r -process remains still unknown and a possible explanation of this difference comes from the hypothesis of a multiplicity of the r -process contributions (see Paper II, Section 3; Travaglio et al. 2004, Qian & Wasserburg 2008, Sneden et al. 2008).

Cu and Al are not produced in AGB stars, as confirmed by the observations. In particular, the negative $[Cu/Fe]$ value is consistent with the observations of unevolved halo stars in the same range of metallicity (see Section 1).

3.2.5 CS 22948-27 (\equiv HE 2134-3940), (Fig. 27)

Barbuy et al. (1997) and Hill et al. (2000), analysed the spectrum of this cool giant, which is heavily contaminated by CH, CN, and C_2 molecular bands. Recently, Barbuy et al. (2005) reviewed this star using high-resolution spectra that permit the detection of lead. Na and Al lines are sensitive to NLTE effects, which decreases the abundance of Na by 0.5 dex and increases the abundance of Al by 0.65 dex (Barbuy et al. 2005). Aoki et al. (2007) confirmed the results by Barbuy et al. (2005), providing updated values for Na and Mg and adopting a slightly higher effective temperature ($T_{\text{eff}} = 5000$ K instead of $T_{\text{eff}} = 4800$ K; $\log g = 1.8$). Strong molecular absorption lines remain the main characteristics of this very cool star. Despite that, the $[El/Fe]$ ratios provided by the different authors agree within the quoted uncertainties; the only exceptions are the metallicity ($[Fe/H] = -2.47$ by Barbuy et al. 2005; $[Fe/H] = -2.21$ by Aoki et al. 2007) and C and N, explained by the different effective temperatures adopted.

Theoretical interpretations of the spectroscopic abundances ($[hs/ls] = 0.93$; $[Pb/hs] = 0.56$) are shown in Fig. 27. A

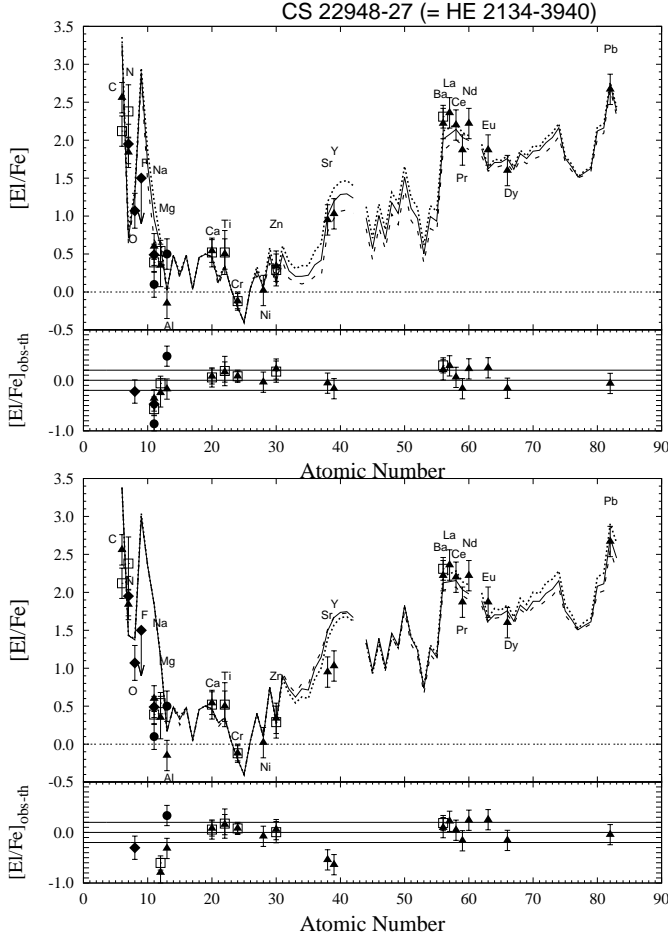


Figure 27. Spectroscopic $[El/Fe]$ abundances of the giant CS 22948-27 ($[Fe/H] = -2.47$; $T_{\text{eff}} = 4800$ K; $\log g = 1.8$, Barbuy et al. 2005; $[Fe/H] = -2.21$; $T_{\text{eff}} = 5000$ K; $\log g = 1.9$; Aoki et al. 2007) compared with AGB models of two initial masses: $M_{\text{ini}}^{\text{AGB}} \sim 1.35 M_{\odot}$, ST/15, $dil = 0.4$ dex and three thermal pulses, 6, 7, 8, see Sections 2.1.1 and 3.1.1 (dashed, solid and dotted lines, respectively; *top panel*); $M_{\text{ini}}^{\text{AGB}} = 1.5 M_{\odot}$, cases ST/6 (dotted line), ST/9 (solid line), ST/12 (dashed line), and $dil = 0.8$ dex (*bottom panel*). Observations are from Barbuy et al. (2005) (filled triangles; filled circles), Aoki et al. (2007) (empty squares), Lucatello et al. (2011) (filled diamonds). Na measured by Barbuy et al. (2007) takes account of NLTE corrections, while values with and without NLTE are shown for the Na measured by Barbuy et al. (2005) (filled circles and triangles, respectively). This star has $[hs/ls] = 0.93$; $[Pb/hs] = 0.56$. The differences $[El/Fe]_{\text{obs-th}}$ displayed in the lower panels refer to the AGB models represented by solid lines. An initial r -process enrichment of $[r/Fe]_{\text{ini}} = 1.5$ is adopted.

large dilution would be required by a giant having suffered the FDU. Instead, the solutions that better fit to the low observed $[Na/Fe]$ and $[Sr, Y/Fe]$ ratios contrast with this hypothesis: we displayed AGB models of $M_{\text{ini}}^{\text{AGB}} \sim 1.35 M_{\odot}$ (pulse 7th), case ST/15 and $dil = 0.4$ dex (*top panel*). AGB models of $M_{\text{ini}}^{\text{AGB}} = 1.5 M_{\odot}$, cases ST/6, ST/9, ST/12 and $dil = 0.8$ dex (see *bottom panel*), would predict $[Na/Fe]$ and $[ls/Fe] \sim 0.5$ dex higher than observed. Similar results are obtained by $M_{\text{ini}}^{\text{AGB}} = 2 M_{\odot}$ models. AGB models predict large $[F/Fe]$ abundances, incompatible with the upper limit detected by Lucatello et al. (2011) (see Paper I; Sec-

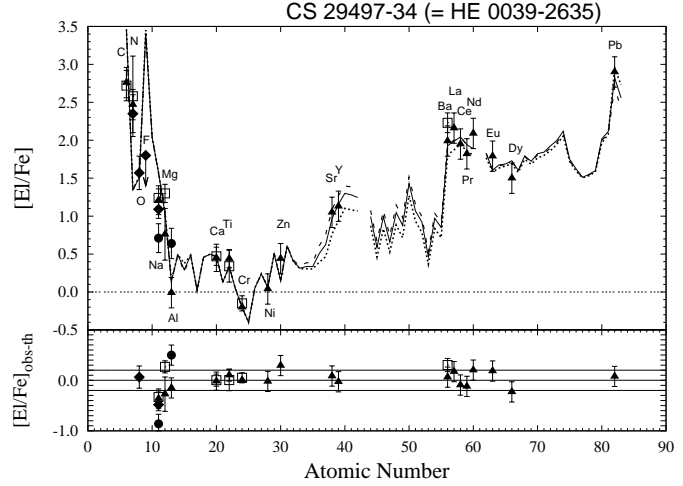


Figure 28. Spectroscopic $[El/Fe]$ abundances of the giant CS 29497-34 ($[Fe/H] = -2.90$; $T_{\text{eff}} = 4800$ K; $\log g = 1.8$) compared with AGB models of $M_{\text{ini}}^{\text{AGB}} = 2 M_{\odot}$, cases ST/6 (dotted line), ST/9 (solid line), ST/12 (dashed line), and $dil = 1.0$ dex. Observations are from Barbuy et al. (2005) (filled triangles; filled circles), Aoki et al. (2007) (empty squares), Lucatello et al. (2011) (filled diamonds). This star shows $[hs/ls]_{\text{obs}} = 0.81$ and $[Pb/hs]_{\text{obs}} = 0.93$. An initial r -process enrichment of $[r/Fe]_{\text{ini}} = 1.5$ is adopted.

tion 2.2.4). Further measurements are desirable.

Preston & Sneden (2001)⁸ first discovered a radial velocity variation for CS 22948-27 with $P = 505$ d. Barbuy et al. (2005) determine a period of 426 days. Aoki et al. (2007) confirm this last value, but further investigations are desirable.

3.2.6 CS 29497-34 (\equiv HE 0039-2635), (Fig. 28)

CS 29497-34 ($[Fe/H] = -2.90$) is a long period binary, with $P = 4130$ days (Preston & Sneden 2001). This very cool giant ($T_{\text{eff}} = 4800$ K and $\log g = 1.8$), affected by strong C_2 and CH molecular bands, was analysed by Barbuy et al. (1997), Hill et al. (2000), Lucatello (2004) and Barbuy et al. (2005). Aoki et al. (2007) adopted a slightly higher effective temperature ($T_{\text{eff}} = 4900$ K), confirming the results by Barbuy et al. (2005), and provided updated values for Na and Mg.

In Fig. 28 we show theoretical interpretations with $M_{\text{ini}}^{\text{AGB}} = 2 M_{\odot}$ (ST/6, ST/9 and ST/12) and $dil = 1$ dex, in agreement with the observed $[hs/ls] = 0.81$ and $[Pb/hs] = 0.93$. The abundances found by the two studies are in agreement within the uncertainties with the exception of Na and Mg, for which Aoki et al. (2007) found 0.4 and 0.5 dex higher values than Barbuy et al. (2005). Aoki et al. (2007) exclude that these discrepancies are due to the small differences in the atmospheric parameters adopted, and highlight the uncertainty of the Na abundance, for which only two very strong lines are available. However, an excess in $[Na/Fe]$ is confirmed by both authors. The enhanced Na observed ($[Na/Fe] = 1.37$, Aoki et al. 2007) is about 0.2 dex lower than that predicted by the AGB model shown in Fig. 28.

⁸ The first measurement by Hill et al. (2000) could not find any clear radial velocity variation due to the low resolution spectra.

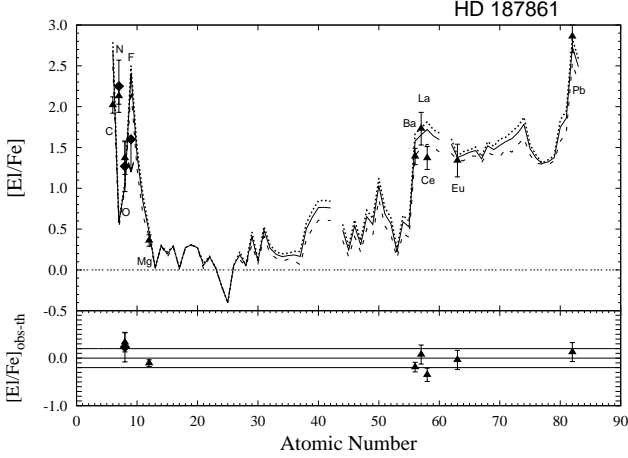


Figure 29. Spectroscopic $[El/Fe]$ abundances of the giant HD 187861 ($[Fe/H] = -2.36$; $T_{\text{eff}} = 4600$ K; $\log g = 1.7$) compared with AGB models of $M_{\text{ini}}^{\text{AGB}} = 1.4 M_{\odot}$, ST/5, and $dil = 0.8$ (dotted line), 0.9 (solid line) and 1.1 dex (dashed line). Observations are from Masseron et al. (2010) (filled triangles) and (Lucatello et al. 2011) (filled diamonds). This giant shows $[Pb/hs] = 1.28$, while no ls elements have been detected by (Masseron et al. 2010) (see text). An initial r -process enrichment of $[r/Fe]_{\text{ini}} = 1.3$ is adopted (see text).

AGB models of $M_{\text{ini}}^{\text{AGB}} = 1.5 M_{\odot}$ (case ST/5 and $dil = 1.0$ dex) overestimate the observed $[Na/Fe]$ by about 0.6 dex. Both Na and Al lines are sensitive to the NLTE effects, which decrease and increase the observations by 0.4 – 0.5 dex and 0.65 dex, respectively (Barbuy et al. 2005; Aoki et al. 2007). Solutions with AGB models of low initial mass and negligible dilution are excluded for this giant having suffered the FDU. As for CS 22948–27 (see also Paper I; Section 2.2.4), AGB models predict a $[F/Fe]$ lower than the value detected by Lucatello et al. (2011). Further measurement are desirable.

3.2.7 HD 187861 (Fig. 29)

This giant was firstly studied by Vanture (1992b). Subsequently, high-resolution spectra were analysed by Van Eck et al. (2003) and Masseron et al. (2010). The abundances by Van Eck et al. (2003) are uncertain because only few lines veiled by molecular bands are available. Masseron et al. (2010) estimate $[Fe/H] = -2.36$, $T_{\text{eff}} = 4600$ K and $\log g = 1.7$. Solutions with $M_{\text{ini}}^{\text{AGB}} = 1.4 M_{\odot}$ models (case ST/5 and $dil \sim 1$ dex) are shown in Fig. 29, compared with spectroscopic observations by Masseron et al. (2010) ($[Pb/hs] = 1.28$). Recently (Lucatello et al. 2011), detected N, O and an upper limit for F (see Section 2.2.4). $[ls/Fe]_{\text{th}} \sim 0.7$ dex is predicted by this model. Van Eck et al. (2003) detected $[Zr/Fe] = 1.3$ by adopting an effective temperature 700 K higher than Masseron et al. (2010), which may explain a difference of about 0.4 dex in $[El/Fe]$. An $[r/Fe]_{\text{ini}} = 1.3$ dex is adopted in order to interpret the observed $[La/Eu]$. The average of $[Ba, La, Ce/Eu]$ suggests even larger initial r -process enhancement. Theoretical interpretations with $M_{\text{ini}}^{\text{AGB}} < 1.4 M_{\odot}$ and negligible dilution would not agree with a giant having suffered the FDU, while $M_{\text{ini}}^{\text{AGB}} = 1.5$ and $2 M_{\odot}$ would overestimated the observed $[Mg/Fe]$. The observations by Masseron et al. (2010) shown in Fig. 29

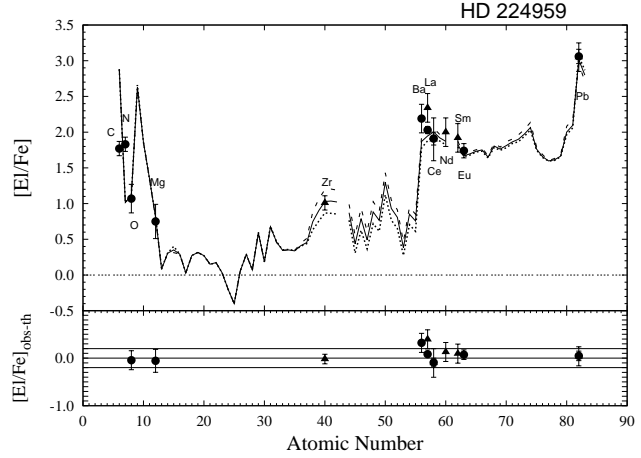


Figure 30. Spectroscopic $[El/Fe]$ abundances of the giant HD 224959 ($[Fe/H] = -2.06$; $T_{\text{eff}} = 4900$ K; $\log g = 2.0$) compared with AGB models of $M_{\text{ini}}^{\text{AGB}} = 1.5 M_{\odot}$, cases ST/2 (dotted line), ST/2.5 (solid line), ST/3 (dashed line), and $dil \sim 1.0$ dex. Observations are from Van Eck et al. (2003) (filled triangles) and Masseron et al. (2010) (filled circles). This star shows $[hs/ls] = 1.12$ and $[Pb/hs] = 1.03$. An $[r/Fe]_{\text{ini}} = 1.6$ dex is adopted.

will be discussed by the authors in Masseron et al., in preparation.

3.2.8 HD 224959 (Fig. 30)

Van Eck et al. (2003) analysed this giant ($[Fe/H] = -2.2$; $T_{\text{eff}} = 5200$ K; $\log g = 1.9$), providing spectroscopic observations for Zr, La, Ce, Nd, Sm and Pb ($[hs/ls] = 1.12$ and $[Pb/hs] = 1.03$). The recent analysis by Masseron et al. (2010) ($[Fe/H] = -2.06$, $T_{\text{eff}} = 4900$ K and $\log g = 2.0$) confirms the previous results and classifies this star as a CEMP- s/r , with $[La/Eu] \sim 0.3$. An initial r -process enhancement of 1.6 dex is adopted. In Fig. 30, we show theoretical interpretations with AGB models of initial mass $1.5 M_{\odot}$ and $dil = 1$ dex (case \sim ST/3), compared with both spectroscopic studies (Van Eck et al. 2003; Masseron et al. 2010). Analogous interpretations are obtained by AGB models of initial mass $2 M_{\odot}$ (ST/3 and $dil = 1$ dex). Solutions with initial masses $M < 1.5 M_{\odot}$ and lower dilutions are discarded, because they would be in contrast with a giant after the FDU.

3.2.9 LP 625–44 (Fig. 31)

Aoki et al. (2002a) carried out a detailed analysis of this giant ($[Fe/H] = -2.7$; $T_{\text{eff}} = 5500$ K; $\log g = 2.5$) with the High Dispersion Spectrograph (HDS) of the Subaru Telescope, subsequently improved by the detection of upper limits for two r -process elements, Os and Ir (Aoki et al. 2006). The binarity was confirmed by radial velocity monitoring (Norris et al. 1997; Aoki et al. 2000), strongly supporting the mass transfer scenario. The period has not been estimated yet, and further measurements of the radial velocity are required to infer orbital parameters for this star. Very enhanced Na and Mg are detected: $[Na/Fe] = 1.75$ and $[Mg/Fe] = 1.12$. The Na abundance was based on five weak lines as well as the strong D lines. The observed $[Na/Fe]$ and $[Mg/Fe]$ are underestimated by AGB models with initial mass $M_{\text{ini}}^{\text{AGB}} \leq 1.35 M_{\odot}$ and case ST/30 (see Bisterzo et al.

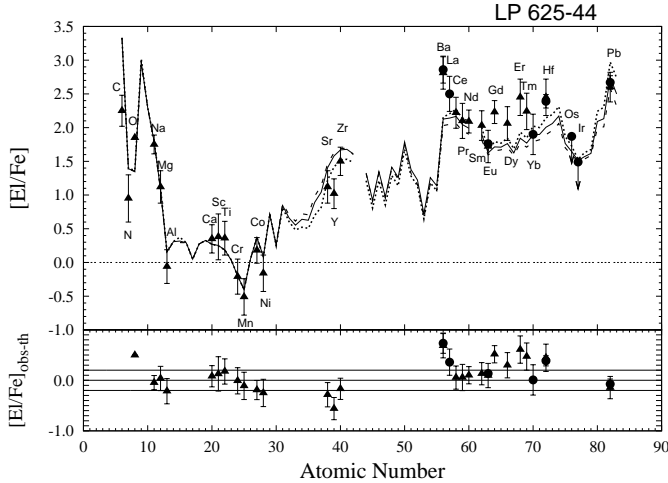


Figure 31. Spectroscopic $[El/Fe]$ abundances of the giant LP 625-44 ($[Fe/H] = -2.7$; $T_{\text{eff}} = 5500$ K; $\log g = 2.5$) compared with AGB models of initial mass $1.5 M_{\odot}$, cases ST/5 (dotted line), ST/8 (solid line), ST/11 (dashed line), and $dil = 0.8$ dex. Observations are from Aoki et al. (2002a) (filled triangles) and Aoki et al. (2006) (filled circles). This star shows $[hs/ls]_{\text{obs}} = 0.93$ and $[Pb/hs]_{\text{obs}} = 0.46$. Note that the $[hs/ls]_{\text{th}}$ is lower than observed, because $[Y/Fe]$ and $[La/Fe]$ are lower and higher than theoretical predictions (see text). An initial r -process enrichment of $[r/Fe]_{\text{ini}} = 1.5$ is adopted.

2009, Fig. 5, bottom panel). Moreover, these models require negligible dilution, in contrast with a giant after the FDU. Fig. 31 shows theoretical interpretations with $M_{\text{ini}}^{\text{AGB}} = 1.5 M_{\odot}$ (cases ST/5, ST/8, ST/11) and $dil = 0.8$ dex, in agreement with the observed $[Na/Fe]$ and $[Mg/Fe]$. The observed $[Y/Fe]$ is about 0.4 dex lower than AGB predictions, while $[Ba/Fe]$ is 0.6 dex higher. Note that the error bar shown for La accounts for uncertainties due to fitting of synthetic spectra and atmospheric parameters. The $[Pb/hs]$ ratio is low in this star (~ 0.46 dex), and low ^{13}C -pockets are needed in order to interpret the s -process distribution. A similar solution is obtained with $M_{\text{ini}}^{\text{AGB}} = 2 M_{\odot}$, but the observed $[Na/Fe]$ is slightly higher than AGB prediction. To match the r -process abundances, we adopt an $[r/Fe]_{\text{ini}} = 1.5$ dex. This choice was assessed on the observed $[Eu/Fe]$ (Aoki et al. 2002a, 2006), as well as on the recent Yb detection and on the upper limit of Ir (Aoki et al. 2006). The observed r -process elements Gd, Er and Tm (7, 6 and 3 lines) are underestimated with the initial r -enhancement assumed in Fig. 31. We underline that four among the neutron capture elements (Y, Ba, Gd, Er) are not interpreted by AGB models. The interpretation of this star remains problematic and further investigations both on spectroscopic and on theoretical point of view are desirable.

3.2.10 CS 22183-015 (\equiv HE 0058-0244); (Fig. 32)

CS 22183-015 has been studied by Johnson & Bolte (2002), Lucatello (2004), Tsangarides (2005), Cohen et al. (2006) and Aoki et al. (2007). Tsangarides (2005) performed radial velocity measurements, but could not confirm the binarity of this star due to the low velocity amplitude. Discrepancies between metallicity and atmospheric parameters are measured by different authors: Johnson & Bolte (2002) report $[Fe/H]$

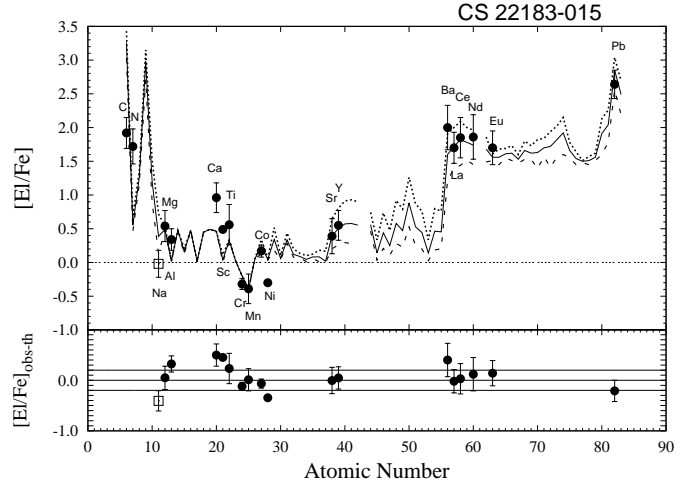


Figure 32. CS 22183-015 has uncertain atmospheric parameters (Cohen et al. 2006; Aoki et al. 2007 and Johnson & Bolte 2002; Tsangarides 2005; see text). We show here spectroscopic $[El/Fe]$ abundances by Cohen et al. (2006) (filled circles) and Aoki et al. (2007) (empty square), ($[Fe/H] = -2.75$; $T_{\text{eff}} = 5620$ K and $\log g = 3.4$, uncertain FDU; $[hs/ls] = 1.21$; $[Pb/hs] = 1.03$), compared with AGB models of $M_{\text{ini}}^{\text{AGB}} \sim 1.3 M_{\odot}$, case ST/12, no dilution. Three thermal pulses are shown: pulses 3 (dashed line), 4 (solid line), 5 (dotted line), (see Sections 2.1.1 and 3.1.1). An initial r -process enrichment of $[r/Fe]_{\text{ini}} = 1.5$ is adopted.

$= -3.12$, $T_{\text{eff}} = 5200$ K and $\log g = 2.5$, while Cohen et al. (2006) give $[Fe/H] = -2.75$, $T_{\text{eff}} = 5620$ K and $\log g = 3.4$. More recently, Lai et al. (2004, 2007) analysed CS 22183-015 with $R \sim 7000$, and found $[Fe/H] = -3.17$, $T_{\text{eff}} = 5178$ K, $\log g = 2.69$, similarly to Johnson & Bolte (2002). Aoki et al. (2007) adopted the atmospheric parameters by Cohen et al. (2006) and determined the Na abundance accounting for NLTE corrections ($\Delta[NLTE] = -0.5$ dex). The strong differences in the atmospheric parameters indicate that the evolutionary phase of this star is uncertain: following Johnson & Bolte (2002) and Lai et al. (2007) it is a giant, while for Cohen et al. (2006) it lies still on the early subgiant phase, where the FDU may not have occurred yet. In Fig. 32, we present possible solutions by adopting the spectroscopic observations by Cohen et al. (2006) and Aoki et al. (2007). The low $[Na/Fe]$ observed together with a high $[hs/Fe]$ are interpreted by AGB models of $M_{\text{ini}}^{\text{AGB}} \sim 1.3 M_{\odot}$ (case ST/12, three TDUs, 3, 4, 5) and $dil = 0$ dex, in agreement with a subgiant having not suffered the FDU episode. An initial r -process enhancement of $[r/Fe]_{\text{ini}} = 1.5$ is adopted. Theoretical interpretations with AGB models of higher initial mass and dilution ($M = 1.4$ to $2 M_{\odot}$; $dil = 0.6 - 1.1$ dex; cases ST/12 – ST/2) would predict a too high $[Na/Fe]$ and $[Sr, Y/Fe]$.

3.3 CEMP-sII/ r I with $[r/Fe]_{\text{ini}} \sim 1.0$

This Section includes four stars with high s -process enhancement ($[hs/Fe] \sim 2$) together with an initial r -enhancement $[r/Fe]_{\text{ini}} \sim 1.0$. Three stars lie on the main-sequence/turnoff phase, HE 0143-0441 by Cohen et al. (2006), SDSS J0912+0216 by Behara et al. (2010), and CS 22887-048, studied by Tsangarides (2005) (PhD Thesis). One star is a giant, HD 209621 by Goswami & Aoki (2010).

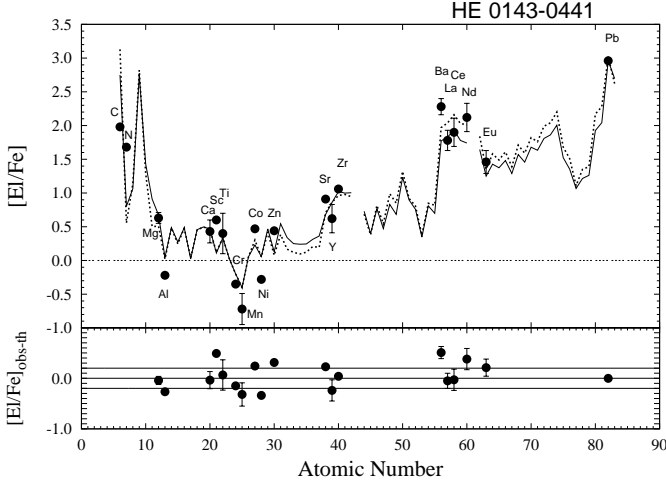


Figure 33. Spectroscopic $[El/Fe]$ abundances of the main-sequence/turnoff star HE 0143-0441 ($[Fe/H] = -2.31$; $T_{\text{eff}} = 6240$ K; $\log g = 3.7$) compared with two AGB models: $M_{\text{ini}}^{\text{AGB}} = 1.3 M_{\odot}$, case ST/9 and $dil = 0.0$ dex (dotted line); $M_{\text{ini}}^{\text{AGB}} = 2 M_{\odot}$, case ST/5 and $dil = 1.0$ dex (solid line). Observations are from Cohen et al. (2006). The observed s -process indicators are $[hs/lr] = 1.12$ and $[Pb/hs] = 1.25$. A spread is observed among the hs elements (see text). The differences $[El/Fe]_{\text{obs-th}}$ displayed in the lower panel refer to the $M_{\text{ini}}^{\text{AGB}} = 2 M_{\odot}$ model (solid line). We adopt an $[r/Fe]_{\text{ini}} = 1.0$.

3.3.1 HE 0143-0441 (Fig. 33)

This is a main-sequence/turnoff star ($[Fe/H] = -2.31$; $T_{\text{eff}} = 6240$ K; $\log g = 3.7$), analysed by Cohen et al. (2004, 2006). Only the most recent data by Cohen et al. (2006) are considered here. We present possible theoretical interpretations with AGB models of different initial masses. Two solutions are shown in Fig. 33: the dotted line corresponds to an AGB model of $M_{\text{ini}}^{\text{AGB}} = 1.3 M_{\odot}$ (case ST/9 and no dilution), the solid line represents an AGB model of $M_{\text{ini}}^{\text{AGB}} = 2 M_{\odot}$ (case ST/5 and $dil = 1$ dex). Both models interpret the observed s -process indicators $[hs/lr] = 1.12$ and $[Pb/hs] = 1.25$. A spread is observed among the hs elements ($[Nd/La] \sim 0.4$ dex; 4 lines are detected for La, 3 lines for Nd as for Ba and Ce), while $[Y/Fe]$ is about 0.2 lower than AGB predictions. Similar solutions may be obtained with AGB models of initial mass $M = 1.5 M_{\odot}$ and $dil = 0.6$ dex. A Na measurement would help to discriminate the AGB initial mass ($[Na/Fe]_{\text{th}} = 0.5$ is predicted by $M_{\text{ini}}^{\text{AGB}} = 1.3 M_{\odot}$, pulse 5 and negligible dilution; $[Na/Fe]_{\text{th}} = 1.1$ with $M_{\text{ini}}^{\text{AGB}} = 1.5 M_{\odot}$, $dil \sim 1$ dex). This would also provide information about the efficiency of the mixing during the main-sequence phase. An initial r -process enrichment $[r/Fe]_{\text{ini}} = 1$ is adopted.

3.3.2 SDSS J0912+0216 (Fig. 34)

This main-sequence star was studied by Behara et al. (2010) with $R = 30000$ ($[Fe/H] = -2.5$; $T_{\text{eff}} = 6500$ K; $\log g = 4.5$ dex). The neutron capture elements are highly enhanced. Large differences are detected among the hs peak elements (e.g., $[Ce/La] \sim 1$) and among the r -elements (e.g., $[Gd/Eu] \sim 1.5$), similarly to the star SDSS J1349-0229 (Section 3.2.3). We assess the initial r -enhancement by the observed $[Eu/Fe]$, while La is chosen as the most representative among the hs peak. In Fig. 34, SDSS J0912+0216 is inter-

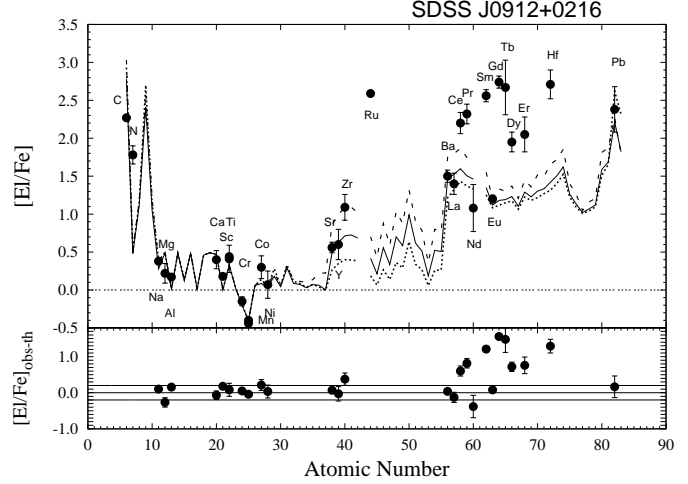


Figure 34. Spectroscopic $[El/Fe]$ abundances of the main-sequence star SDSS J0912+0216 ($[Fe/H] = -2.5$; $T_{\text{eff}} = 6500$ K; $\log g = 4.5$) compared with AGB models of $M_{\text{ini}}^{\text{AGB}} = 1.3 M_{\odot}$, cases ST/9 (dotted line), ST/18 (solid line), ST/24 (dashed line), $dil \sim 0.6$ dex. Observations are from Behara et al. (2010). For a discussion of the differences between observations and predictions for Zr, Ru and elements from Ba to Hf see text. On average $[hs/lr]_{\text{obs}} = 0.84$ and $[Pb/hs]_{\text{obs}} = 0.64$. $[C/Fe]$ and $[N/Fe]$ from CH bands are displayed. 3D model atmospheres calculations reduce these values to 1.67 and 1.07 dex, respectively (Behara et al. 2010). An initial r -process enrichment of $[r/Fe]_{\text{ini}} = 1.0$ is adopted, in agreement with the observed $[Eu/Fe]$ (see text).

preted with a $M_{\text{ini}}^{\text{AGB}} = 1.3 M_{\odot}$ model (case ST/18 and $dil = 0.6$ dex). This star lies on the main-sequence, and the dilution provided by this model suggests that mixing has been efficient during this phase. However, the large spread affecting the hs elements leave this conclusion very uncertain. Solutions with negligible dilutions may be obtained by decreasing the number of TDUs (e.g., $M_{\text{ini}}^{\text{AGB}} = 1.2 M_{\odot}$, pulse number 3), but the predicted $[Na/Fe]$ would be 0.3 dex lower than that observed. The detected $[La/Eu]$ ratio needs an initial r -process enhancement of $[r/Fe]_{\text{ini}} = 1$ dex. However, we are not able to interpret the discrepancy observed among Eu and the other r -elements. Similarly, Ru is highly enhanced, at the same level of Gd and Tb. The low $[Na/Fe]$ would exclude models with $M_{\text{ini}}^{\text{AGB}} \geq 1.5 M_{\odot}$. Note that by increasing the AGB initial mass and with a proper choice of the ^{13}C -pocket and dilution factor, we may find theoretical solutions for the high $[Ce, Pr/Fe]$ observed, but several observed elements ($[Na, Mg, Sr, Y, Ba, La, Nd, Eu/Fe]$) would be overestimated by models. Behara et al. (2010) provide 3D atmospheric model corrections for C and N, which decrease the observations shown in Fig. 34 by 0.5 and 0.67 dex, respectively.

Further investigations are strongly desirable for this star, especially in the light of the large discrepancies outlined both among hs and r -elements that can not be explained by AGB models.

3.3.3 HD 209621 (\equiv HIP 108953, BD +205071), (Fig. 35)

This giant with $[\text{Fe}/\text{H}] \sim -1.93$ ($T_{\text{eff}} = 4500$ K and $\log g = 2.0$) has been recently observed by Goswami & Aoki (2010). HD 209621 was one of the CH stars analysed by Vanture (1992b) with lower resolution spectra ($R = 20\,000$ instead of 50 000 by Goswami & Aoki 2010). The metallicity of the star was estimated as $[\text{Fe}/\text{H}] = -0.9$, significantly higher than that derived by Goswami & Aoki (2010) ($[\text{Fe}/\text{H}] = -1.93$). HD 209621 was found to be a long-period binary by McClure & Woodworth (1990), with $P \sim 400$ d. This supports the hypothesis of mass transfer of s -rich material from an AGB companion. The spectra of this star are dominated by molecular absorption lines of CH, CN and C_2 . Goswami & Aoki (2010) carefully considered only the unblended lines for the determination of the spectroscopic abundances. They found a large spread among the observed ls element (e.g., $[\text{Zr}/\text{Y}] = 1.4$). This disagrees with theoretical AGB models, which predict $[\text{Y}/\text{Fe}] \sim [\text{Zr}/\text{Fe}]$. However, we recall that only one reliable line has been adopted for the analysis of Sr, Y e Zr in this cool giant. In Fig. 35 we select to fit Zr among the ls elements, according with a low ^{13}C -pocket (ST/15), which interpret both $[\text{hs}/\text{Zr}]$ and $[\text{Pb}/\text{hs}]$. $M_{\text{ini}}^{\text{AGB}} = 2 M_{\odot}$ models with a large dilution in agreement with a giant ($\text{dil} = 0.9$ dex) are shown. The low $[\text{Na}/\text{Fe}]$ is calculated with the resonance doublet Na I D lines at 5890 and 5896 Å with a LTE analysis. Lower AGB initial mass and lower dilutions are discarded because in contrast with a giant after the FDU (e.g., a model of $M_{\text{ini}}^{\text{AGB}} = 1.5 M_{\odot}$ and ST/15 would imply a $\text{dil} = 0.6$ dex). An $[\text{r}/\text{Fe}]^{\text{ini}} = 1$ is adopted to interpret the $[\text{hs}/\text{Eu}]$ ratio. The observed $[\text{Er}/\text{Fe}]$ is lower than theoretical predictions, but only one line is detected for this element. Note that W, similarly to Hf, is mostly an s -process element ($\sim 60\%$ of solar W is produced by the main- s process). Therefore, our theoretical prediction would not be largely affected by higher initial r -process enhancements. However, Goswami & Aoki (2010) explicitly mention a potential overestimation of the $[\text{W}/\text{Fe}]$ abundance owing to a possible blending.

Goswami & Aoki (2010) provided theoretical interpretations with a parametric model, based on the solar system s and r -process isotopic abundances (scaled to the metallicity of the star) of each isotope provided by Arlandini et al. (1999). This method does not account for the dominant contribution to Pb and Bi by the strong component at low metallicities. Indeed, in order to estimate the solar r -process percentage of Pb and Bi, we adopt a Galactic Chemical Evolution model, which accounts for the s -process contribution of all AGB masses and all metallicities (Travaglio et al. 2004, Paper II).

3.3.4 CS 22887-048 (Fig. 36)

CS 22887-048, with $[\text{Fe}/\text{H}] = -1.7$, was studied by Tsangarides (2005), PhD thesis. This star shows an effective temperature typical of main-sequence/turnoff stars ($T_{\text{eff}} = 6500$ K), while its surface gravity is rather low ($\log g = 3.35$). Johnson et al. (2007) included this star in a sample of metal-poor N-rich candidates. They estimated a metallicity 1 dex lower than Tsangarides (2005), ($[\text{Fe}/\text{H}] = -2.79$). Although the period remains unknown, Tsangarides (2005)

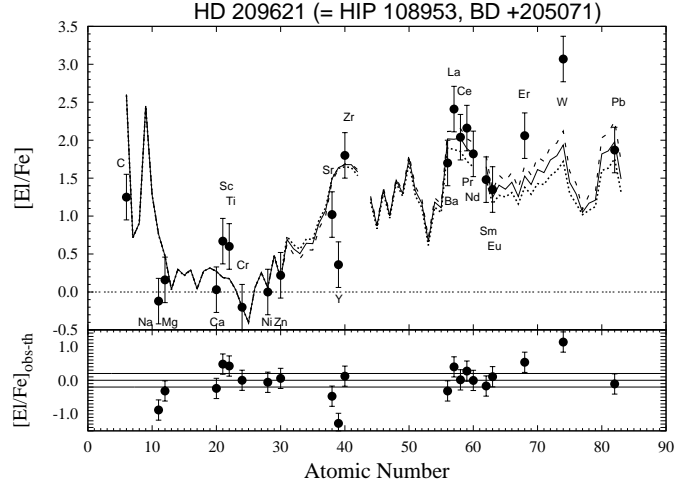


Figure 35. Spectroscopic $[\text{El}/\text{Fe}]$ abundances of the giant HD 209621 ($[\text{Fe}/\text{H}] = -1.93$; $T_{\text{eff}} = 4500$ K; $\log g = 2.0$) compared with AGB models of $M_{\text{ini}}^{\text{AGB}} = 2 M_{\odot}$, cases ST/12 (dashed line), ST/15 (solid line), ST/18 (dotted line). We adopt $\text{dil} = 0.9$ dex. Observations are from Goswami & Aoki (2010). A spread in the ls elements is observed, while $[\text{Pb}/\text{hs}] \sim 0$. For discussions about differences between observed and predicted Na, Y, Er and W see text. An initial r -process enrichment of $[\text{r}/\text{Fe}]^{\text{ini}} = 1.0$ is adopted.

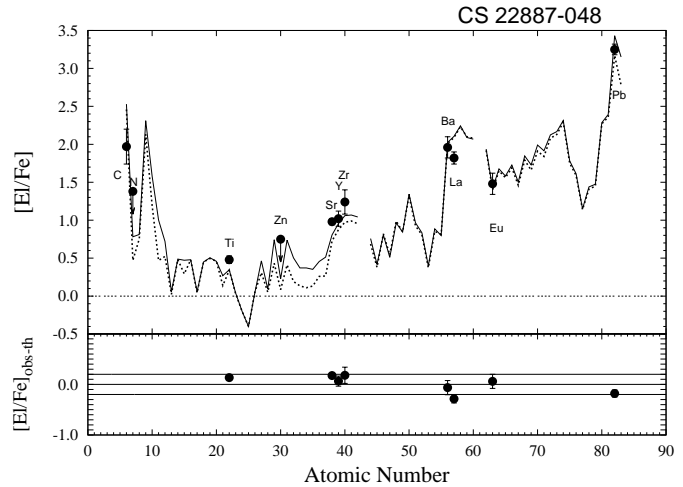


Figure 36. Spectroscopic $[\text{El}/\text{Fe}]$ abundances of the main-sequence/turnoff star CS 22887-048 ($[\text{Fe}/\text{H}] = -1.7$; $T_{\text{eff}} = 6500$ K; $\log g = 3.35$) compared with different AGB models: $M_{\text{ini}}^{\text{AGB}} = 1.4 M_{\odot}$, case ST/2 and no dilution (dotted line), or $M_{\text{ini}}^{\text{AGB}} = 1.5 M_{\odot}$, case ST $\times 1.2$ and $\text{dil} = 0.3$ dex (solid line). Observations are from Tsangarides (2005), who found $[\text{hs}/\text{ls}] = 0.80$ and $[\text{Pb}/\text{hs}] = 1.49$. The differences $[\text{El}/\text{Fe}]_{\text{obs-th}}$ displayed in the lower panel refer to the $M_{\text{ini}}^{\text{AGB}} = 1.5 M_{\odot}$ model. An initial r -process enrichment of $[\text{r}/\text{Fe}]^{\text{ini}} = 1.0$ is adopted.

confirms the binarity of this star, supporting the mass transfer scenario.

In Fig. 36, possible interpretations with AGB models are shown: $M_{\text{ini}}^{\text{AGB}} = 1.4 M_{\odot}$, case ST/2, and no dilution, and $M_{\text{ini}}^{\text{AGB}} = 1.5 M_{\odot}$, case ST $\times 1.2$ and $\text{dil} = 0.3$ dex. Note that this star needs the most efficient ^{13}C -pocket strength of all CEMP- s (and CEMP- s/r) sample. Both solutions sustain that moderate mixing had occurred in this star. An initial r -process enhancement $[\text{r}/\text{Fe}]^{\text{ini}} = 1.0$ is adopted in order to interpret a $[\text{Ba}/\text{Eu}]$ ratio of 0.5 dex. $[\text{La}/\text{Fe}]$ is ~ 0.3 dex

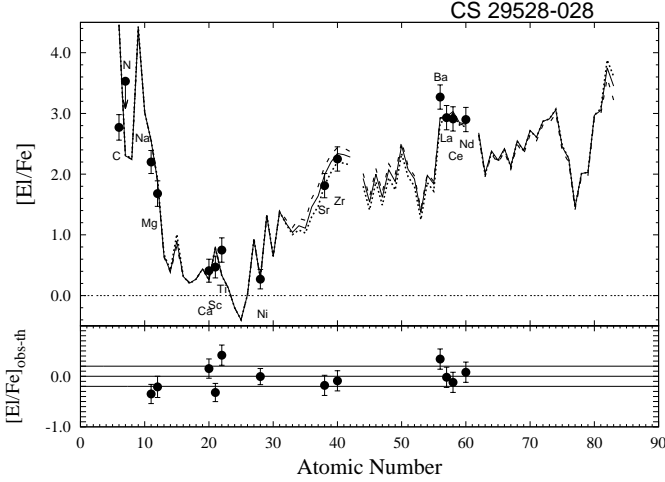


Figure 37. Spectroscopic $[El/Fe]$ abundances of the main-sequence star CS 29528-028 ($[Fe/H] = -2.86$; $T_{\text{eff}} = 6800$ K; $\log g = 4.0$) compared with AGB models of $M_{\text{ini}}^{\text{AGB}} = 2 M_{\odot}$, cases ST/8 (dotted line), ST/12 (solid line), ST/15 (dashed line), and no dilution. Observations are from Aoki et al. (2007), who detected $[hs/ls] = 0.62$. This model predicts $[Pb/Fe]_{\text{th}} \sim 3.8$. An $[r/Fe]_{\text{ini}} = 0.5$ is adopted.

lower than AGB models: a smaller $[hs/Fe]_{\text{th}}$ value would be obtained by a lower ^{13}C -pocket efficiency (e.g. the case ST/3 for $M_{\text{ini}}^{\text{AGB}} = 1.5 M_{\odot}$), with a significant decrease in lead ($[Pb/Fe]_{\text{th}} = 2.7$). Note that $[La/Eu] = 0.24$ would require a higher initial r -process enrichment. Further AGB model constraints may be obtained by detecting Na and additional hs elements.

4 CEMP-s STARS WITH NO Eu MEASUREMENT

In this Section, we analyse CEMP-sII and CEMP-sI stars with no Eu detection. These stars are interpreted by an initial r -process enrichment $[r/Fe]_{\text{ini}} = 0.5$, chosen as representative of the average of $[Eu/Fe]$ observed in halo field stars (see Section 1).

4.1 CEMP-sII with no Eu

Six stars show a high s -process enhancement and no Eu measurement: three stars are main-sequence/turnoff, CS 29528-028 by Aoki et al. (2007), HE 1430-1123 by Barklem et al. (2005), and SDSS 0126+06 by Aoki et al. (2008). Other three stars are giants, HD 201626 by Van Eck et al. (2003), HD 5223 by Goswami et al. (2006), and HE 0212-0557 by Cohen et al. (2006).

4.1.1 CS 29528-028 (Fig. 37)

CS 29528-028 is the hottest main-sequence star among the sample studied by Aoki et al. (2007), ($[Fe/H] = -2.86$; $T_{\text{eff}} = 6800$ K; $\log g = 4.0$). The authors detected several s -elements, Sr, Zr, Ba, La, Ce and Nd, showing a great s -enhancement, about 1 dex higher than the average of CEMP-s stars: $[ls/Fe] \sim 2$ and $[hs/Fe] \sim 3$. Moreover, this star exhibits high Na and Mg ($[Na/Fe] = 2.33$ and

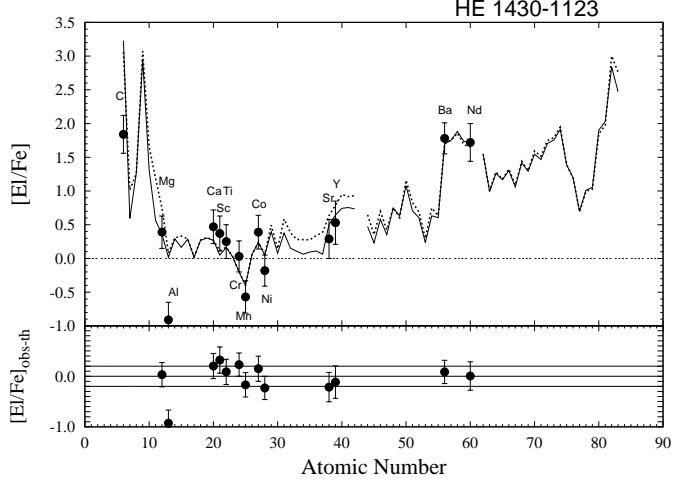


Figure 38. Spectroscopic $[El/Fe]$ abundances of the turnoff/subgiant HE 1430-1123 ($[Fe/H] = -2.71$; $T_{\text{eff}} = 5915$ K; $\log g = 3.75$, before the FDU) compared with AGB models of initial mass $1.3 M_{\odot}$ (ST/12 and $dil = 0.2$ dex; solid line) and $2 M_{\odot}$ (ST/5 and $dil = 1.0$ dex; dotted line). Observations are from Barklem et al. (2005), who found $[hs/ls] = 0.94$. An $[r/Fe]_{\text{ini}} = 0.5$ is adopted.

$[Mg/Fe] = 1.69$). No solutions are attained using AGB models of initial mass $M_{\text{ini}}^{\text{AGB}} \lesssim 1.4 M_{\odot}$, because the observed $[Na, Mg, ls, hs/Fe]$ would be too high. In Fig. 37, interpretations with $M_{\text{ini}}^{\text{AGB}} = 2 M_{\odot}$ are shown, (cases ST/8, ST/12, ST/15 and no dilution). This model predicts $[Pb/Fe]_{\text{th}} \sim 3.8$. AGB models of $M_{\text{ini}}^{\text{AGB}} = 1.5 M_{\odot}$ are excluded, because they overestimate the observed Na and Mg ($[Na/Fe]_{\text{th}} = 3.00$; $[Mg/Fe]_{\text{th}} = 2.25$, case ST/5 and no dilution). The lack of dilution suggests that no efficient mixing had occurred. This star shows the highest $[ls/Fe]$ and $[hs/Fe]$ known. Observations of Eu and Pb would be very useful. A similar behaviour has been observed in SDSS 1707+58 by Aoki et al. (2008), ($[Sr/Fe] = 2.3$ and $[Ba/Fe] = 3.4$), as described in Appendix A. Further investigations on these two stars are strongly suggested.

4.1.2 HE 1430-1123 (Fig. 38)

This turnoff/subgiant shows $[Fe/H] = -2.71$, $T_{\text{eff}} = 5915$ K and $\log g = 3.75$ (Barklem et al. 2005). In Fig. 38, theoretical interpretations are shown using AGB models of $M_{\text{ini}}^{\text{AGB}} = 2 M_{\odot}$, case ST/5 and $dil = 1.0$ dex (dotted line) and $M_{\text{ini}}^{\text{AGB}} = 1.3 M_{\odot}$, case ST/12 and a negligible dilution ($dil = 0.2$ dex, solid line). The model with a lower number of TDUs better interprets the observed $[Mg/Fe]$, even if the value predicted by $M_{\text{ini}}^{\text{AGB}} = 2 M_{\odot}$ still agrees within the errors. Solutions with $M_{\text{ini}}^{\text{AGB}} = 1.5 M_{\odot}$ predict a higher $[Mg/Fe]$ than observed. A Na measurement would help to provide constraints on the AGB initial mass and on the efficiency of possible mixing.

4.1.3 SDSS 0126+06 (Fig. 39)

A high s -process enhancement is shown by the main-sequence star SDSS 0126+06 ($[Fe/H] = -3.11$, $T_{\text{eff}} = 6600$ K, $\log g = 4.1$): $[Zr/Fe] \sim 1.9$, $[La/Fe] \sim 2.4$ and $[Pb/Fe]$

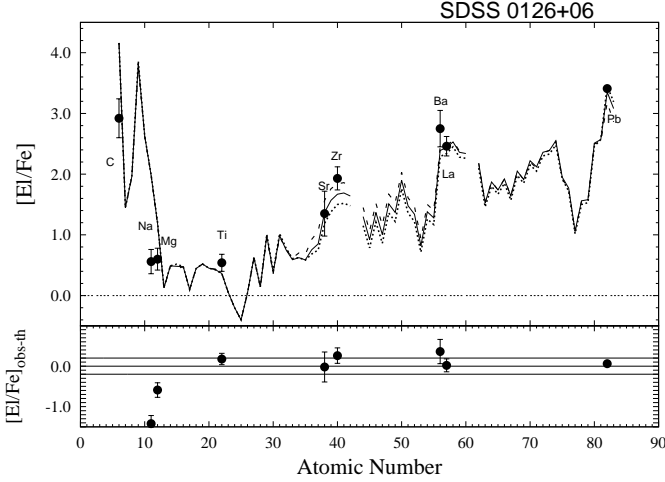


Figure 39. Spectroscopic $[El/Fe]$ abundances of the main-sequence star SDSS 0126+06 ($[Fe/H] = -3.11$; $T_{\text{eff}} = 6600$ K; $\log g = 4.1$) compared with AGB models of initial mass $M_{\text{ini}}^{\text{AGB}} = 1.4 M_{\odot}$, cases ST/9 (dotted line), ST/12 (solid line), ST/18 (dashed line), and no dilution. Observations are from Aoki et al. (2008). This star shows a very high s -process enhancement, $[La/Fe] = 2.46$ ($[hs/ls] = 0.58$ and $[Pb/hs] = 1.08$), impossible to interpret with AGB models of lower initial mass ($M_{\text{ini}}^{\text{AGB}} = 1.2 - 1.3 M_{\odot}$, which undergo a limited number of TDUs). This leads to an overestimation of the observed $[Na/Fe]$. An $[r/Fe]_{\text{ini}} = 0.5$ is adopted.

~ 3.4 (Aoki et al. 2008). A possible theoretical interpretation is displayed in Fig. 39 by models of $M_{\text{ini}}^{\text{AGB}} = 1.4 M_{\odot}$, no dilution and three ^{13}C -pockets (cases ST/9, ST/12 and ST/18). Note that the observed $[Na/Fe]$ and $[Mg/Fe]$ are largely overestimated by models. Similar solutions are found by $M_{\text{ini}}^{\text{AGB}} = 1.5$ and $2 M_{\odot}$ models (with $dil \sim 0.4$ dex, suggesting a moderate mixing), but the observed $[Na/Fe]$ and $[Mg/Fe]$ would be 1 dex (or more) higher than AGB predictions. Models of $M_{\text{ini}}^{\text{AGB}} = 1.3 M_{\odot}$, which undergo 5 TDUs, would provide lower $[Na/Fe]$ and $[Mg/Fe]$, but they can not reach the high $[La/Fe]$ observed.

4.1.4 HD 201626 (Fig. 40)

For this giant ($[Fe/H] = -2.1$; $T_{\text{eff}} = 5190$ K; $\log g = 2.25$), Zr, La, Ce, Nd, Sm and Pb have been detected by Van Eck et al. (2003) ($[hs/ls] = 0.73$ and $[Pb/hs] = 1.00$). The only constraint for AGB models is provided by the occurrence of the FDU, which imply a dilution of the order of 1 dex or more. Possible theoretical interpretations are shown in Fig. 40, for $M_{\text{ini}}^{\text{AGB}} = 1.5 M_{\odot}$, cases ST/2, ST/3, ST/5, and $dil = 1.3$ dex. Analogous solutions are obtained for $M_{\text{ini}}^{\text{AGB}} = 2 M_{\odot}$ (ST/3 and $dil = 1.3$ dex). Models with $M_{\text{ini}}^{\text{AGB}} < 1.4 M_{\odot}$ are excluded because dilutions lower than ~ 0.5 dex would be in contrast with a giant after the FDU. Observations of Na or Mg would provide information on the AGB initial mass.

4.1.5 HD 5223 (Fig. 41)

HD 5223 is a cold giant ($[Fe/H] = -2.06$; $T_{\text{eff}} = 4500$ K; $\log g = 1.0$), analysed by Goswami et al. (2006). The high hs -peak ($[hs/Fe] = 1.8$) confirms the evidence of an AGB contribution, also supported by a binary scenario

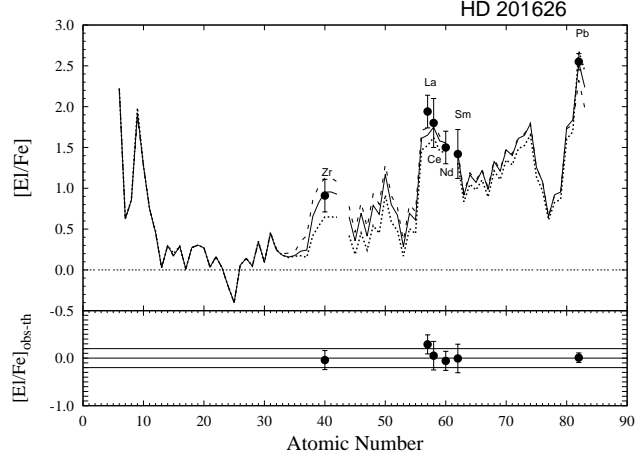


Figure 40. Spectroscopic $[El/Fe]$ abundances of the giant HD 201626 ($[Fe/H] = -2.1$; $T_{\text{eff}} = 5190$ K; $\log g = 2.25$) compared with AGB models of $M_{\text{ini}}^{\text{AGB}} = 1.5 M_{\odot}$, cases ST/2 (dotted line), ST/3 (solid line), ST/5 (dashed line), and $dil = 1.3$ dex. Observations are from Van Eck et al. (2003), who detected $[hs/ls] = 0.73$ and $[Pb/hs] = 1.00$. An $[r/Fe]_{\text{ini}} = 0.5$ is adopted.

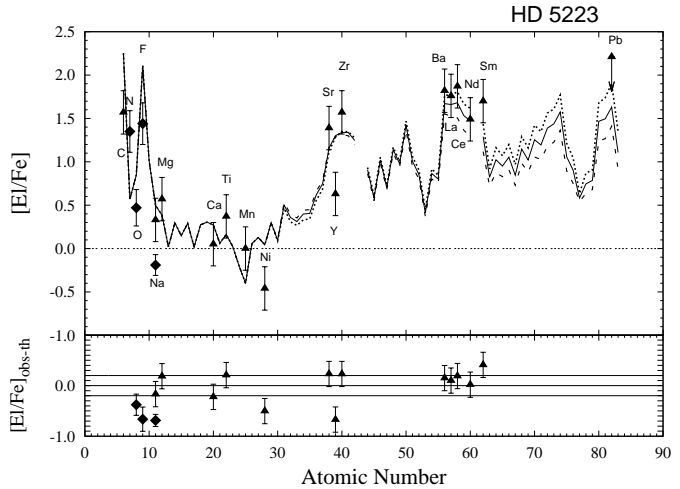


Figure 41. Spectroscopic $[El/Fe]$ abundances of the giant HD 5223 ($[Fe/H] = -2.06$; $T_{\text{eff}} = 4500$ K; $\log g = 1.0$) compared with AGB models of $M_{\text{ini}}^{\text{AGB}} = 2 M_{\odot}$, cases ST/12 (dotted line), ST/15 (solid line), ST/18 (dashed line), and $dil = 1.2$ dex. Observations are from Goswami et al. (2006) (filled circles) and Lucatello et al. (2011) (filled diamonds). A spread in the ls elements is observed. See text for the discussion about Y and Na. An $[r/Fe]_{\text{ini}} = 0.5$ is adopted.

(McClure & Woodsworth 1990). Large uncertainties affect the ls elements ($[Zr/Y] \sim 0.8$ dex), in disagreement with AGB theoretical predictions⁹. Only an upper limit for Pb is detected ($[Pb/hs] \leq 0.55$). Note that NLTE effects were not considered to determine the abundances. The single Pb line at 4057 Å is strongly affected by molecular absorption bands. Possible interpretations with AGB models of $M_{\text{ini}}^{\text{AGB}} = 2 M_{\odot}$, cases ST/12, ST/15, ST/18, and $dil = 1.2$ dex are

⁹ Two other stars studied by Goswami et al. (2006) show a similar spectroscopic behaviour: HE 1305+0007, discussed in Section 3.1.6 with $[Zr/Y] \sim 1.3$, and HE 1152-0355 for hs -peak with $[La/Nd] \sim 1.3$ (see Section 4.2).

displayed in Fig. 41. Higher ^{13}C -pocket efficiencies may explain the observed $[\text{Y}/\text{Fe}]$, but the upper limit of Pb would be overestimated by these models ($[\text{Pb}/\text{Fe}]_{\text{th}} \sim 2.9$, case ST/3, $dil \sim 1$ dex). We exclude solutions with $M_{\text{ini}}^{\text{AGB}} = 1.5 M_{\odot}$ models, since the observed $[\text{Na}/\text{Fe}]$ would be overestimated. On the other side, AGBs with lower initial mass ($M_{\text{ini}}^{\text{AGB}} = 1.3 M_{\odot}$; case ST/24) have negligible dilutions, in contrast with a giant having suffered the FDU. The $[\text{Na}/\text{Fe}]$ observed by Lucatello et al. (2011) is about 0.5 dex lower than the AGB predictions. Lucatello et al. (2011) detected $[\text{F}/\text{Fe}]$ in this star¹⁰. The AGB models shown in Fig. 41 overestimated the observed $[\text{F}/\text{Fe}]$ by about 0.5 dex.

4.1.6 HE 0212-0557 (Fig. 42)

This giant HE 0212-0557 ($[\text{Fe}/\text{H}] = -2.27$; $T_{\text{eff}} = 5075$ K; $\log g = 2.15$) has been analysed by Cohen et al. (2006). It is a cool star, affected by molecular absorption from CH and CN bands (Cohen et al. 2006). The Na I D line is too strong for a reliable abundance determination. Concerning the ls elements, Zr is not detected, one line is available for Sr, and three lines for Y.

Possible solutions with an AGB initial mass of $M_{\text{ini}}^{\text{AGB}} = 2 M_{\odot}$ are shown in Fig. 42, (cases ST/5, ST/8, ST/12 and $dil = 0.8$ dex). These models predict $[\text{Pb}/\text{Fe}]_{\text{th}} \sim 3$ dex. The main problem is the observed $[\text{Y}/\text{Fe}]$ ($[\text{hs}/\text{Y}]_{\text{obs}} = 1.5$), about 1 dex lower than the AGB predictions¹¹. A better solution for $[\text{Y}/\text{Fe}]$ would be obtained with a case ST/3, but the low dilution (~ 0.5 dex) barely agrees with a giant after the FDU. Although the low $[\text{Mg}/\text{Fe}]$ observed would better interpret the value predicted by $M_{\text{ini}}^{\text{AGB}} = 1.3 M_{\odot}$ models, solutions with no dilution are in contrast with a giant having suffered the FDU.

4.2 CEMP-sI with no Eu

Eleven stars show mild s-process enhancement ($[\text{hs}/\text{Fe}] < 1.5$) for which Eu measurements are not available. Four stars lie before the occurrence of the FDU: HE 0231-4016, HE 0430-4404 and HE 2150-0825 by Barklem et al. (2005), HE 2232-0603 by Cohen et al. (2006). Six stars are giants: BD +04°2466 by (Pereira & Drake 2009; Zhang et al. 2009; Ishigaki et al. 2010), HD 189711, HD 198269 and V Ari by Van Eck et al. (2003), HE 1031-0020, HE 1434-1442 by Cohen et al. (2006). Similarly to HD 26 and HD 206983, the giant HE 1152-0355, with $[\text{Fe}/\text{H}] = -1.3$ (Goswami et al. 2006), will be discussed in Section 5.

4.2.1 HE 0231-4016 (Fig. 43), HE 0430-4404 (Fig. A3) and HE 2150-0825 (Fig. A4)

These three stars, analysed by Barklem et al. (2005), are discussed together because they show similar abundance patterns ($[\text{hs}/\text{ls}] \sim 0.5 - 0.6$).

HE 0231-4016 ($[\text{Fe}/\text{H}] = -2.08$; $T_{\text{eff}} = 5972$ K; $\log g =$

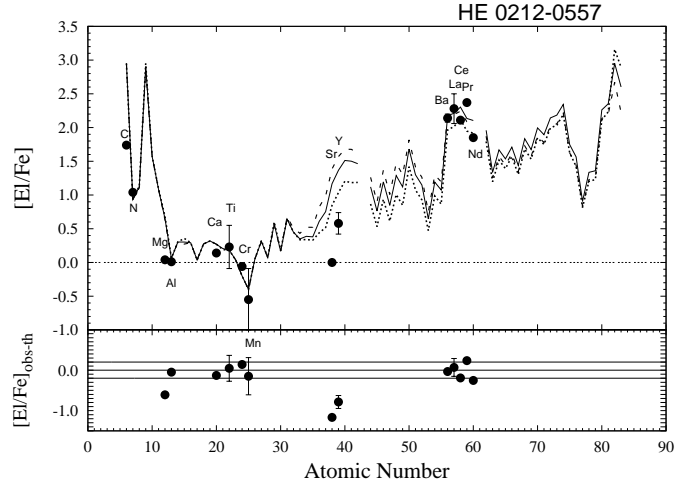


Figure 42. Spectroscopic $[\text{El}/\text{Fe}]$ abundances of the giant HE 0212-0557 ($[\text{Fe}/\text{H}] = -2.27$; $T_{\text{eff}} = 5075$ K; $\log g = 2.15$) compared with AGB models of $M_{\text{ini}}^{\text{AGB}} = 2 M_{\odot}$, cases ST/5 (dotted line), ST/8 (solid line), ST/12 (dashed line), and $dil = 0.8$ dex. Observations are from Cohen et al. (2006). The first s-peak is very uncertain, because Zr is not measured and only one line is available for Sr. Three lines are detected for Y. An $[\text{r}/\text{Fe}]_{\text{ini}} = 0.5$ is adopted.

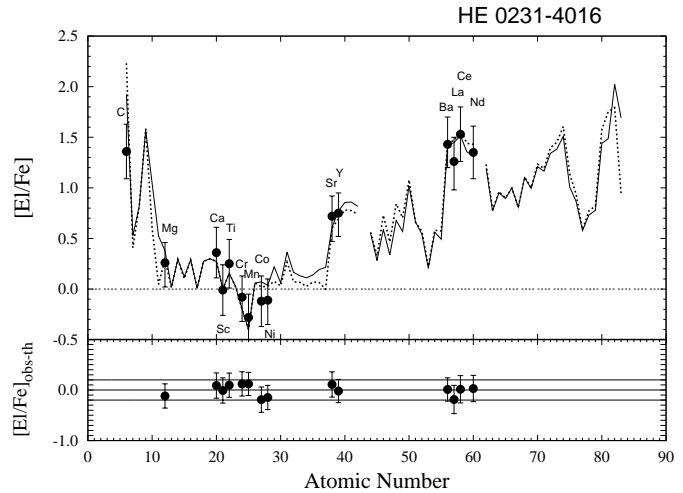


Figure 43. Spectroscopic $[\text{El}/\text{Fe}]$ abundances of the subgiant HE 0231-4016 ($[\text{Fe}/\text{H}] = -2.08$; $T_{\text{eff}} = 5972$ K; $\log g = 3.59$, before the occurrence of the FDU) compared with two AGB models: $M_{\text{ini}}^{\text{AGB}} = 1.2 M_{\odot}$, case ST/12, $dil = 0.2$ dex (dotted line), or $M_{\text{ini}}^{\text{AGB}} = 1.5 M_{\odot}$, case ST/5, $dil = 1.6$ dex (solid line). Observations are from Barklem et al. (2005), who found $[\text{hs}/\text{ls}] = 0.5$. We predict $[\text{Pb}/\text{Fe}]_{\text{th}} \sim 1.9$. The differences $[\text{El}/\text{Fe}]_{\text{obs-th}}$ displayed in the lower panel refer to the $M_{\text{ini}}^{\text{AGB}} = 1.5 M_{\odot}$ model (solid line). Similar solutions are obtained for two other CEMP-s, HE 2150-0825 and HE 0430-4404, as described in Appendix A. An $[\text{r}/\text{Fe}]_{\text{ini}} = 0.5$ is adopted.

3.59) and HE 2150-0825 ($[\text{Fe}/\text{H}] = -1.98$; $T_{\text{eff}} = 5960$ K; $\log g = 3.67$) lie on the subgiant phase or close to the turnoff, while HE 0430-4404 is a main-sequence star ($[\text{Fe}/\text{H}] = -2.07$; $T_{\text{eff}} = 6214$ K; $\log g = 4.27$). No lead has been detected. In Fig. 43, we show theoretical interpretations for HE 0231-4016, using AGB models of $M_{\text{ini}}^{\text{AGB}} = 1.2 M_{\odot}$ (case ST/12 and $dil = 0.2$ dex; dotted line) and $M_{\text{ini}}^{\text{AGB}} = 1.5 M_{\odot}$ (case ST/5 and $dil = 1.6$ dex; solid line). All AGB initial

¹⁰ Fluorine has been measured in two other CEMP-s stars: HE 1152-0355 by Lucatello et al. (2011) ($[\text{F}/\text{Fe}] = 0.64$; Section 5.3) and HE 1305+0132 by Schuler et al. (2008) (see Section A6.7).

¹¹ Note that in Paper II we calculated $[\text{hs}/\text{ls}] = 1$ (see Table 2), by considering $[\text{ls}/\text{Fe}]$ as an average between $[\text{Y}/\text{Fe}]_{\text{obs}}$ and $[\text{Zr}/\text{Fe}]_{\text{th}}$.

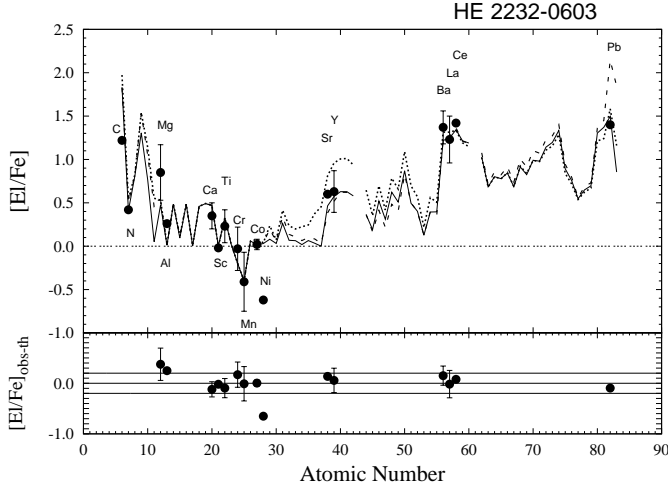


Figure 44. Spectroscopic $[El/Fe]$ abundances of the subgiant HE 2232-0603 ($[Fe/H] = -1.85$; $T_{\text{eff}} = 5750$ K; $\log g = 3.5$, uncertain FDU) compared with an AGB model of $M_{\text{ini}}^{\text{AGB}} = 1.3 M_{\odot}$, case ST/12 and $dil = 1.0$ dex shown by solid line. Observations are from Cohen et al. (2006). This star shows $[hs/ls] = 0.53$ and $[Pb/hs] = 0.25$. Solutions with $M_{\text{ini}}^{\text{AGB}} = 1.5 M_{\odot}$ are also shown: cases ST/5 and ST/3, $dil \sim 1.7$ dex, represented with dotted and dashed lines, respectively (see text). Large uncertainties affect the observed $[C/Fe]$ and $[N/Fe]$, for which no error bars are provided by the authors. An $[r/Fe]_{\text{ini}} = 0.5$ is adopted.

masses in the range $1.2 M_{\odot} \lesssim M_{\text{ini}}^{\text{AGB}} \lesssim 2 M_{\odot}$ can equally interpret the spectroscopic observations with a proper ^{13}C -pocket and dilution. Similar ^{13}C -pocket efficiencies and dilutions are adopted for HE 0430-4404 and HE 2150-0825 (see Fig. A3 and A4, Appendix A). For these three stars we predict $[Pb/Fe]_{\text{th}} \sim 1.6 - 2.2$. A Na investigation may help to discriminate the AGB initial mass and the efficiency of mixing during the main-sequence phase.

4.2.2 HE 2232-0603 (Fig. 44)

The mild s -process subgiant HE 2232-0603 ($[Fe/H] = -1.85$; $T_{\text{eff}} = 5750$ K; $\log g = 3.5$, with uncertain FDU) has been analysed by Cohen et al. (2006). It shows $[hs/Fe] \sim 1.15$ and $[Pb/Fe] \sim 1.4$. An AGB model of $M_{\text{ini}}^{\text{AGB}} = 1.3 M_{\odot}$ (case ST/12 and $dil = 1.0$ dex) interprets the neutron capture elements, as displayed in Fig. 44 by the solid line. Similar results may be obtained by $M_{\text{ini}}^{\text{AGB}} = 1.2$ and $1.4 M_{\odot}$ models ($dil = 0.4$ and 1.3 dex, respectively). By increasing the number of thermal pulses we can not find solutions for all three s -peaks: e.g., for $M_{\text{ini}}^{\text{AGB}} = 1.5 M_{\odot}$, the observed $[Sr/Fe]$ and $[Y/Fe]$ would be lower than the AGB models (case ST/5; dotted lines) or the predicted $[Pb/Fe]$ would be ~ 0.7 dex higher than observed (case ST/3; dashed line), as shown in Fig. 44. However, Cohen et al. (2006) remarked the uncertainty of the observed Pb, with only one line detected. The high observed $[Mg/Fe]$ ratio agrees within the error bars with the AGB predictions ($[Mg/Fe] = 0.85 \pm 0.32$, 5 lines).

4.2.3 BD+04°2466 (\equiv HIP 55852), (Fig. 45)

This giant has been recently analysed by different authors: Pereira & Drake (2009), Zhang et al. (2009), Ishigaki et al. (2010), ($[Fe/H] \sim -2$; $T_{\text{eff}} = 5100$ K; $\log g = 1.8$). It was

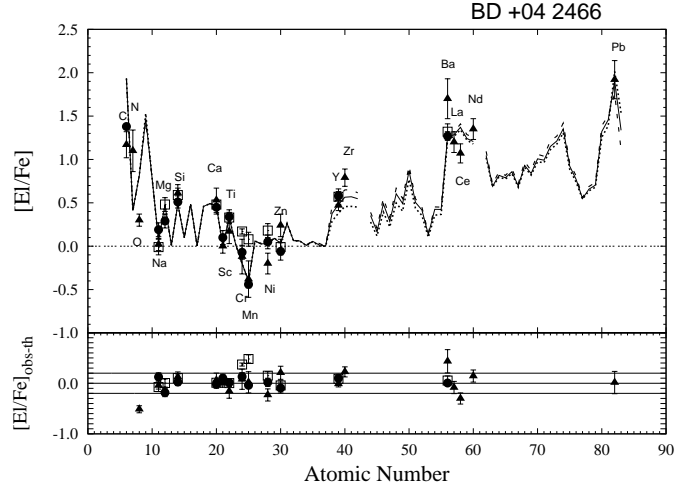


Figure 45. Spectroscopic $[El/Fe]$ abundances of the giant BD+04°2466 ($[Fe/H] \sim -2$; $T_{\text{eff}} = 5100$ K; $\log g = 1.8$) compared with AGB models of $M_{\text{ini}}^{\text{AGB}} = 1.3 M_{\odot}$, cases ST/6 (dotted line), ST/9 (solid line), ST/12 (dashed line), and $dil = 0.9$ dex. Observations are from Pereira & Drake (2009) (filled triangles), Zhang et al. (2009) (filled circles), Ishigaki et al. (2010) (empty squares). The two s -process indicators are $[hs/ls] = 0.6$ and $[Pb/hs] = 0.7$. The observed $[O/Fe]$ is about 0.5 dex lower than predicted by the models (see text). An $[r/Fe]_{\text{ini}} = 0.5$ is adopted.

firstly identified as a metal-poor star by Bond (1980), and afterwards it was classified as CH star or "metal-deficient barium star" by Luck & Bond (1991). Jorissen et al. (2005) confirm the binary scenario, finding radial velocity variations with a period $P = 4593$ days.

Large dilutions are needed in order to interpret the mild s -process observed ($[ls/Fe] = 0.6$, $[hs/Fe] = 1.2$, $[Pb/Fe] = 1.9$), even using AGB models with low initial mass. In Fig. 45, we show solutions with $M_{\text{ini}}^{\text{AGB}} = 1.3 M_{\odot}$, cases ST/6, ST/9, ST/12, and $dil = 0.9$ dex. Among the hs elements, the observed $[Ce/Fe]$, with 5 detected lines, is about 0.3 dex lower than the AGB predictions. Nd is the most reliable with 12 detected lines. The $[Na/Fe] \sim 0$ observed by Ishigaki et al. (2010), would be slightly overestimated by AGB models with higher initial mass, although the s -process elements are equally well interpreted: for instance, $M_{\text{ini}}^{\text{AGB}} = 1.5 M_{\odot}$ predicts $[Na/Fe]_{\text{th}} = 0.3$ (case ST/3; $dil = 1.8$ dex). The observed $[C/Fe]$ is ~ 0.6 dex lower than the AGB prediction. The low $^{12}\text{C}/^{13}\text{C}$ ratio detected (15^{+5}_{-3}) confirms that efficient mixing has taken place. The predicted $[O/Fe]$ is ~ 0.5 dex higher than observed. Note that the uncertainty shown for $[O/Fe]$ in Fig. 45, may be underestimated, because C, N, and O measured by Pereira & Drake (2009) are interdependent.

4.2.4 HD 198269 (Fig. 46)

The mild s -process enhanced giant HD 198269, with $[Fe/H] \sim -2.2$, $T_{\text{eff}} = 4800$ K and $\log g = 1.3$, has been studied by Van Eck et al. (2003). Only Zr is measured among the ls elements, while the hs peak is better determined with La, Ce, Nd and Sm ($[hs/ls] = 0.94$). One line is detected for Pb ($[Pb/hs] = 1.07$). As said by the authors, the derived abundances may be uncertain owing to the presence of molecular

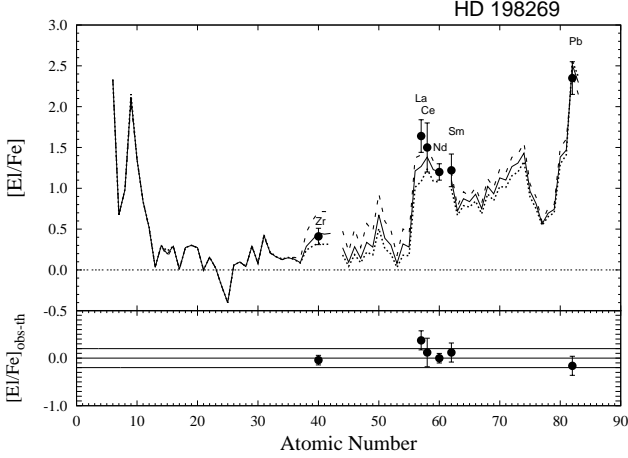


Figure 46. Spectroscopic $[\text{El}/\text{Fe}]$ abundances of the giant HD 198269 ($[\text{Fe}/\text{H}] \sim -2.2$; $T_{\text{eff}} = 4800$ K; $\log g = 1.3$) compared with AGB models of $M_{\text{ini}}^{\text{AGB}} = 1.5 M_{\odot}$, cases ST/1.5 (dotted line), ST/2 (solid line), ST/3 (dashed line), and $dil = 1.5$ dex. Observations are from Van Eck et al. (2003), who found $[\text{hs}/\text{ls}] = 0.94$ and $[\text{Pb}/\text{hs}] = 1.07$. An $[\text{r}/\text{Fe}]_{\text{ini}} = 0.5$ is adopted.

lines in the spectra. The most reliable is Ce, for which more lines are available. Possible theoretical interpretations are displayed in Fig. 46, for AGB models with initial mass $M = 1.5 M_{\odot}$, cases ST/1.5, ST/2, ST/3 and $dil = 1.5$ dex. Analogous solutions are obtained for $M_{\text{ini}}^{\text{AGB}} = 2 M_{\odot}$ (ST/2 and $dil = 1.5$ dex). Models with $M_{\text{ini}}^{\text{AGB}} < 1.4 M_{\odot}$ are excluded because dilutions lower than ~ 0.5 dex would be in contrast with a giant after the FDU. No light elements are available for this giant. Observations of Na or Mg would provide key information on the AGB initial mass.

4.2.5 HD 189711 (Fig. A1); V Ari (Fig. A2)

We analyse these two mild *s*-process enhanced stars together, because they show similar *s*-process distributions ($[\text{hs}/\text{ls}] \sim 0.2$; $[\text{Pb}/\text{hs}] \sim -0.3$).

As said before, the abundances by Van Eck et al. (2003) are uncertain because only few lines are available in a very crowded region of the spectrum, veiled by molecular lines. The difficulties increase for the coolest stars, as the giants HD 189711 ($[\text{Fe}/\text{H}] \sim -1.8$; $T_{\text{eff}} = 3500$ K; $\log g = 0.5$) and V Ari ($[\text{Fe}/\text{H}] \sim -2.4$; $T_{\text{eff}} = 3580$ K; $\log g = -0.2$), for which the abundance determination represent a real challenge for the spectroscopists, and the errors are of the order of ± 0.4 dex. Caution is suggested for these stars. An attempt to interpret the $[\text{El}/\text{Fe}]$ observations is given in Figs. A1 and A2 (Appendix A). Very low *s*-process efficiencies are adopted (ST/24 and ST/30), in order to obtain $[\text{Pb}/\text{hs}] \sim -0.42$ and -0.22 , respectively. For HD 189711, Kipper et al. (1996) measured $[\text{Eu}/\text{Fe}] = 1.45$, which may suggest a possible initial *r*-process enhancement. However, the metallicities detected by Van Eck et al. (2003) and Kipper et al. (1996) are discrepant ($[\text{Fe}/\text{H}] = -1.8$ and -1.15 , respectively), and further Eu investigations are desirable in this star.

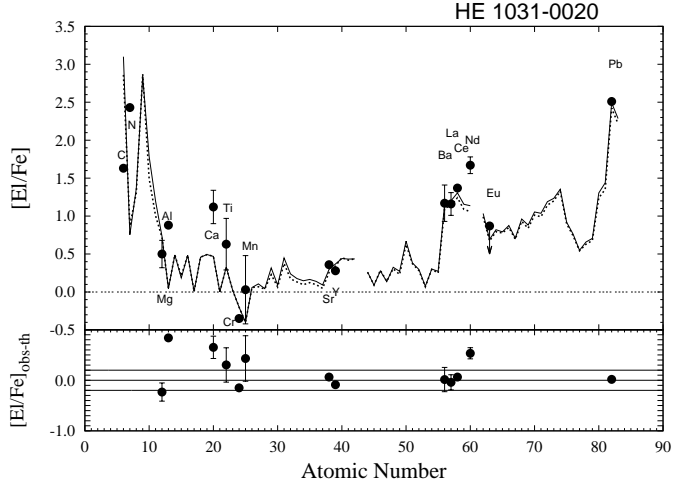


Figure 47. Spectroscopic $[\text{El}/\text{Fe}]$ abundances of the giant HE 1031-0020 ($[\text{Fe}/\text{H}] = -2.86$; $T_{\text{eff}} = 5080$ K; $\log g = 2.2$) compared with two AGB models: $M_{\text{ini}}^{\text{AGB}} = 1.4 M_{\odot}$, case ST/5 and $dil = 1.2$ dex (solid line), or $M_{\text{ini}}^{\text{AGB}} = 2 M_{\odot}$, case ST/5 and $dil = 1.6$ dex (dotted line). Observations are from Cohen et al. (2006), who detected $[\text{hs}/\text{ls}] = 0.94$ and $[\text{Pb}/\text{hs}] = 1.37$. For discussion about Nd see text. The differences $[\text{El}/\text{Fe}]_{\text{obs-th}}$ displayed in the lower panel refer to the $M_{\text{ini}}^{\text{AGB}} = 1.4 M_{\odot}$ model (solid line). An $[\text{r}/\text{Fe}]_{\text{ini}} = 0.5$ is adopted.

4.2.6 HE 1031-0020 (Fig. 47)

The giant HE 1031-0020 is one of the coolest stars analysed by Cohen et al. (2006), ($[\text{Fe}/\text{H}] = -2.86$; $T_{\text{eff}} = 5080$ K; $\log g = 2.2$). It is affected by molecular absorption from CH and CN bands, and the metallicity is probably underestimated. The Na I D line is too strong and no reliable abundance can be obtained. A large uncertainty is reported by Cohen et al. (2006) for Ti (± 0.4 dex) with 15 detected lines.

The detection of Mg is, in general, accurate, with an uncertainty of about ± 0.2 dex. Caution is suggested by Cohen et al. (2006) for Sr and Ba detections. This giant shows mild enhancement in ls and hs: $[\text{ls}/\text{Fe}] = 0.35$ and $[\text{hs}/\text{Fe}] = 1.29$. Instead, a very high $[\text{Pb}/\text{Fe}]$ is observed ($[\text{Pb}/\text{Fe}] = 2.66$; $[\text{Pb}/\text{hs}] = 1.37$). However, Pb is uncertain in this star, because the single line detected is strongly blended by CH features. Possible solutions with two AGB initial masses are shown in Fig. 47: for $M_{\text{ini}}^{\text{AGB}} = 1.4 M_{\odot}$, $dil = 1.2$ dex is required (solid line), while for $M_{\text{ini}}^{\text{AGB}} = 2 M_{\odot}$ a $dil = 1.6$ dex is adopted (dotted line). A case ST/5 is needed for both models. AGBs with lower initial mass may equally interpret the spectroscopic data: $M_{\text{ini}}^{\text{AGB}} = 1.3 M_{\odot}$, case ST/15 and $dil = 0.8$ dex, in agreement with a giant after the FDU. Among the hs elements, a difference of about 0.5 dex is observed between La and Nd (four lines detected for both elements). This discrepancy contrasts with AGB predictions. In Fig. 47 we consider La as more reliable among the hs elements, with a proper choice of the ^{13}C -pocket and dilution factor, we may find theoretical solutions for the observed $[\text{Nd}/\text{Fe}]$, but in this case the observed $[\text{Mg}/\text{Fe}]$ and $[\text{ls}/\text{Fe}]$ would be overestimated. AGB models of $M_{\text{ini}}^{\text{AGB}} = 1.5 M_{\odot}$ would predict a larger $[\text{Mg}/\text{Fe}]$ than observed. No error bars are provided by the authors for C and N.

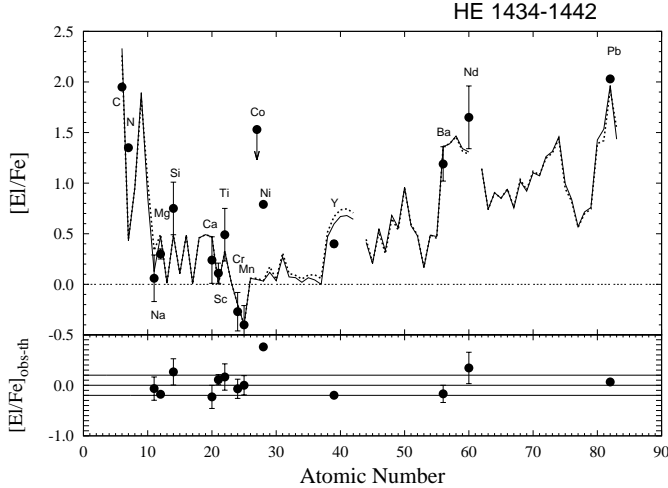


Figure 48. Spectroscopic $[\text{El}/\text{Fe}]$ abundances of the subgiant HE 1434-1442 ($[\text{Fe}/\text{H}] = -2.39$; $T_{\text{eff}} = 5420$ K; $\log g = 3.15$, having suffered the FDU) compared with two AGB models: $M_{\text{ini}}^{\text{AGB}} = 1.3 M_{\odot}$, case ST/15, $dil = 0.8$ dex (solid line), or $M_{\text{ini}}^{\text{AGB}} = 1.4 M_{\odot}$, case ST/12, $dil = 1.2$ dex (dotted line). Observations are from Cohen et al. (2006). This solution is indicative owing to the limited number of s -elements observed ($[\text{hs}/\text{ls}] \sim 0.9$; $[\text{Pb}/\text{hs}] \sim 0.8$, see text). The differences $[\text{El}/\text{Fe}]_{\text{obs-th}}$ displayed in the lower panel refer to the $M_{\text{ini}}^{\text{AGB}} = 1.3 M_{\odot}$ model. An $[\text{r}/\text{Fe}]^{\text{ini}} = 0.5$ is adopted.

4.2.7 HE 1434-1442 (Fig. 48)

The giant HE 1434-1442 has $[\text{Fe}/\text{H}] = -2.39$, $T_{\text{eff}} = 5420$ K and $\log g = 3.15$ (Cohen et al. 2006). As other stars studied by Cohen et al. (2006), it is affected by molecular absorption from CH and CN bands. A limited number of s elements is observed: Ba (three lines), Y and Nd (two lines), and Pb (one line). Fig. 48 shows possible theoretical interpretations with AGB models of low initial mass ($M_{\text{ini}}^{\text{AGB}} = 1.3$ and $1.4 M_{\odot}$, solid and dotted line, respectively), in agreement with $[\text{hs}/\text{ls}] = 0.89$ and $[\text{Pb}/\text{hs}] = 0.77$. These solutions interpret the observed $[\text{Na}/\text{Fe}] \sim 0$. This star lies on the subgiant phase after the FDU, according to the large dilution adopted ($dil = 0.8 - 1.2$ dex). AGB models of $M_{\text{ini}}^{\text{AGB}} = 1.5 M_{\odot}$ (case \sim ST/6) are excluded because they predict a high Na abundance ($[\text{Na}/\text{Fe}]_{\text{th}} = 0.6$). A lower Na value is obtained by $M_{\text{ini}}^{\text{AGB}} = 2 M_{\odot}$, case ST/9 and $dil = 1.6$ dex ($[\text{Na}/\text{Fe}]_{\text{th}} = 0.4$). While the neutron capture elements may be interpreted with all AGB initial masses in the range $1.3 M_{\odot} \leq M_{\text{ini}}^{\text{AGB}} \leq 2 M_{\odot}$, Na agrees with $M_{\text{ini}}^{\text{AGB}} \leq 1.4 M_{\odot}$ models. However, Na is explicitly mentioned by the authors as very uncertain for this cool star. C and N are not very reliable, because no error bars are provided by Cohen et al. (2006).

5 STARS AT $[\text{Fe}/\text{H}] \sim -1.2$

In this Section, we consider three stars with $[\text{Fe}/\text{H}] \gtrsim -1.4$: HD 26 ($[\text{Fe}/\text{H}] = -1.25$, -1.02 ; Van Eck et al. 2003, Masseron et al. 2010), HD 206983 ($[\text{Fe}/\text{H}] = -0.99$, -1.43 ; Masseron et al. 2010, Junqueira & Pereira 2001), HE 1152-0355 ($[\text{Fe}/\text{H}] = -1.27$; Goswami et al. 2006); for two other stars, CS 29503-010 ($[\text{Fe}/\text{H}] = -1.06$; Aoki et al. 2007) and HE 0507-1653 ($[\text{Fe}/\text{H}] = -1.38$, -1.42 ; Aoki et al. 2007; Schuler et al. 2008), only Ba is detected among the

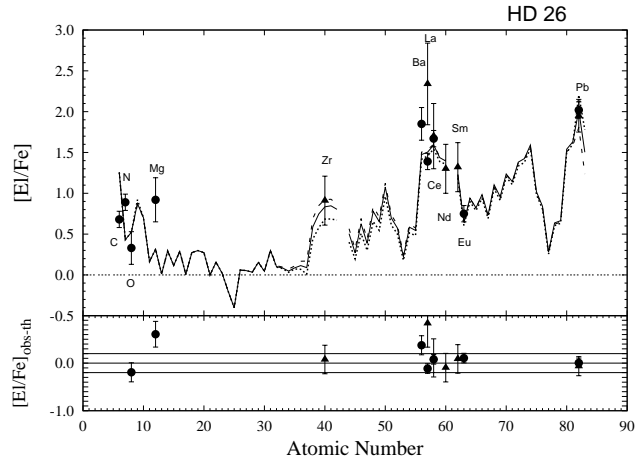


Figure 49. Spectroscopic $[\text{El}/\text{Fe}]$ abundances of the giant HD 26 ($[\text{Fe}/\text{H}] = -1.25$, $T_{\text{eff}} = 5170$ K, $\log g = 2.2$, Van Eck et al. 2003; $[\text{Fe}/\text{H}] = -1.02$, $T_{\text{eff}} = 4900$ K, $\log g = 1.5$, Masseron et al. (2010)) compared with AGB models of initial mass $M = 1.5 M_{\odot}$, cases ST/1.5 (dotted line), ST/2 (solid line), ST/2.5 (dashed line), and $dil = 1$ dex. Observations are from Van Eck et al. (2003) (filled triangles) and Masseron et al. (2010) (filled circles). This giant shows $[\text{hs}/\text{ls}] = 0.5$ and $[\text{Pb}/\text{hs}] = 0.7$. An $[\text{r}/\text{Fe}]^{\text{ini}} = 0.0$ is adopted.

s -process elements. All these stars show enhanced $[\text{C}/\text{Fe}]$ and s -process elements. Their metallicity is close to disc stars and their atmospheric parameters are far from the TP-AGB phase. These stars may be considered as a link between CEMP- s and s -rich giants or dwarfs of disc metallicity (e.g., barium stars¹², CH stars, MS/S stars with no Tc, symbiotic stars), because the carbon and s -enrichment on their surface is commonly ascribed to a binary scenario with mass transfer by stellar winds. Some of these stars are not CH stars, and, starting from Luck & Bond (1991), they have been classified as “metal-poor barium stars”.

5.1 HD 26 (Fig. 49)

Vanture (1992,b) studied for the first time HD 26, deriving spectroscopic abundances for C, N, O, and heavier elements. They classified this giant as a CH star. Later on, Van Eck et al. (2003) and Masseron et al. (2010) reported spectroscopic observations obtained with high-resolution spectra. We discuss here only these most recent values. A model constraint is given by the occurrence of the FDU ($T_{\text{eff}} = 5170$ K and $\log g = 2.2$ by Van Eck et al. 2003; $T_{\text{eff}} = 4900$ K and $\log g = 1.5$ by Masseron et al. 2010), which requires a dilution of the order of 1 dex. The abundances by Van Eck et al. (2003) are uncertain because only few lines veiled by molecular bands are available; they refer to Ce as

¹² Barium stars are giants (and dwarfs) showing Ba and Sr overabundances by the presence of singly ionised barium, Ba II, at $\lambda = 4554 \text{ \AA}$ and Sr II ($\lambda = 4077 \text{ \AA}$, $\lambda = 4215 \text{ \AA}$), as well as CH G band and CN bands also enhanced (Allen & Barbuy 2006; Smiljanic et al. 2007). Values of $[\text{Pb}/\text{Fe}] > 1$ dex have been observed for the first time in barium stars by Allen & Barbuy (2006), explained with efficient ^{13}C -pockets in the AGB companion. Theoretical interpretations of barium stars have been discussed by Husty et al. (2008, 2009).

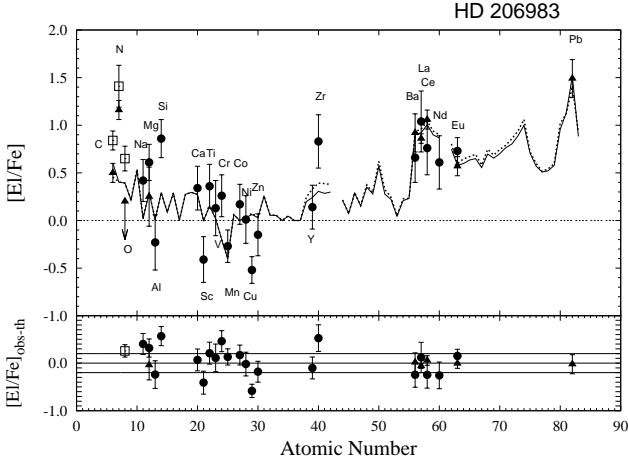


Figure 50. Spectroscopic $[El/Fe]$ abundances of the giant HD 206983 ($[Fe/H] = -0.99$; $T_{\text{eff}} \sim 4200$ K; $\log g = 0.6$, Masseron et al. 2010) compared with AGB models of $M_{\text{ini}}^{\text{AGB}} = 1.3$ or $1.5 M_{\odot}$, case ST, $dil = 0.7$ or 1.6 dex (solid or dotted lines, respectively). Observations are from Masseron et al. (2010) (filled triangles), Drake & Pereira (2008) (empty squares), Junqueira & Pereira (2001) (filled circles). This giant shows $[hs/ls] = 0.38$ and $[Pb/hs] = 0.67$ (Masseron et al. 2010). See text for discussion about Cu. An $[r/Fe]_{\text{ini}} = 0.5$ is adopted.

the most reliable element among the hs-peak. Besides five neutron capture elements (Zr, La, Ce, Nd, and Sm), they detected the Pb I line at 4057.812 \AA , clearly resolved thanks to the high-resolution $R = \lambda/\Delta\lambda = 135\,000$. Masseron et al. (2010) provided new observations for C, N, O, Mg, and Eu, as well as updated results for Ba, La, Ce, and Pb ($[hs/ls] = 0.5$; $[Pb/hs] = 0.7$). In Fig. 49 we show theoretical interpretations with AGB models of $M_{\text{ini}}^{\text{AGB}} = 1.5 M_{\odot}$, cases ST/1.5, ST/2, ST/2.5, and $dil = 1$ dex. Similar solutions are obtained with higher AGB initial masses (e.g., $M_{\text{ini}}^{\text{AGB}} = 2 M_{\odot}$). No initial *r*-process enhancement is adopted for this star. The observed $[Mg/Fe]$ is higher than the AGB predictions. The observations by Masseron et al. (2010) shown in Fig. 49 will be discussed by the authors in Masseron et al., in preparation.

5.2 HD 206983 (Fig. 50)

This giant ($T_{\text{eff}} \sim 4200$ K, $\log g = 0.6$) has been analysed by Masseron et al. (2010), Drake & Pereira (2008) (who studied C, N, O), and Junqueira & Pereira (2001).

In Fig. 50, we show theoretical interpretations using AGB models of initial masses $M = 1.3$ and $1.5 M_{\odot}$, case ST, $dil = 0.7$ and 1.6 dex, respectively. We considered Y (seven detected lines) more reliable than Zr (four lines available), (Junqueira & Pereira 2001). Discrepant $[C/Fe]$ and $[O/Fe]$ ratios are found by Drake & Pereira (2008) and Masseron et al. (2010): note that Drake & Pereira (2008) adopted the stellar parameters obtained by Junqueira & Pereira (2001), which provided a metallicity 0.4 dex lower than $[Fe/H] = -0.99$ by Masseron et al. (2010). In Fig. 50, we display solutions with AGB models of $[Fe/H]_{\text{th}} = -1$, which agree with $[C/Fe]$ detected by Masseron et al. (2010). Instead, the observed $[N/Fe]$ is about 0.7 dex higher than AGB predictions. Note that, by decreasing metallicity, a larger primary amount of $[C/Fe]$

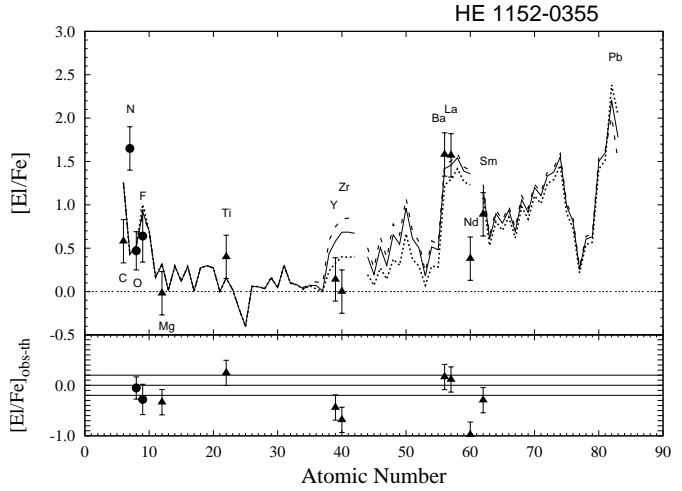


Figure 51. Spectroscopic $[El/Fe]$ abundances of the giant HE 1152-0355 ($[Fe/H] = -1.27$; $T_{\text{eff}} = 4000$ K; $\log g = 1.0$) compared with a AGB stellar models of $1.5 M_{\odot}$, cases ST (dotted line), ST/1.5 (solid line), ST/2 (dashed line), and $dil = 1.0$ dex. Observations are from Goswami et al. (2006) (filled triangles) and Lucatello et al. (2011) (filled circles). The observed $[Y/Fe]$, $[Zr/Fe]$ and $[Nd/Fe]$ ratios are overestimated by AGB models (see text). An $[r/Fe]_{\text{ini}} = 0.0$ is adopted.

is predicted. C and N are also affected by uncertainty in 3D atmosphere models that may decrease the observations (Asplund et al. 2009). $[Na/Fe]_{\text{obs}}$ (two lines) is 0.4 dex higher than AGB models, but no NLTE corrections are considered by Junqueira & Pereira (2001). Note that Junqueira & Pereira (2001) detected $[Cu/Fe] = -0.5$, by assuming $[Fe/H] = -1.4$. At this metallicity, spectroscopic observations of unevolved stars show on average similar values. Indeed, as discussed in Section 1, for halo stars ($[Fe/H] \lesssim -1.7$) $[Cu/Fe]$ shows a negative constant ratio close to -0.7 dex. By increasing the metallicity, $[Cu/Fe]$ increases starting from $[Fe/H] \sim -1.5$ and reaching solar values at $[Fe/H] \sim -0.5$.

5.3 HE 1152-0355 (Fig. 51)

The giant HE 1152-0355 is a very cool star ($[Fe/H] = -1.27$; $T_{\text{eff}} = 4000$ K; $\log g = 1.0$) affected by strong molecular contaminations, probably inducing the spread observed among the hs elements ($[La/Nd] \sim 1$ dex). Moreover, Goswami et al. (2006) could not estimate Na for the highly blended lines present in the spectra. A possible interpretation is shown in Fig. 51, for AGB models of $M_{\text{ini}}^{\text{AGB}} = 1.5 M_{\odot}$ (case ST, ST/1.5, ST/2 and $dil = 1.0$ dex). Note the low $[Nd/Fe]$ with respect to $[Ba, La/Fe]$: we have considered La as the most reliable among the hs elements. These models predict $[Pb/Fe]_{\text{th}} \sim 2$. By considering lower $[hs/Fe]_{\text{th}}$, we may interpret the observed $[ls/Fe]$ under the hypothesis of higher dilutions. However, the large uncertainties of the observations do not permit to provide accurate theoretical discussions. Lucatello et al. (2011) determined $[F/Fe]$ abundance for this star, in agreement with theoretical AGB predictions.

5.4 CS 29503–010

This main-sequence star ($T_{\text{eff}} \sim 6500$ K and $\log g = 4.5$; $[\text{Fe}/\text{H}] = -1.06$) has only Ba detected among the *s*-elements, with $[\text{Ba}/\text{Fe}] = 1.5$. AGB models with initial mass in the range $1.3 \leq M/M_{\odot} \leq 2$ may equally interpret the observations, by adopting different ^{13}C -pockets and dilutions. However, at present, this star seems not to belong to binary system (Tsangarides 2005), and further spectroscopic investigations are desirable.

5.5 HE 0507–1653

Only barium among the *s*-process elements is measured for this giant with $T_{\text{eff}} \sim 5000$ K and $\log g = 2.4$ ($[\text{Fe}/\text{H}] = -1.38, -1.42$; Aoki et al. 2007; Schuler et al. 2008). Schuler et al. (2008) detected C and N, in agreement with previous results by Aoki et al. (2007). Due to the limited number of spectroscopic observations, a range higher than 1 dex may be predicted for the ls peak and Pb.

6 EFFECT OF ^{22}Ne , ^{12}C AND ^{16}O AT LOW METALLICITY

The aim of this Section is to provide a more detailed discussion about the impact of the $^{22}\text{Ne}(\text{n}, \gamma)^{23}\text{Ne}$ reaction, both as neutron poison and as neutron seed, and about the effect of the $^{12}\text{C}(\text{n}, \gamma)^{13}\text{C}$ and $^{16}\text{O}(\text{n}, \gamma)^{17}\text{O}$ reactions as neutron poisons. Additional tests with respect to Paper I (see Section 4 and Appendix C) are presented, by changing the AGB initial mass and the ^{13}C -pocket.

The *s*-process distribution observed in several stars can be interpreted by AGB models with different initial masses and a proper choice of the ^{13}C -pocket. In particular, at $[\text{Fe}/\text{H}] \sim -2.5$, comparable $[\text{hs}/\text{ls}]$ and $[\text{Pb}/\text{hs}]$ are obtained with $M = 1.3 M_{\odot}$ model and $\sim\text{ST}/12$ or $M = 1.5 M_{\odot}$ and case $\sim\text{ST}/3$. This is mainly due to the large amount of primary ^{22}Ne at low metallicities, which acts both as neutron poison and as neutron seed. In addition to ^{22}Ne , neutron poisons by primary ^{12}C and ^{16}O also affect the *s*-process abundances. This result highlights the importance of a study focused on the production of the light elements, the reactions involved and their uncertainties, as well as their effects on the *s*-process path.

6.1 ^{22}Ne

At low metallicities, ^{22}Ne has two effects: it acts both as neutron seed and as neutron poison. The first effect leads to a production of ^{56}Fe by neutron captures on ^{22}Ne ; then, ^{56}Fe becomes seed for the nucleosynthesis of the *s*-elements. Therefore, both iron seeds and the number of neutrons released change.

Concerning the effect of ^{22}Ne as neutron seed, we report in Fig. 52, left panel, a comparison of the envelope abundances for an AGB model of $M = 1.5 M_{\odot}$ at $[\text{Fe}/\text{H}] = -2.6$ and a case ST/3 (red solid line), with a test case in which we set to zero the initial abundances of all isotopes from ^{56}Fe to ^{209}Bi (blue dotted line). Owing to the abundant primary ^{22}Ne , the $^{22}\text{Ne}(\text{n}, \gamma)^{23}\text{Ne}$ reaction drives a neutron chain that extends up to ^{56}Fe and beyond, producing a large amount of

s-elements. A similar effect is obtained for an AGB model of initial mass $M = 1.3 M_{\odot}$ and case ST/12 (Fig. 52, right panel).

Concerning the effect of neutron poison, we made additional tests by setting to zero the $^{22}\text{Ne}(\text{n}, \gamma)^{23}\text{Ne}$ reaction.

We report in Fig. 53, the results of AGB models of $M = 1.5 M_{\odot}$ (20 TDUs) at $[\text{Fe}/\text{H}] = -2.6$ (red solid lines), compared with a test case in which the $^{22}\text{Ne}(\text{n}, \gamma)^{23}\text{Ne}$ channel is set to zero (blue dotted lines). Two ^{13}C -pockets are considered: ST/12 (left panel) and ST/3 (right panel). By excluding the $^{22}\text{Ne}(\text{n}, \gamma)^{23}\text{Ne}$ channel, the production of the three *s*-process peaks in general increases. When a case ST/3 is adopted, major effects are observed for the ls elements, while the hs peak is almost unchanged; for case ST/12, the effect on Pb is large.

For AGB models with $M = 1.4 M_{\odot}$ (10 TDUs) we obtain results similar to $M = 1.5 M_{\odot}$ models.

For AGB models of initial mass $M = 1.3 M_{\odot}$, the effect of the $^{22}\text{Ne}(\text{n}, \gamma)^{23}\text{Ne}$ reaction is marginal owing to the limited number of thermal pulses (5 TDUs).

For AGB models with $M \sim 1.35 M_{\odot}$ at the 6th and 7th TDU, we obtain results similar to $M = 1.3 M_{\odot}$ models.

6.2 ^{12}C and ^{16}O

In Fig. 54, we compare an AGB model of $M = 1.3 M_{\odot}$ at $[\text{Fe}/\text{H}] = -2.6$ (red solid lines), with a test case in which both $^{12}\text{C}(\text{n}, \gamma)^{13}\text{C}$ and $^{16}\text{O}(\text{n}, \gamma)^{17}\text{O}$ channels have been set to zero (blue dotted lines). Two ^{13}C -pockets are considered: ST/12 (left panel) and ST/3 (right panel). The variation of the ls and hs elements is evident because of the low $[\text{ls}/\text{Fe}]$ and $[\text{hs}/\text{Fe}]$ abundances.

For AGB models with $M \sim 1.35 M_{\odot}$ at the 6th and 7th TDU, we obtain results similar to $M = 1.3 M_{\odot}$ models.

Instead, by setting to zero both the $^{12}\text{C}(\text{n}, \gamma)^{13}\text{C}$ and $^{16}\text{O}(\text{n}, \gamma)^{17}\text{O}$ channels in AGB models of $M = 1.5 M_{\odot}$, variations lower than ~ 0.2 dex are produced. Note that the neutron poison effect of the very abundant primary ^{12}C is almost cancelled by $^{13}\text{C}(\alpha, \text{n})^{16}\text{O}$ recycling.

For AGB models with $M = 1.4 M_{\odot}$ (10th TDU) we obtain results similar to $M = 1.5 M_{\odot}$ models.

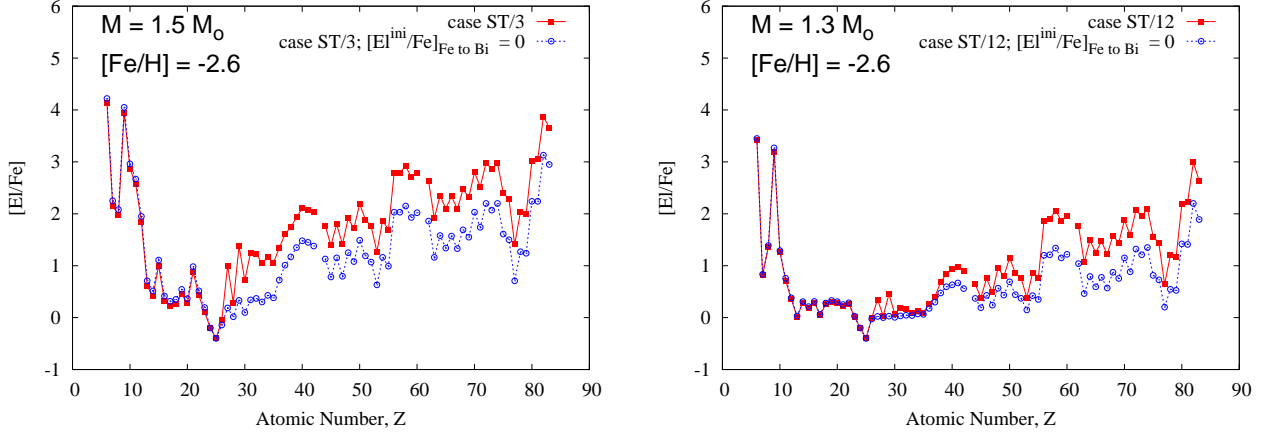


Figure 52. Left panel: we compare an AGB model of $M = 1.5 M_{\odot}$ at $[\text{Fe}/\text{H}] = -2.6$ (red solid line) and case ST/3, with a test case in which we set to zero the initial abundances of all isotopes from ^{56}Fe to ^{209}Bi (blue dotted line). (See the electronic paper for a colour version of the figures of this Section. Right panel: the same as left panel but for an AGB model of $M = 1.3 M_{\odot}$ and case ST/12.

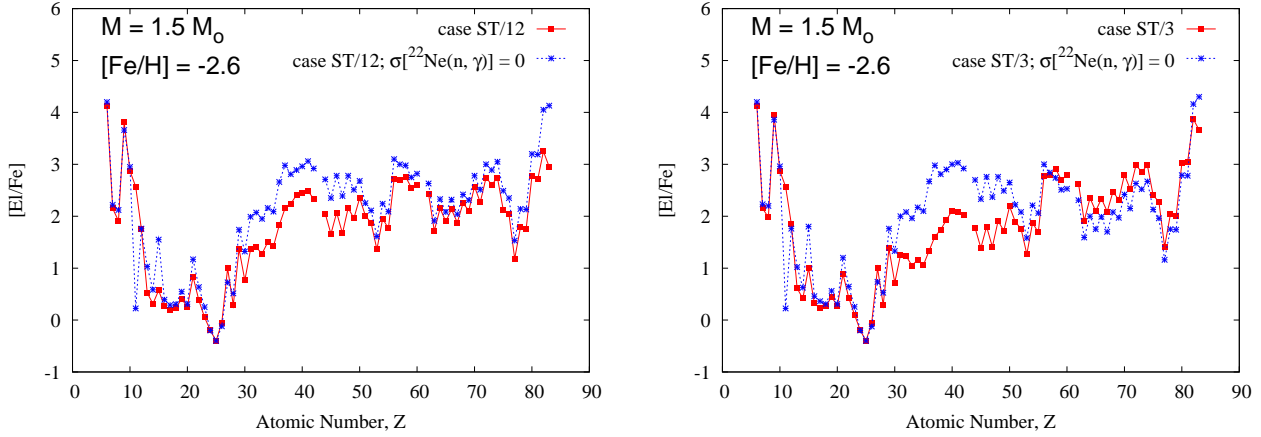


Figure 53. AGB models of $M = 1.5 M_{\odot}$ (20th TDU) at $[\text{Fe}/\text{H}] = -2.6$ (red solid lines), compared with a test case in which the $^{22}\text{Ne}(\text{n}, \gamma)^{23}\text{Ne}$ channel is set to zero (blue dotted lines). Two ^{13}C -pockets are considered: ST/12 (left panel) and ST/3 (right panel).

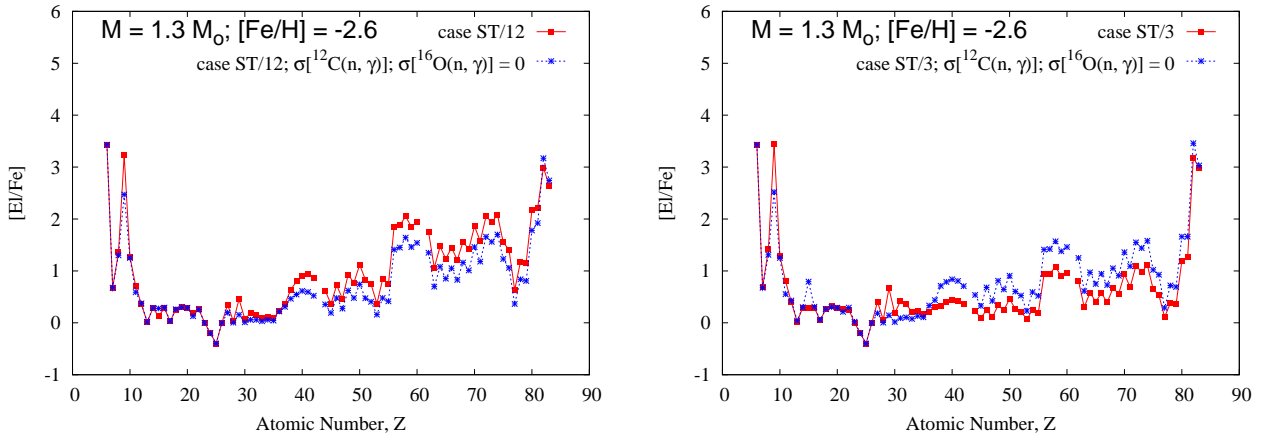


Figure 54. AGB model of $M = 1.3 M_{\odot}$ at $[\text{Fe}/\text{H}] = -2.6$ (red solid lines), compared with a test case in which both the $^{12}\text{C}(\text{n}, \gamma)^{13}\text{C}$ and $^{16}\text{O}(\text{n}, \gamma)^{17}\text{O}$ channels have been set to zero (blue dotted lines). Two ^{13}C -pockets are considered: ST/12 (left panel) and ST/3 (right panel).

7 SUMMARY AND CONCLUSIONS

We have presented a detailed discussion of 94 CEMP-*s* and CEMP-*s/r* stars collected from the literature. This paper is strictly related to Paper II, in which we provided a general description of the sample and the main results obtained.

The theoretical interpretation of CEMP-*s/r* stars is still largely debated, because the *s* and *r*-processes are ascribed to different physical environments. We remind the hypothesis adopted here and described in Paper II: we assumed an initial *r*-process enhancement in the molecular cloud from which the binary system formed, followed by *s*-process nucleosynthesis during the TP-AGB phase.

In the analysis we followed the star classification provided in Paper II. We considered all single species, the number of lines detected and the error bars determined by the authors, with particular attention to the three *s*-process peaks, ls, hs and Pb. For each star, AGB models that better interpret the observations have exhaustively discussed (a summary of the results has already been presented in Paper II, Tables 10 and 11). We considered separately those stars for which a limited number of observations among the *s*-process elements are available (Appendix A). Five stars with $[\text{Fe}/\text{H}] > -1.5$ were discussed in a separate Section: HD 206983, HD 26 and HE 1152–0355, as well as CS 29503–010 and HE 0507–1653, which have a limited number of *s*-element observations. Note that some CEMP-*s* stars analysed here were previously classified as CH stars (e.g., Van Eck et al. 2003). As firstly suggested by McClure (1990) and Luck & Bond (1991), these objects, showing strong features of CN and CH bands as well as high *s*-process abundances, may be considered a link between barium stars (with disk metallicity) and CEMP-*s* stars (with halo metallicity). Indeed, they all belong to binary systems with mass transfer from the most evolved companion having already undergone the TP-AGB phase.

As discussed in Paper II, interpretations of spectroscopic data are obtained for AGB initial masses in the range $M \sim 1.3$ to $2 M_{\odot}$, provided that different dilutions and ^{13}C -pocket strengths are chosen. The AGB initial mass is mainly defined by the occurrence of the FDU (which implies a dilution of at least 1 dex) and by the observed $[\text{Na}/\text{Fe}]$ (and $[\text{Mg}/\text{Fe}]$). Major information on the efficiency of the ^{13}C -pocket is provided by both $[\text{hs}/\text{ls}]$ and $[\text{Pb}/\text{hs}]$. For a given metallicity, a range of ^{13}C -pocket strengths is required in order to interpret observations of CEMP-*s* and CEMP-*s/r* stars: for models with $M_{\text{ini}}^{\text{AGB}} \sim 1.3 M_{\odot}$, ^{13}C -pockets close to case ST/12 (with a range from cases ST/6 to ST/15) are needed, while for $M_{\text{ini}}^{\text{AGB}} \sim 1.5 M_{\odot}$, ^{13}C -pockets close to case ST/3 (with a range from cases ST/2 to ST/12)¹³ are required (see Section 6). However, as highlighted in this study, such a classification is only indicative. Indeed, the analysis of individual stars provided in this paper is necessary in order to point out the peculiar characteristics of each star. For instance, several stars do not have Na or Pb detected, which are useful to constrain the AGB initial mass or the

^{13}C -pocket strength. Also, for many stars we do not have information about Eu, and we can not argue about any possible initial *r*-process enhancement. Finally, 40% of the star sample has a limited number of spectroscopic observations. For all these reasons, an averaged analysis could not be realistic. Actually, six stars need ^{13}C -pockets \leq case ST/24 (Table 3), below the ranges indicated above: CS 22942–019, CS 31062–012, HE 0336+0113 as well as V Ari, HE 1135+0139 and HD 189711, having more uncertain observations because their spectra are veiled by strong molecular lines (Van Eck et al. 2003) or have lower resolution (HE 1135+0139 with $R = 20\,000$, Barklem et al. 2005).¹⁴ For CS 22942–019, CS 31062–012 and HE 0336+0113, we do not exclude different interpretations. For instance, in AGBs of low mass and metallicity ($[\text{Fe}/\text{H}] \lesssim -2.5$), (Hollowell et al. 1990; Iwamoto et al. 2004; Campbell & Lattanzio 2008; Cristallo et al. 2009b; Campbell, Lugaro, Karakas 2010), a proton ingestion episode may modify the *s*-process pattern. However, the AGB initial mass and the metallicity at which this proton ingestion starts to occur would be decreased if an initial oxygen enhancement is adopted (Straniero et al. 2011). Moreover, a possible contribution from AGB models of initial mass $3 \lesssim M_{\text{ini}}^{\text{AGB}}/M_{\odot} \lesssim 7$ (intermediate AGBs, IMS) may be investigated. In Paper I, we briefly discuss the nucleosynthesis in IMS of disc metallicity. In IMS the temperatures at the bottom of the convective pulse is higher than in low mass AGBs ($1.2 \lesssim M_{\text{ini}}^{\text{AGB}}/M_{\odot} \lesssim 2$, LMS), and the neutron source $^{22}\text{Ne}(\alpha, n)^{25}\text{Mg}$ is more efficiently activated. This may increase the *s*-process contribution to the ls elements with respect to the other *s*-peaks (Travaglio et al. 2004), as observed in CS 22942–019 ($[\text{ls}/\text{Fe}] > [\text{hs}/\text{Fe}] > [\text{Pb}/\text{Fe}]$). However, the mass of the He-intershell in IMS is smaller than LMS by one order of magnitude. This reduces the TDU efficiency and the final $[\text{El}/\text{Fe}]$ abundances observed in the envelope. Moreover, in this AGB mass range, Hot Bottom Burning (HBB) also modifies the final C and N abundances (Sugimoto 1971, Iben 1973, Karakas & Lattanzio 2003, Ventura & D’Antona 2005), destroying C and producing a large amount of N (NEMPs, nitrogen-enhanced metal-poor stars Johnson et al. 2007), contrary to that observed in CS 22942–019, CS 31062–012 and HE 0336+0113. In addition, IMS stars with $[\text{Fe}/\text{H}] \lesssim -2.3$, undergo an hot TDU, in which the envelope deeply penetrates into the intershell burning protons at its base (Goriely & Siess 2004; Herwig 2004; Campbell & Lattanzio 2008; Lau et al. 2009), possibly modifying the structure and the evolution of the star. Further investigations are desirable.

Note that the spread of the ^{13}C -pocket strengths obtained here is larger than that found by Bončić Marinović et al. (2007). However, it may reflect the uncertainties affecting the formation of the ^{13}C -pocket: the H profile (and then the amount of ^{13}C and ^{14}N), the mass of the pocket, and the physical mechanisms involved (e.g., the treatment of the mixing process at the radiative/convective interfaces,

¹³ The three giants HD 5223, HD 209621 and HE 1305+0007 may be interpreted with $M_{\text{ini}}^{\text{AGB}} \sim 2 M_{\odot}$ and case ST/15, which is slightly lower than the given range, but still within the uncertainties considering that the spectra of these stars are highly blended.

¹⁴ Among the star with a limited number of data, three CEMP-*s* need low *s*-process efficiencies, CS 22956–28, CS 22891–171 and HE 1001–0243. Further spectroscopic investigations are desirable for these objects (e.g., no ls elements are available for CS 22891–171 and HE 1001–0243).

models including rotation, magnetic fields or gravity waves) are object of study (Herwig et al. 1997; Langer et al. 1999; Herwig et al. 2003; Denissenkov & Tout 2003; Siess et al. 2004; Straniero et al. 2006; Cristallo et al. 2009a).

As well as [Na/Fe] (and [Mg/Fe]), in some cases the [ls,hs/Fe] and their ratio [hs/ls] may provides indications on the AGB initial mass. In five stars (CS 22183-015, CS 22880-074, CS 22898-027, HE 0338-3945, HE 2148-1247) the low observed [ls/Fe] (corresponding to a high [hs/ls]) is better interpreted by AGB models with low initial mass ($M \sim 1.3 M_{\odot}$). On the other side, two stars among the sample show an extremely large *s*-process enhancement ([ls/Fe] ~ 2 and [hs/Fe] ~ 3), about 1 dex higher than the average of the CEMP-sII (or CEMP-sII/*r*) stars: CS 29528-028 and SDSS 1707+58. Both stars can only be interpreted by AGB models with initial mass $M = 2 M_{\odot}$, which undergo a larger number of TDUs. Further investigations are strongly suggested, especially for SDSS 1707+58, which has a limited number of observations available.

Among the sample listed in Table 1 (in which stars with a large number of observations are reported), 17 stars lie on the main-sequence/turnoff. The degree of dilution obtained for these stars may provide information on the effect of mixing as thermohaline, gravitational settlings and radiative levitation. We find that ten of them (CS 22881-036, CS 22898-027, CS 29497-030, CS 29526-110, CS 29528-028, CS 31062-012, HE 0338-3945, HE 2148-1247, SDSS 0216+06, SDSSJ1349-0229) have only one theoretical interpretation with negligible dilution, from which we may hypothesise that low mixing had occurred. Three stars (HE 0143-0441, HE 0430-4404, HE 1152+0027) may have different theoretical interpretations with different AGB initial masses (in the range of $1.2 - 2 M_{\odot}$). For each star, a solution with $dil = 0.0$ dex may be found: HE 0143-0441 and HE 1152+0027 with $M = 1.3 M_{\odot}$; HE 0430-4404 with $M = 1.2 M_{\odot}$. Higher dilutions can be found with higher initial masses. Two stars, CS 22887-048 and BS 16080-175, were analysed by Tsangarides (2005), PhD Thesis. CS 22887-048 has solutions with different AGB models, but with low or negligible dilution: $M = 1.4 M_{\odot}$ and $dil = 0$ dex, $M = 1.5$ or $2 M_{\odot}$ and $dil = 0.3$ dex. Tsangarides (2005) estimated a metallicity 1 dex higher than Johnson et al. (2007). A more detailed analysis is desirable. BS 16080-175 has three possible interpretations: $M = 1.35 M_{\odot}$ and $dil = 0.6$ dex, $M = 1.5 M_{\odot}$ and $dil = 1.2$ dex, $M = 2 M_{\odot}$ and $dil = 1.2$ dex. CS 22964-161 has solutions with $M = 1.2 M_{\odot}$ and $dil = 0.4$ dex, $M = 1.3 M_{\odot}$ and $dil = 0.9$ dex, suggesting moderate mixing. The interpretation of SDSS J0912-0229 is uncertain, and no information on possible mixing can be deduced.

The main goal of this paper is to present a detailed study of spectroscopic observations star by star, through an analysis of the AGB models presented in Paper I and II. In general, we found possible agreements between theoretical predictions and spectroscopic data. The major discrepancies are summarised here below. This aims to provide potential indications for future studies, also of spectroscopic nature, and suggests important starting points of yet unsolved issues.

One of the main problems concerns C and N. As highlighted in Paper II (Section 5.3), the observed [C/Fe], [N/Fe] and the carbon isotopic ratio $^{12}\text{C}/^{13}\text{C}$ can not be interpreted by AGB models. Large uncertainties are

present in both spectroscopic (NLTE and 3D atmospheric models; Collet et al. 2007, 2009; Grevesse et al. 2007; Asplund et al. 2009; Caffau et al. 2009; Frebel & Norris 2011) and AGB models, as extra-mixing processes (CBP), thermohaline, or rotation and magnetic fields which may induce the mixing (Stancliffe et al. 2009; Stancliffe 2010; Charbonnel & Lagarde 2010). The hypothesis of the CBP, in order to reconcile theoretical predictions and observations in stars (or SiC presolar grains), has been remarked by different authors (Nollett et al. 2003; Domínguez et al. 2004a,b; Cristallo et al. 2007; Busso et al. 2010; Palmerini et al. 2011). The effects of the CBP on ^{12}C and ^{14}N cannot be exactly quantified by models and the physical processes involved are not clear yet. In several CEMP-*s* stars the predicted [C/Fe] is much higher than reported by spectroscopic observations. The contemporary measurement of a very low $^{12}\text{C}/^{13}\text{C}$ ratio observed, in the typical range 4 to 10, indicates the impact of a strong extra-mixing, which have not been included in our AGB models nor in our treatment of the envelope of the observed low mass star after mass accretion by the more massive AGB companion. This will imply a concomitant reduction of the expected [C/Fe] and $^{12}\text{C}/^{13}\text{C}$ ratio, but at the same time a strong increase of the predicted [N/Fe]. In several cases one would expect CEMP-*s* stars to be even more N-rich than C-rich. A discussion of this issue is deferred to further work (Bisterzo et al., in preparation). An additional process that may increase ^{13}C and ^{14}N is the proton ingestion episode occurring in low mass AGBs of low metallicity (see Section 2.1.1).

Among the light elements, also fluorine is largely produced by AGB models, while recent spectroscopic determinations in CEMP-*s* stars provide [F/Fe] about 1 dex (or more) lower than theoretical predictions (Lucatello et al. 2011). Note that recently, Palmerini et al. (2011) studied the effect of extra-mixing in AGB stars on the light-elements, suggesting a possible decrease of [F/Fe] at low metallicities. However, further studies both on the theoretical and spectroscopic point of view are strongly desirable.

Another discrepancy concerns the elements belonging to the ls and hs peaks. AGB models predict (within 0.3 dex) similar abundances for the first *s*-peak (Sr, Y, and Zr) and for the second *s*-peak (for Ba, La, Ce, Pr and Nd), (with a slightly increasing or decreasing trend of [El/Fe] with atomic number depending on the ^{13}C -pocket, see Paper I, Appendix B). This is strongly supported by the reliable neutron cross section measurements and solar abundances in the ls and hs regions. Instead, some CEMP-*s* stars show an internal spread among ls and hs elements greater than 0.5 dex. In several stars the observed [Ba/Fe] is higher than the average of [hs/Fe] (e.g., HD 26, CS 30301-015, HE 0143-0441, HE 0336+0113, LP 625-44); the most evident example is CS 31062-050 (Aoki et al. 2006), where [Ba/Fe] is about 0.5 dex higher than the other hs elements (Section 3.2.4). In general, Sr is more uncertain than other ls elements, with a limited number of lines detected. In our analysis, we exclude Sr from the ls elements and Ba from the hs peak, which are mainly affected by higher spectroscopic uncertainties (Busso et al. 1995) due to NLTE effects (Andrievsky et al. 2009, 2011; Mashonkina et al. 2008; Short & Hauschildt 2006), especially by decreasing the metallicity. However, even excluding Sr and Ba from the analysis, very large spreads between Y and Zr and among the hs elements have been

observed in some stars: $[\text{Zr}/\text{Y}] \gtrsim 1$ in the cold giants HD 5223, HD 206983, HD 209621 and HE 1305+0007; $[\text{La}/\text{Ce}] \sim -1$ in the main-sequence CEMP-sII/ r stars SDSS J1349-0229 and SDSS J0912+0216; $[\text{La}/\text{Nd}] \sim 1$ in the cold giant HE 1152-0355. Lower $[\text{La}/\text{Nd}]$ (~ 0.5) were observed in the giant HE 1031-0020 and lower $[\text{Zr}/\text{Y}]$ (~ 0.5) were detected in CS 29497-030, CS 31062-050 and HE 0143-0441, HE 0338-3945, HE 2148-1247, CS 29513-032, HK II 17435-00532, LP 625-44. Note that the recent estimation of NLTE effects for Zr II lines (+0.3 dex) in low metallicity stars by Velichko, Mashonkina, Nilsson (2010) would further increase the discrepancy between Zr and Y observed in some stars.

At the state of the art, differences larger than 0.5 dex among the hs elements can not be obtained by AGB models. Concerning the ls elements, low metallicity unevolved Galactic stars show a large spread in $[\text{Sr}, \text{Y}, \text{Zr}/\text{Fe}]$ for $[\text{Fe}/\text{H}] \leq -2.5$. For instance, $[\text{Sr}/\text{Fe}]$ has minimum observed values of -1 for $[\text{Fe}/\text{H}] \sim -2.7$ down to -2 for $[\text{Fe}/\text{H}] \leq -3$ (see e.g., Fig. 20 of Käppeler et al. 2011; or Andrievsky et al. 2011, who account for NLTE effects). A similar spread is observed for $[\text{Y}/\text{Fe}]$ and $[\text{Zr}/\text{Fe}]$. This may be due to non homogeneous or incomplete mixing of the gas in the Galactic halo or to a multiplicity of primary r -process components (see Travaglio et al. 2004, Qian & Wasserburg 2008, Sneden et al. 2008). Therefore, the hypothesis of an extreme initial deficiency of Sr, Y and Zr in the molecular cloud seems plausible. In some CEMP-s stars, we assumed an $[\text{Sr}, \text{Y}, \text{Zr}/\text{Fe}]^{\text{ini}}$ (or one of them) $= -1$, in order to interpret the observations (e.g., the CEMP-sI star CS 30322-023 by Masseron et al. 2006 and CS 29513-032 by Roederer et al. 2010a). However, in general, the s -process contribution is large and overcomes initial deficient compositions (e.g., CS CS29497-030 by Ivans et al. 2005 or CS 31062-012 Aoki et al. 2002d, 2007, 2008). Then, the discrepancy within the ls elements remains an open problem. From the theoretical point of view, the nucleosynthesis of the ls elements is highly debated. Specifically, a primary contribution of about $\lesssim 20\%$ to solar Sr, Y and Zr (lighter element primary process, LEPP Travaglio et al. 2004) has been hypothesised in order to interpret the observations of $[\text{Sr}, \text{Y}, \text{Zr}/\text{Fe}]$ versus $[\text{Fe}/\text{H}]$ in of Galactic metal-poor stars¹⁵. However, the exact contribution from this primary process to individual ls elements is not well established and its origin is still under investigation (e.g., Montes et al. 2007; see also the recent Arcones & Montes 2011 and references therein). Among CEMP-s/ r stars, five stars (CS 22898027, CS 29497030, HE 03383945, HE 1305+0007 and HE 21481247) require the highest r -enhancement $[\text{r}/\text{Fe}]^{\text{ini}} = 2.0$, with an observed $[\text{La}/\text{Eu}] \sim 0$, together with $[\text{La}/\text{Fe}] \sim 2$. As discussed in Paper II (Section 3), the hypothesis of an initial r -process enhancement is adopted in the region between Ba and Bi. Indeed, observations of elements between Mo and Cs

are lacking. For neutron-capture elements lighter than Ba, different initial r -process enrichment could be introduced under the assumption of a multiplicity of r -process components (Sneden et al. 2003a). Only Johnson & Bolte (2004) detected Pd for CS 31062-050. About 50% of solar Pd is produced by the s -process (see Paper II, Table 5); the remaining 50% is ascribed to the r -process. The $[\text{r}/\text{Fe}]^{\text{ini}} = 1.6$, adopted in order to interpret the observed r -elements from Eu to Ir, would overestimate the $[\text{Pd}/\text{Fe}]_{\text{obs}}$ by ~ 1 dex. Lower initial light- r -enhancements $[\text{light-r}/\text{Fe}]^{\text{ini}} \sim 0.5 - 1.0$ are assumed (Section 3.2.4), likely confirming a multiplicity of the r -processes. This is the only reliable detection among the elements included between Mo and Cs in CEMP-s or CEMP-s/ r stars. The upper limits for Ag in CS 29497-030 (Ivans et al. 2005) and HE 0338-3945 (Jonsell et al. 2006) do not provide significant constraints. When allowed, further investigations on the light- r elements are desirable. Behara et al. (2010) detected a very enhanced Ru in the main-sequence star SDSS J0912+0216 ($[\text{Ru}/\text{Fe}] = 2.6$). Even if no error bar is provided by the authors, the Ru observed in this star seems to agree with some among the heavy- r process elements, as Gd and Tb. The abundances observed in SDSS J0912+0216 are peculiar, both for s - and r -process elements: indeed, in addition to the already mentioned large spread among the hs peak, this star shows a large spread among the r -elements (e.g., $[\text{Gd}/\text{Eu}] \sim 1.5$). A similar behaviour is found in SDSS J13490229, studied by the same authors. The spread is confirmed in both stars, and highlights a crucial problem from the point of view of the theoretical interpretation. Other three stars show discrepancies of about 0.5 dex between observed and predicted r -elements: CS 31062-050 (Er, Yb, Lu), LP 625-44 (Gd, Er) and HE 0338-3945 (Dy, Tm). These stars may be considered important starting point for future studies. In general, further investigations on the r -elements in CEMP-s and CEMP-s/ r stars would be strongly useful.

We recall that the theoretical interpretations presented here are thought as test for AGB models, obtained with post-process nucleosynthesis models based on old FRANEC models (Gallino et al. 1998; Straniero et al. 2003). A new generation of FRANEC code is developing. These new full evolutionary models account for new opacities, updated reaction rates, a mixing algorithm to obtain the ^{13}C -pocket, a new evaluation of the mass loss rate based on the observed correlation with the pulsational period (Straniero et al. 2006; Cristallo et al. 2009b,a, 2011). Future investigations are planned in order to update our predictions accounting for low metallicity fully FRANEC models, once a whole spectrum of masses and metallicities will be completed.

¹⁵ Galactic Chemical Evolution models (Travaglio et al. 2004; Serminato et al. 2009), that account for the main and strong s -process in low and intermediate mass AGB stars of different stellar populations, predict s contributions of $\sim 64\%$, $\sim 67\%$, and $\sim 60\%$ to solar Sr, Y, and Zr, respectively. The weak- s process in massive stars is estimated to contribute to $\sim 9\%$ to solar Sr, $\sim 10\%$ to solar Y, and $\sim 0\%$ to solar Zr. The r -process contribution is $\sim 12\%$, 8% and 15% for solar Sr, Y and Zr, respectively.

Table 3. Summary of theoretical interpretations for six CEMP-*s* and CEMP-*s/r* stars that need low ^{13}C -pocket efficiencies (\leq case ST/24). The AGB initial mass, ^{13}C -pocket, dilution factor, and initial *r*-enhancement are reported. Asterisks in column 9 indicate that no Eu has been observed. The Figure number associated to the theoretical interpretation is given in column 10.

Star (1)	Ref. (2)	[Fe/H] (3)	FDU (4)	Type (5)	$M_{\text{ini}}^{\text{AGB}}$ (6)	pocket (7)	dil (8)	[r/Fe] ⁱⁿⁱ (9)	Fig. (10)
CS 22942-019	A02c,d,PS01,Sch08,M10,L11	-2.64,-2.43	yes	sI	2	ST/50	0.7	0.5	9
CS 31062-012	I01,A07,A02c,d,A08	-2.55	no	sII/rII	1.3	ST/30	0.0	1.5	24
HE 0336+0113	C06	-2.68	no	sII	1.4	ST/55	0.0	0.5	2
”	”	”	”	”	2	ST/45	0.3	”	”
V Ari	VE03	-2.40	yes	sI/—	1.5	ST/30	0.9	0.5*	A2
HE 1135+0139	B05	-2.33	yes	sI	1.3	ST/24	1.2	0.0	14
”	”	”	”	”	1.5;2	ST/6	1.8	”	”
HD 189711	VE03	-1.80	yes	sI/—	1.5;2	ST/24	0.9	0.5*	A1

ACKNOWLEDGMENTS

We are deeply indebted to T. C. Beers, J. J. Cowan, I. I. Ivans, C. Pereira, G. W. Preston, I. U. Roederer, C. Sneden, I. B. Thompson, S. Van Eck, S. Vauclair, for enlightening discussions about CEMP-*s* and CEMP-*s/r* stars. Special acknowledgments are addressed to W. Aoki and P. Bonifacio for precious comments on four peculiar stars (LP 625–44, HD 209621; SDSS J1349–0229, SDSS J0912–0216). Heartfelt thanks go to Dr Maria Lugaro for helping us to improve the discussion of the main results of the paper. This work has been supported by the MIUR and KIT (Karlsruhe Institute of Technology).

REFERENCES

- Abia, C., Busso, M., Gallino, R., Domínguez, I., Straniero, O., Isern, J., 2001, *ApJ*, 559, 1117
- Abia, C., et al., 2002, *ApJ*, 579, 817
- Abia, C. et al. 2010, *ApJ*, 715, L94
- Allen, D. M., Barbuy, B., 2006, *A&A*, 454, 895
- Andrievsky, S. M., et al., 2007, *A&A*, 464, 1081
- Andrievsky, S. M., et al., 2009, *A&A*, 494, 1083
- Andrievsky, S. M., Spite, F., Korotin, S. A., François, P., Spite, M., Bonifacio, P., Cayrel, R., Hill, V., 2011, *A&A*, 530, 105
- Aoki, W., Norris, J. E., Ryan, S. G., Beers, T. C., Ando, H., 2000, *ApJ*, 536, 97
- Aoki, W. et al., 2001, *ApJ*, 561, 346
- Aoki, W. et al., 2002a, *PASJ*, 54, 427
- Aoki, W., Norris, J. E., Ryan, S. G., Beers, T. C., Ando, H., 2002b, *PASJ*, 54, 933
- Aoki, W., Ryan, S. G., Norris, J. E., Beers, T. C., Ando, H., Tsangarides, S., 2002c, *ApJ*, 580, 1149
- Aoki, W. et al., 2003, *ApJ*, 592, 67
- Aoki, W., Bisterzo, S., Gallino, R., Beers, T. C., Norris, J. E., Ryan, S. G., Tsangarides, S., 2006, *ApJ*, 650, 127
- Aoki, W., Beers, T., Christlieb, N., Norris, J. E., Ryan, S. G., Tsangarides, S., 2007, *ApJ*, 655, 492
- Aoki, W. et al., 2008, *ApJ*, 678, 1351
- Arcones, A., Montes, F., 2011, *ApJ*, 731, 5
- Arlandini, C., Käppeler, F., Wisshak, K., Gallino, R., Lugaro, M., Busso, M., Straniero, O., 1999, *ApJ*, 525, 886
- Asplund, M., 2005, *ARA&A*, 43, 481
- Asplund, M., Grevesse, N., Sauval, A. J., Scott, P., 2009, *ARA&A*, 47, 481
- Barbuy, B., Cayrel, R., Spite, M., Beers, T. C., Spite, F., Nordstroem, B., Nissen, P. E., 1997, *A&A*, 317, 63
- Barbuy, B., Spite, M., Spite, F., Hill, V., Cayrel, R., Plez, B., Petitjean, P., 2005, *A&A*, 429, 1031
- Barklem, P. S., et al., 2005, *A&A*, 439, 129
- Beers, T. C., Christlieb, N., 2005, *ARA&A*, 43, 531
- Beers, T. C., Sivarani, T., Marsteller, B., Lee, Y., Rossi, S., Plez, B., 2007, *AJ*, 133, 1193
- Behara, N. T., Bonifacio, P., Ludwig, H.-G., Sbordone, L., González Hernández, J. I., Caffau, E., 2010, *A&A*, 513, 72
- Bergemann, M., Gehren, T., 2008, *A&A*, 492, 823
- Bisterzo, S., Gallino, R., Pignatari, M., Pompeia, L., Cunha, K., Smith, V., 2004, *Mem. Soc. Astron. Ital.*, 75, 741
- Bisterzo, S., Gallino, R., Straniero, O., Ivans, I. I., Preston, G. W., Aoki, W., 2008, First Stars III Conference, in *AIP Conference Proceedings*, edited by B. W. O’Shea, A. Heger, T. Abel, 990, 330
- Bisterzo, S., Gallino, R., Straniero, O., Aoki, W., 2009, *PASA*, 26, 314
- Bisterzo, S., Gallino, R., Straniero, O., Cristallo, S., Käppeler F., 2010, *MNRAS*, 404, 1529 (Paper I)
- Bisterzo, S., Gallino, R., Straniero, O., Cristallo, S., Käppeler F., 2011, *MNRAS*, 418, 284 (Paper II)
- Bond, H. E., 1980, *ApJS*, 44, 517
- Bončić Marinović A., Izzard R. G., Lugaro M., Pols O. R., 2007, *A&A* 469, 1013
- Busso, M., Lambert, D. L., Beglio, L., Gallino, R., Raiteri, C. M., Smith, V. V., 1995, *ApJ*, 446, 775
- Busso, M., Gallino, R., Wasserburg, G. J., 1999, *ARA&A*, 37, 239
- Busso, M., Gallino, R., Lambert, D. L., Travaglio, C., Smith, V. V., 2001, *ApJ*, 557, 802
- Busso, M., Palmerini, S., Maiorca, E., Cristallo, S., Straniero, O., Abia, C., Gallino, R., La Cognata, M., 2010, *ApJ*, 717, L47
- Caffau, E., et al., 2009, *A&A*, 498, 877
- Campbell, S. W., Lattanzio, J. C., 2008, *A&A*, 490, 769
- Campbell, S. W., Lugaro, M., Karakas, A. I., 2010, *A&A*, 522, 6
- Cayrel, R. et al., 2004, *A&A*, 416, 1117
- Charbonnel, C., Lagarde, N. 2010, *A&A*, 522, 10
- Carretta, E., Gratton, R., Cohen, J. G., Beers, T. C., Christlieb, N., 2002, *AJ*, 124, 481
- Chieffi, A., Straniero, O., 1989, *ApJS*, 71, 47
- Cohen, J. G., Christlieb, N., Beers, T. C., Gratton, R., Carretta, E., 2002, *AJ*, 124, 470
- Cohen, J. G., Christlieb, N., Qian, Y. Z., Wasserburg, G. J., 2003, *ApJ*, 588, 1082
- Cohen, J. G. et al., 2004, *ApJ*, 612, 1107
- Cohen, J. G. et al., 2006, *AJ*, 132, 137
- Collet, R., Asplund, M., Trampedach, R., 2007, *A&A*, 469, 687
- Collet, R., Asplund, M., Nissen, P. E., 2009, *PASA*, 26, 330
- Corliss, C. H., Bozman, W. R., 1962, *Experimental Transitions Probabilities for Spectral lines of Seventy Elements*, NBS Monographs 32 (Washington: GPO)
- Cristallo, S., Gallino, R., Straniero, O., Piersanti, L., Domínguez, I., 2006, *Mem. Soc. Astron. Ital.*, 77, 774
- Cristallo, S., Straniero, O., Lederer, M. T., Aringer, B., 2007, *ApJ*, 667, 489
- Cristallo, S., Straniero, O., Gallino, R., Piersanti, L., Domínguez, I., Lederer, M. T., 2009a, *ApJ*, 696, 797
- Cristallo, S., Piersanti, L., Straniero, O., Gallino, R., Domínguez, I., Käppeler, F., 2009b, *PASA*, 26, 139
- Cristallo, S., Piersanti, L., Straniero, O., Gallino, R., Domínguez, I., Abia, C., Di Rico, G., Quintini, M., Bisterzo, S., 2011, *ApJS*, 197, 17
- Cui, W. Y., Zhang, B. M. K., Zhang, L., 2007, *ApJ*, 657, 1037
- Denissenkov, P. A., & Tout, C. A. 2003, *MNRAS*, 340, 722
- Domínguez, I., Abia, C., Straniero, O., Cristallo, S., Pavlenko, Y. V. , 2004a, *A&A*, 422, 1045
- Domínguez, I., Abia, C., Straniero, O., 2004b, *Mem. Soc. Astron. Ital.*, 75, 601
- Drake, M. A., Pereira, C. B., 2008, *ApJ*, 135, 1070

- François, P., Matteucci, F., Cayrel, R., Spite, M., Spite, F., Chiappini, C., 2004, *A&A*, 421, 613
- François, P., et al., 2007, *A&A*, 476, 935
- Frebel, A., Norris, J. E., 2011, To appear in Vol. 5 of Planets, Stars and Stellar Systems, by Springer, in 2012, arXiv:1102.1748v2
- Gallino, R., et al., 1998, *ApJ*, 497, 388
- Gallino, R., Bisterzo, S., Husti, L., Käppeler, F., Cristallo, S., Straniero, O., 2006, Proceedings of the International Symposium on Nuclear Astrophysics - Nuclei in the Cosmos - IX, 25-30 June, CERN, Geneva, Switzerland, Proceedings of Science, 100
- Gallino, R., Bisterzo, S., Cristallo, S., Straniero, O., 2010, *Mem. Soc. Astron. Ital.*, 81, 998
- Goriely, S., Mowlavi, N., 2000, *A&A*, 362, 599
- Goriely, S., Siess, L., 2004, *A&A*, 421, 25
- Goswami, A., Aoki, W., Beers, T. C., Christlieb, N., Norris, J. E., Ryan, S. G., Tsangarides, S., 2006, *MNRAS*, 372, 343
- Goswami, A., Aoki, W., 2010, *MNRAS*, 404, 253
- Grevesse, N., Asplund, M., & Sauval, A. J., 2007, *Sp. Sci. Rev.*, 130, 105
- Gratton, R. G., Carretta, E., Eriksson, E., Gustafsson, B., 1999, *A&A*, 350, 955
- Helmi, A., White, S. D. M., 1999, *MNRAS*, 307, 495
- Herwig, F., Blöcker, T., Schönberner, D., El Eid, M. 1997, *A&A*, 324, L81
- Herwig F., Langer N., Lugaro M., 2003, *ApJ*, 593, 1056
- Herwig F., 2004, *ApJS*, 155, 651
- Herwig, F., 2005, *ARA&A*, 43, 435
- Hill, V., et al., 2000, *A&A*, 353, 557
- Hollowell, D., Iben, I. I., Fujimoto, M. Y., 1990, *ApJ*, 351, 245
- Husti, L., Gallino, R., Bisterzo, S., Cristallo, S., Straniero, O., 2007, *Mem. Soc. Astron. Ital.*, 78, 523
- Husti, L., Gallino, R., Straniero, O., 2008, First Stars III Conference, in AIP Conference Proceedings, edited by B. W. O'Shea, A. Heger, T. Abel, 990, 161
- Husti, L., Gallino, R., Bisterzo, S., Straniero, O., Cristallo, S., 2009, *PASA*, 26, 176
- Iben, I. Jr., 1973, *ApJ*, 185, 209
- Ivans, I. I., Sneden, C., Gallino, R., Cowan, J. J., Preston, G. W., 2005, *ApJ*, 627, 145
- Ishigaki, M., Chiba, M., 2010, *PASJ*, 62, 143
- Israelian, G., Rebolo, R., Garcia Lopez, R. J., Bonifacio, P., Molaro, P., Basri, G., Shchukina, N., 2001, *ApJ*, 551, 833
- Israelian, G., Shchukina, N., Rebolo, R., Basri, G., González Hernández, J. I., Kajino, T., 2004, *A&A*, 419, 1095
- Iwamoto, N., Kajino, T., Mathews, G. J., Fujimoto, M. Y., Aoki, W., 2004, *ApJ*, 602, 377
- Johnson, J. A., Bolte, M., 2002, *ApJ*, 579, 87
- Johnson, J. A., Bolte, M., 2004, *ApJ*, 605, 462
- Johnson, J. A., Herwig, F., Beers, T. C., Christlieb, N., 2007, *ApJ*, 658, 1203
- Jonsell, K., Barklem, P. S., Gustafsson, B., Christlieb, N., Hill, V., Beers, T. C., Holmberg, J., 2006, *A&A*, 451, 651
- Jorissen, A., Zács, L., Uldry, S., Lindgren, H., Musaev, F. A., 2007, *A&A*, 441, 1135
- Junqueira, S., Pereira, C. B. 2001, *A&A*, 122, 360
- Käppeler, F., Gallino, R., Bisterzo, S., Aoki, W., 2011, *Rev. Mod. Phys.*, 83, 157
- Karakas, A., Lattanzio, J., 2003, *PASA*, 20, 279
- Kipper, T., Jørgensen, U. G., Klochkova, V. G., Panchuk, V. E., 1996, *A&A*, 306, 489
- Korn, A. J., Shi, J., Gehren, T., 2003, *A&A*, 407, 691
- Kurucz, R. L., 1995, CD-ROMs, Cambridge, SAO
- Lai, D. K., Bolte, M., Johnson, J. A., Lucatello, S., 2004, *AJ*, 128, 2402
- Lai, D. K., Johnson, J. A., Bolte, M., Lucatello, S., 2007, *ApJ*, 667, 1185
- Lau, H. H. B., Stanciliffe, R. J., & Tout, C. A. 2009, *MNRAS*, 396, 1046
- Langer, N., Heger, A. Wellstein, S., Herwig, F. 1999, *A&A*, 346, L37
- Lodders, K., Palme, H., Gail, H.-P., 2009, edited by J.E. Trümper, Landolt-Börnstein, Berlin
- Lucatello, S., Gratton, R., Cohen, J. G., Beers, T. C., Christlieb, N., Carretta, E., Ramirez, S., 2003, *ApJ*, 125, 875
- Lucatello, S., 2004, Ph.D. Thesis, 'C-enhanced metal poor stars', Università di Padova, Italy
- Lucatello, S., Masseron, T., Johnson J. A., 2009, *PASA*, 26, 303
- Lucatello, S., Masseron, T., Johnson, J. A., Pignatari, M., Herwig, F., 2011, *ApJ*, 729, 40
- Luck, R. E., Bond, H. E., 1991, *ApJS*, 77, 515
- Lugaro, M., et al. 2008, *A&A*, 484, L27
- Lugaro, M., Campbell, S. W., de Mink, S. E., 2009, *PASA*, 24, 322
- Mashonkina, L. et al., 2008, *A&A*, 478, 529
- Masseron, T. et al., 2006, *A&A*, 455, 1059
- Masseron, T., Johnson, J. A., Plez, B., Van Eck, S., Primas, F., Goriely, S., Jorissen, A., 2010, *A&A*, 509, A93
- McClure, R.D., Woodsworth, A. W., 1990, *ApJ*, 352, 709
- McClure, R.D., 1989, in Evolution of Peculiar Red Giants, ed. H. R. Johnson, and R. Zuckerman, (Cambridge Univ. Press) 196
- Montes, F., et al., 2007, *ApJ*, 671, 1685
- Mowlavi, N., 1999, *A&A*, 350, 73
- Nollett, K. M., Busso, M., Wasserburg, G. J., 2003, *ApJ*, 582, 1036
- Norris, J. E., Ryan, G., Beers, T. C., 1997, *ApJ*, 488, 350
- Palmerini, S., La Cognata, M., Cristallo, S., Busso, M., *ApJ*, 729, 3
- Pereira, C. B., Drake, N. A. 2009, *A&A*, 496, 791
- Preston, G. W., Sneden, C., 2000, *AJ*, 120, 1014
- Preston, G. W., Sneden, C., 2001, *AJ*, 122, 1545
- Preston, G. W., 2009, *PASA*, 26, 372
- Qian, Y.-Z. Wasserburg, G. J., 2003, *ApJ*, 588, 1099
- Qian, Y.-Z. Wasserburg, G. J., 2008, *ApJ*, 687, 272
- Richard, O., Michaud, G., Richer, J., 2002a, *ApJ*, 580, 1100
- Richard O., Michaud G., Richer J., Turcotte S., Turck-Chièze S., Vandenberg D. A., 2002b, *ApJ*, 568, 979
- Roederer, I. U., et al., 2008, *ApJ*, 679, 1549
- Roederer, I. U., Sneden, C., Thompson, I. B., Preston, G. W., Shectman, S. A., 2010a, *ApJ*, 7119, 573
- Romano, D., Matteucci, F., 2007, *MNRAS*, 378, L59
- Schuler, S. C., Cunha, K., Smith, V. V., Sivarani, T., Beers, T. C., Sun Lee, Y., 2007, *AJ*, 667, L81
- Schuler, S. C., Margheim, S. J., Sivarani, T., Asplund, M., Smith, V. V., Cunha, K., Beers, T. C., 2008, *AJ*, 136, 2244
- Schuler, S. C., Cunha, K., Smith, V. V., Sivarani, T., Beers, T. C., 2008, 10th Symposium on Nuclei in the Cosmos,

- July 27 - August 1 2008, Mackinac Island, Michigan, USA,
in *Nuclei in the Cosmos - X, Proceedings of Science (PoS)*,
76
- Serminato, A., Gallino, R., Travaglio, C., Bisterzo, S.,
Straniero, O., *PASA*, 26, 153
- Short, C. I., Hauschildt, P. H., 2006, *ApJ*, 641, 494
- Siess, L., Goriely, S., & Langer, N. 2004, *A&A*, 415, 1089
- Sivarani, T. et al., 2004, *A&A*, 413, 1073
- Sivarani, T. et al., 2006, *A&A*, 459, 125
- Smiljanic, R., Porto de Mello, G. F., da Silva, L., 2007,
A&A, 468, 679
- Snedden, C., McWilliam, A., Preston, G. W., Cowan, J. J.,
Burris, D. L., Armosky, B. J., 1996, *ApJ*, 467, 819
- Snedden, C. et al. 2003a, *ApJ*, 591, 936
- Snedden, C., Preston, G. W., Cowan, J. J., 2003, *ApJ*, 592,
504
- Snedden, C., Cowan, J. J., Gallino, R., 2008, *ARA&A*, 46,
241
- Stancliffe, R. J., Glebbeek, E., Izzard, R. G., Pols, O. R.,
2007, *A&A*, 464, 57
- Stancliffe, R. J. Glebbeek, E., 2008, *MNRAS*, 389, 1828
- Stancliffe, R. J., Church, R. P., Angelou, G. C., Lattanzio,
J. C., 2009, *MNRAS*, 396, 2313
- Stancliffe, R. J. 2010, *MNRAS*, 403, 505
- Stephens, A., Boesgaard, A. M., 2002, *AJ*, 123, 1647
- Straniero, O., Domínguez, I., Cristallo, S., Gallino, R.,
2003, *PASA*, 20, 389
- Straniero, O., Gallino, R., Cristallo, S., 2006, *Nucl. Phys.*
A, 777, 311
- Straniero, O., Cristallo, S., Piersanti, L., Gallino, R.,
Domínguez, I., Bisterzo, S., 2011, *Why galaxies care about*
AGB stars II: shining examples and common inhabitants,
16-20 August 2010, Vienna, Austria, *ASP. Conf. Ser.*,
edited by F. Kerschbaum, T. Lebzelter, and R. F. Wing,
Vol. 445
- Sugimoto, D., 1971, *Progr. Theor. Phys.*, 45, 761
- Theado S., Vauclair S., 2010, *Astrophys. Space Sci.*, 328,
209
- Thévenin, F., Idiart, T. P., 1999, *ApJ*, 521, 753
- Thompson, I. B., et al., 2008, *ApJ*, 677, 556
- Travaglio, C., Gallino, R., Arnone, E., Cowan, J., Jordan,
F., Sneden, C., 2004, *ApJ*, 601, 864
- Tsangarides, S. A., 2005, *Ph.D. Thesis*, Open University
(United Kingdom), DAI-C 66/04
- Van Eck, S., Goriely, S., Jorissen, A., Plez, B., 2003, *A&A*,
404, 291
- Vanture, E. D. 1992, *AJ*, 104, 1986
- Vanture, E. D. 1992b, *AJ*, 104, 1997
- Vauclair, S., 2004, *ApJ*, 605, 874
- Velichko, A. B., Mashonkina, L. I., Nilsson, H., 2010, *As-*
tron. Lett., 36, 664
- Ventura, P., D'Antona, F., 2005, *A&A*, 431, 279
- Wanajo, S., Nomoto, K., Iwamoto, N., Ishimaru, Y., Beers,
T. C. 2006b, *ApJ*, 636, 842
- Wasserburg, G. J., Busso, M., Gallino, R., Nollett, K. M.,
2006, *Nucl. Phys. A*, 777, 5
- Wickliffe, M. E., Lawler, J. E., 1997, *Journal of the Optical*
Society of America B, 14, 737
- Zhang, L., Ishigaki, M., Aoki, W., Zhao, G., Chiba, M.,
2009, *ApJ*, 706, 1095
- Zijlstra, A. A., 2004, *MNRAS*, 348, L23
- Zinner, E., et al., 2006, *ApJ*, 650, 350

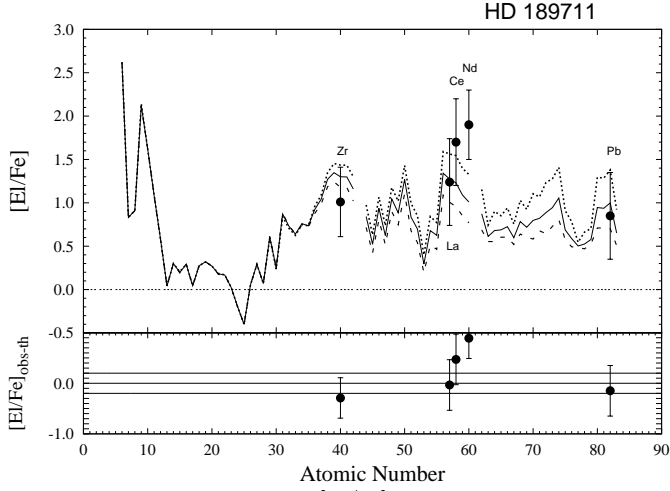


Figure A1. Spectroscopic [El/Fe] abundances of the giant HD 189711 ($[\text{Fe}/\text{H}] = -1.8$; $T_{\text{eff}} = 3500$ K; $\log g = 0.5$) compared with AGB models of initial mass $M = 1.5 M_{\odot}$, cases ST/18 (dotted line), ST/24 (solid line), ST/30 (dashed line), and $dil = 0.9$ dex. Observations are from Van Eck et al. (2003), who detected $[\text{hs}/\text{ls}] \sim 0.2$ and $[\text{Pb}/\text{hs}] \sim -0.4$ (see Section 4.2.5). An $[\text{r}/\text{Fe}]^{\text{ini}} = 0.5$ is adopted.

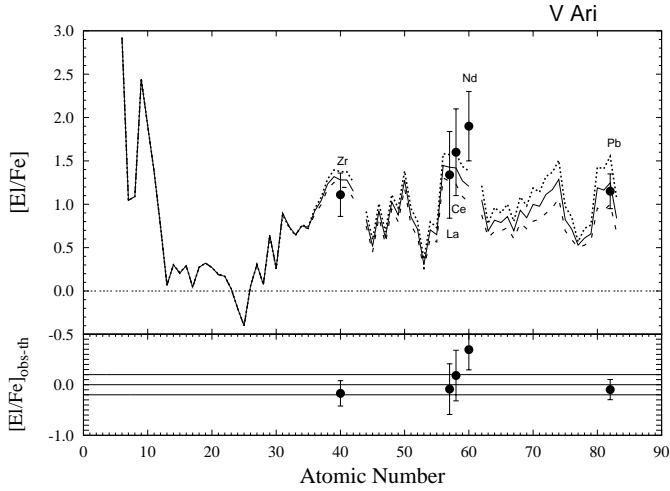


Figure A2. Spectroscopic [El/Fe] abundances of the giant V Ari ($[\text{Fe}/\text{H}] = -2.4$; $T_{\text{eff}} = 3580$ K; $\log g = -0.2$) compared with AGB models of initial mass $M = 1.5 M_{\odot}$, cases ST/24 (dotted line), ST/30 (solid line), ST/36 (dashed line), and $dil = 0.9$ dex. Observations are from Van Eck et al. (2003), who detected $[\text{hs}/\text{ls}] \sim 0.2$ and $[\text{Pb}/\text{hs}] \sim -0.2$. An $[\text{r}/\text{Fe}]^{\text{ini}} = 0.5$ is adopted.

APPENDIX A: ONLINE MATERIAL

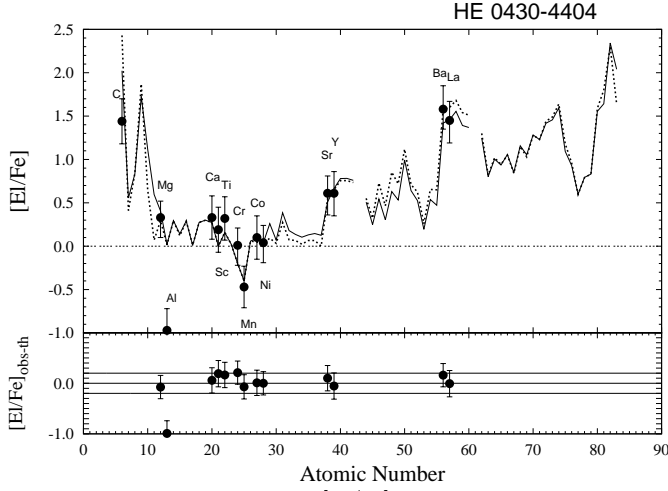


Figure A3. Spectroscopic $[El/Fe]$ abundances of the main-sequence star HE 0430-4404 ($[Fe/H] = -2.07$; $T_{\text{eff}} = 6214$ K; $\log g = 4.27$) compared with two AGB models: $M_{\text{ini}}^{\text{AGB}} = 1.2 M_{\odot}$, case ST/9, $dil = 0.0$ dex (dotted line), or $M_{\text{ini}}^{\text{AGB}} = 1.5 M_{\odot}$, case ST/3, $dil = 1.5$ dex (solid line). Observations are from Barklem et al. (2005), who detected $[hs/lr] = 0.65$. An $[r/Fe]_{\text{ini}} = 0.5$ is adopted. The theoretical interpretation provided for this star is similar to HE 0231-4016 (see Section 4.2.1).

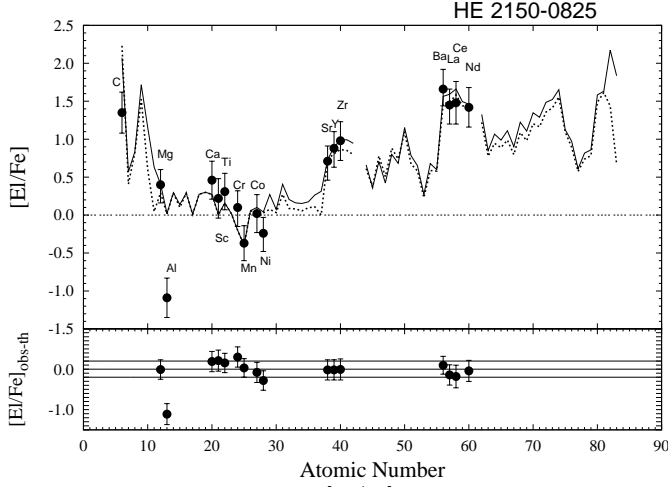


Figure A4. Spectroscopic $[El/Fe]$ abundances of this turnoff/subgiant HE 2150-0825 ($[Fe/H] = -1.98$; $T_{\text{eff}} = 5960$ K; $\log g = 3.67$, before the FDU) compared with two AGB models: $M_{\text{ini}}^{\text{AGB}} = 1.2 M_{\odot}$, case ST/15, $dil = 0.2$ dex (dotted line), or $M_{\text{ini}}^{\text{AGB}} = 1.5 M_{\odot}$, case ST/5, $dil = 1.5$ dex (solid line). Observations are from Barklem et al. (2005), who derived $[hs/lr] = 0.5$. An $[r/Fe]_{\text{ini}} = 0.5$ is adopted. The theoretical interpretation provided for this star is similar to HE 0231-4016 (see Section 4.2.1).

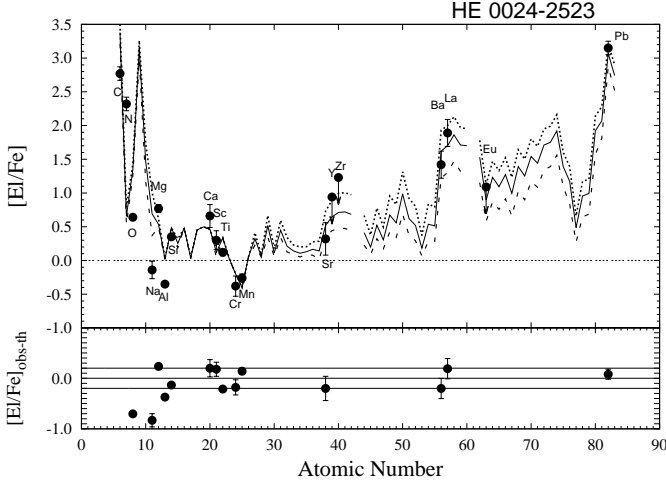


Figure A5. Spectroscopic $[El/Fe]$ abundances of main-sequence star HE 0024-2523 ($[Fe/H] = -2.72$; $T_{\text{eff}} = 6625$ K; $\log g = 4.3$) compared with AGB models of initial mass $M = 1.3 M_{\odot}$, case ST/9 and $dil \sim 0.0$ dex. Three thermal pulses with TDU are shown: pulse 4 (dashed line), 5 (solid line), 6 (dotted line). Observations are from Lucatello et al. (2003), ($[hs/ls] = 1.3$; $[Pb/hs] = 1.7$). An $[r/Fe]_{\text{ini}} = 0.0$ is adopted.

A1 Interpretations of CEMP-*s* and CEMP-*s/r* stars with a limited number of spectroscopic observations (see Paper II, Table 3)

The number of elements detected for the stars discussed in Sections 2 and 3 provide important constraints for AGB models. Unfortunately, many CEMP-*s* stars have a limited number of *s*-process elements available. For instance, only Ba is detected in nineteen stars (Aoki et al. 2007; Cohen et al. 2006); for other stars, Sr among the ls and Ba among the hs elements are measured. Possible solutions have been provided in Paper II, Table 11. These theoretical interpretations have to be considered as indicative examples, because many AGB models may interpret the observations as well.

A2 CEMP-*s*II

Three main-sequence stars with a limited number of data belong to this group: HE 0024-2523 by Lucatello et al. (2003), CS 22967-07 and CS 30323-107 by Lucatello (2004), for which a very low upper limit is reported for Eu, excluding high initial *r*-process enhancements.

A2.1 HE 0024-2523 (Fig. A5)

This is a very metal-poor main-sequence star ($[Fe/H] = -2.7$; $T_{\text{eff}} = 6625$ K; $\log g = 4.3$), analysed by Cohen et al. (2002), Carretta et al. (2002) (who detected Sr and Ba among the *s*-elements), and Lucatello et al. (2003). Lucatello et al. (2003) provide the most complete study of this star, with a deep discussion about the orbital parameters. HE 0024-2523 is a short-period spectroscopic binary, with $P = 3.4$ days. Although the exact values of the individual masses are unknown, limits have been derived from the available photometric and spectroscopic informations: the observed star has a mass of about $0.9 M_{\odot}$; for the AGB companion (now a white dwarf) Lucatello et al. (2003) estimated a mass range $0.6 \leq M/M_{\odot} \leq 1.4$. The values of $[O/Fe]$, $[Na/Fe]$ and $[Al/Fe]$ take into account the NLTE effects according to the prescription by Gratton et al. (1999). The lines of C, N, Eu, La, and Pb were derived from spectral synthesis, because they are very weak or somewhat blended with nearby lines of other species (Lucatello et al. 2003). Only Sr with two lines is detected among the ls elements, while for Y and Zr upper limits are provided. The authors estimated an uncertainty of 0.1 dex for Pb because hyperfine structure and isotopic splitting were not included in the analysis. Fig. A5 shows possible theoretical interpretations with AGB models of initial mass $M_{\text{ini}}^{\text{AGB}} = 1.3 M_{\odot}$, case ST/9 and no dilution. No initial *r*-process enrichment is necessary to interpret the observed $[La/Eu] \geq 0.7$. For higher initial masses ($M_{\text{ini}}^{\text{AGB}} = 1.5 - 2 M_{\odot}$) dilutions higher than 1 dex are necessary. With these models, Mg and the neutron capture elements Ba, La and Pb would be equally fitted, while the observed $[Na/Fe]$ approaches to the solution with $M_{\text{ini}}^{\text{AGB}} = 1.3 M_{\odot}$. The low carbon isotopic ratio $^{12}C/^{13}C = 6 \pm 1$ sustains the hypothesis of efficient mixing.

A2.2 CS 22967-07

This is a main-sequence star ($[Fe/H] = -1.81$; $T_{\text{eff}} = 6479$ K; $\log g = 4.2$), (Lucatello 2004). The solar $[Na/Fe]$ agrees with AGB models of initial mass $1.3 M_{\odot}$ (case ST/9, $dil = 0.0$ dex). No initial *r*-process enhancement is needed in order to interpret the observed $[La/Eu] = 0.7$ dex.

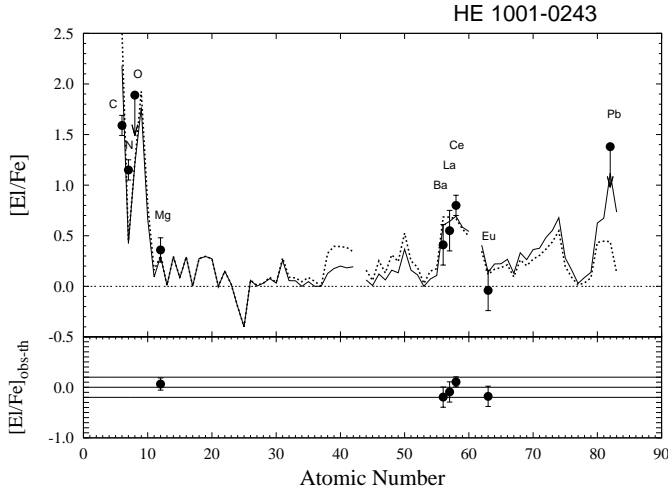


Figure A6. Spectroscopic $[El/Fe]$ abundances of the giant HE 1001-0243 ($[Fe/H] = -2.88$; $T_{\text{eff}} = 5000$ K; $\log g = 2.0$) compared with AGB models of initial mass $M = 1.3 M_{\odot}$, cases ST/30 and ST/75, $dil \sim 1.7 - 1.3$ dex, solid and dotted lines, respectively. Similar solutions can be obtained by AGB models of higher initial mass ($M = 1.5$ and $2 M_{\odot}$) and $dil \sim 2$ dex. Observations are from Masseron et al. (2010), who detected $[Pb/hs] \lesssim 0.9$. An $[r/Fe]_{\text{ini}} = 0.0$ is adopted.

A2.3 CS 30323-107

CS 30323-107 is a main-sequence star ($[Fe/H] = -1.75$; $T_{\text{eff}} = 6126$ K; $\log g = 4.4$) studied by Lucatello (2004). A difference of 0.6 dex is observed between $[Ba/Fe]$ and $[La, Ce/Fe]$. The authors detected $[Na/Fe] = -0.7$, which can not be explained by an initial solar Na scaled with the metallicity. We suggest a solution with $M_{\text{ini}}^{\text{AGB}} = 1.3 M_{\odot}$ (case ST/3, $dil = 0.3$ dex), which approaches $[Na/Fe] \sim 0$. A low upper limit is measured for Eu, excluding a high initial r -process enhancement ($[La/Eu] \geq 0.5$).

A3 CEMP-sI

In this Section we describe three giants, CS 29495-42 by Lucatello (2004), HE 1001-0243 and HE 1419-1324 by Masseron et al. (2010), without observations of ls elements, and one star with uncertain occurrence of the FDU, CS 30315-91 (Lucatello 2004).

A3.1 CS 29495-42

CS 29495-42 is classified as a CEMP-sI star, with $[Sr/Fe] = 0.2$, $[La/Fe] = 1.3$ and $[Pb/Fe] = 1.3$. As observed in other stars, Ba (three lines) is about 0.5 dex higher than La and Ce (three and two lines, respectively). This star has $T_{\text{eff}} = 5544$ K and $\log g = 3.4$ (Lucatello 2004), ($[Fe/H] = -1.88$). The occurrence of the FDU is uncertain in this star. Recently, Johnson et al. (2007) obtained $T_{\text{eff}} = 5400$ K and $\log g = 3.3$ with low resolution spectra, surely after the occurrence of the FDU. Solutions are found with AGB models of initial mass $1.3 M_{\odot}$ and $dil = 0.9$ dex. A low ^{13}C -pocket is needed to interpret the negative $[Pb/hs]$ (ST/18), but the observed $[Sr/Fe]$ (one detected line) is overestimated by the models. Higher ^{13}C -pockets agree with the observed $[hs/Sr]$, but the predicted $[Pb/Fe]$ would be higher than observed. The $[Na/Fe]$ prediction may be considered in agreement with the observed value within an uncertainty of 0.2 dex. AGB models with higher initial mass would overestimate the observed $[Na/Fe]$ and $[Sr/Fe]$.

A3.2 HE 1001-0243 and HE 1419-1324 (Figs A6, A7)

These two newly discovered giants have been recently studied by Masseron et al. (2010). Unfortunately no ls elements have been published so far. Observations by Masseron et al. (2010) will be discussed by the authors in a forthcoming paper. Both stars are giants with very low metallicity: HE 1001-0243 has $[Fe/H] = -2.88$, $T_{\text{eff}} = 5000$ K and $\log g = 2.0$, while HE 1419-1324 shows $[Fe/H] = -3.05$, $T_{\text{eff}} = 4900$ K and $\log g = 1.8$. For HE 1001-0243 the hs elements are very low ($[hs/Fe] = 0.6$) and only an upper limit for Pb is measured, but HE 1419-1324 shows high lead ($[Pb/Fe] = 2.15$; $[Pb/hs] = 1.31$) in accordance with an efficient s -process. We present here possible theoretical interpretations in Figs. A6 and A7.

A3.3 CS 30315-91

As for CS 29495-42, for the subgiant CS 30315-91 the occurrence of the FDU remains uncertain ($[Fe/H] = -1.68$; $T_{\text{eff}} = 5536$ K, $\log g = 3.4$, Lucatello 2004). Due to the mild s -process enhancement (CEMP-sI), a large dilution has to be applied even with AGB models of low initial mass. Solutions with negligible dilution may be found only with $M_{\text{ini}}^{\text{AGB}} = 1.2 M_{\odot}$ models.

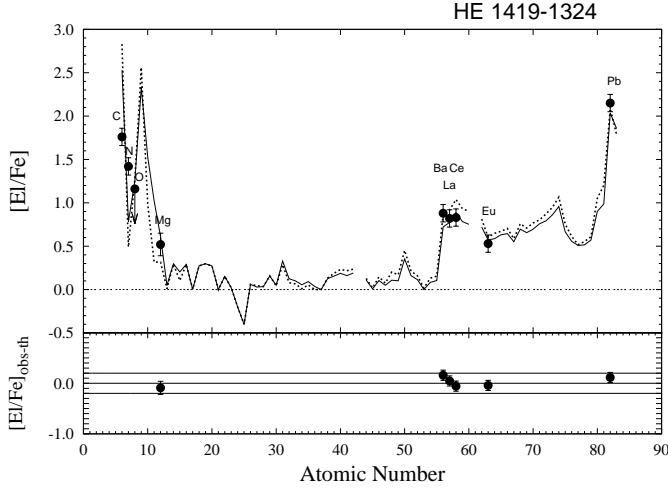


Figure A7. Spectroscopic $[El/Fe]$ abundances of the giant HE 1419-1324 ($[Fe/H] = -3.05$; $T_{\text{eff}} = 4900$ K; $\log g = 1.8$) compared with AGB models of initial mass $M = 1.3$ and $1.5 M_{\odot}$, cases ST/14 and ST/2, dil $\sim 1.0 - 2.0$ dex, dotted and solid lines, respectively. Observations are from Masseron et al. (2010) ($[Pb/hs] = 1.31$). An $[r/Fe]_{\text{ini}} = 0.5$ is adopted.

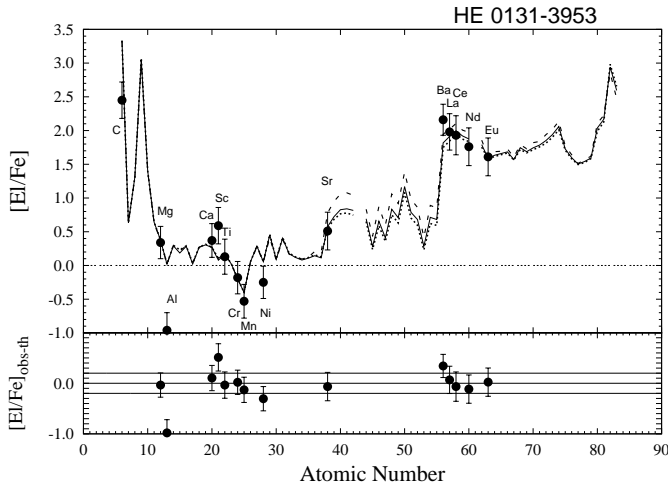


Figure A8. Spectroscopic $[El/Fe]$ abundances of the turnoff/subgiant HE 0131-3953 ($[Fe/H] = -2.71$; $T_{\text{eff}} = 5928$ K; $\log g = 3.83$, before the FDU) compared with AGB models of $M_{\text{ini}}^{\text{AGB}} = 1.3 M_{\odot}$, cases ST/10 (dotted line), ST/12 (solid line), ST/15 (dashed line), and no dilution. Observations are from Barklem et al. (2005), who detected $[hs/ls] = 1.5$. We predict $[Pb/Fe]_{\text{th}} \sim 3$. An initial r -process enrichment $[r/Fe]_{\text{ini}} = 1.5$ is assumed.

AGB models with higher initial mass ($M_{\text{ini}}^{\text{AGB}} = 1.5$ and $2 M_{\odot}$) agree with the observed $[Na/Fe] \sim 0$. No initial r -process enrichment is needed in order to interpret the observed $[La/Eu] < 0.89$.

A4 CEMP-*s*II/*r*II with $[r/Fe]_{\text{ini}} \sim 1.5$

The turnoff star HE 0131-3953 observed by Barklem et al. (2005), with a limited number of spectroscopic data among the ls elements (only Sr with one detected line), may belong to this group due to the high s - and r -process enhancement. For the giant CS 22891-171 by Masseron et al. (2010) no observations are available among the ls elements, but the authors detected Ba, La, Ce and Eu, adding this star to the CEMP-*s*II/*r*II class. The giant CS 30338-089 has been detected by Lucatello (2004) and by Aoki et al. (2007), with discrepant metallicities ($\Delta[Fe/H] \sim 0.7$ dex). Lucatello (2004) found a high Eu enhancement, not confirmed by Aoki et al. (2007), who detected only Ba and Na. At the state of the art this star belongs to CEMP-*s*II/*r*II, but further measurements are needed.

A4.1 HE 0131-3953 (Fig. A8)

This star lies close to the turnoff (Barklem et al. 2005, $[Fe/H] = -2.71$; $T_{\text{eff}} = 5928$ K; $\log g = 3.83$). The low $[Mg/Fe] = 0.3$ (three lines) is interpreted with AGB models of initial mass $M_{\text{ini}}^{\text{AGB}} = 1.3 M_{\odot}$, low s -process efficiencies (ST/10, ST/12 and ST/15) and no dilution (Fig. A8). A $[Na/Fe]$ lower than 0.6 dex would confirm this interpretation. Solutions with higher initial mass predict a large $[Mg/Fe]_{\text{th}}$, about 0.2 dex out of the error bars, and $[Na/Fe]_{\text{th}} \geq 1$ dex. The lead prediction is very

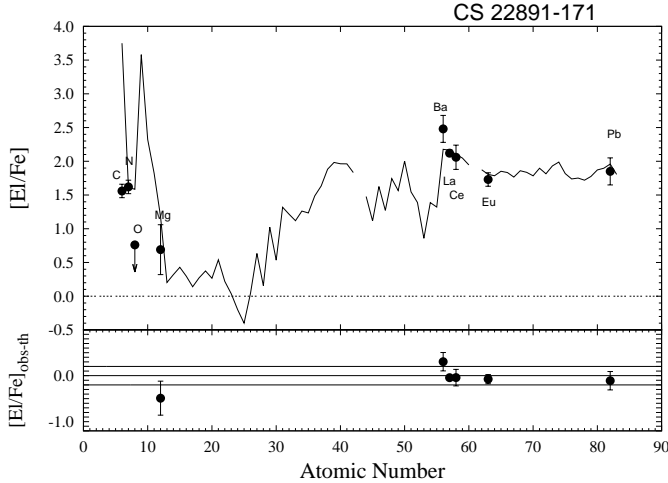


Figure A9. Spectroscopic $[El/Fe]$ abundances of the giant CS 22891-171 ($[Fe/H] = -2.25$; $T_{\text{eff}} = 5100$ K; $\log g = 1.6$) compared with AGB models of initial mass $M = 2 M_{\odot}$, case ST/45 and $dil \sim 0.3$ dex. Observations are from Masseron et al. (2010), who detected $[Pb/hs] = -0.4$. An initial r -process enrichment of $[r/Fe]^{\text{ini}} = 1.8$ is adopted.

uncertain because it depends strictly on the ls elements, for which only Sr is observed. At this state, we predict $[Pb/Fe]_{\text{th}} \sim 3$. An initial r -process enrichment of $[r/Fe]^{\text{ini}} = 1.5$ is needed in order to predict $[La/Eu] = 0.3$.

A4.2 CS 22891-171 (Fig. A9)

The giant CS 22891-171 ($[Fe/H] = -2.25$; $T_{\text{eff}} = 5100$ K; $\log g = 1.6$) has been analysed by Masseron et al. (2010). No ls elements have been detected, while the observed $[Pb/hs] \sim 0$ suggests a low s -process efficiency. In Fig. A9 we provide a possible theoretical interpretation with an AGB model of initial mass $M = 2 M_{\odot}$ and a very low ^{13}C -pocket efficiency (case ST/45). High $[hs/Fe] (\gtrsim 2$ dex), together with a low $[Pb/hs]$ ratio ($\lesssim 0$), can not be obtained by AGB models with low initial mass ($M_{\text{ini}}^{\text{AGB}} = 1.3 - 1.4 M_{\odot}$), which undergo a lower number of thermal pulses with TDU. Even for the case shown in Fig. A9 a low dilution is applied, $dil = 0.3$ dex, hardly compatible with a giant having suffered the FDU. The low upper limit for oxygen is about 1 dex lower than the predictions. No satisfactory theoretical interpretations may be found for the observed C, N and O. However, we highlight that in CEMP stars these light elements are affected by large uncertainties. A high initial r -process enhancement $[r/Fe]^{\text{ini}} = 1.8$ is required to explain the the observed $[La/Eu]$ ratio (~ 0.4). For a further discussion of this star, Masseron et al. (2010) refer to a paper in preparation.

A4.3 CS 30338-089

For this giant, discrepant metallicities have been detected by Aoki et al. (2007) ($[Fe/H] = -2.45$) and Lucatello (2004) ($[Fe/H] = -1.75$). As shown in Paper II, Table A.1, Lucatello (2004) found lower $[Fe/H]$ ratios also for other stars compared to other authors. This may be due to a systematic effect. The high $[Eu/Fe]$ detected by Lucatello (2004) classifies this star as a possible CEMP-sII/r, but further investigations are desirable. We considered here the spectroscopic data by Aoki et al. (2007). The occurrence of the FDU ($T_{\text{eff}} = 5000$ K and $\log g = 2.1$) together with a high s -process enhancement, would exclude solutions with AGB models of $M_{\text{ini}}^{\text{AGB}} = 1.3 M_{\odot}$. Indeed, the large mixing occurring during the FDU are simulated by a large dilution, which can not be applied if the AGB undergoes a limited number of TDUs. Possible solutions are listed in Paper II, Table 11, for $M_{\text{ini}}^{\text{AGB}} = 1.5$ and $2 M_{\odot}$ with $dil = 0.5$ dex (case ST/2). However, these models disagree with the low observed $[Na/Fe]$ (~ 0.46).

A5 CEMP-sII without Eu detection

Stars with a limited number of data may be classified in this group: the main-sequence/turnoff stars SDSS 0924+40, SDSS 1707+58, SDSS 2047+00 by Aoki et al. (2008); the giants HE 0206-1916, HE 0400-2030, HE 1157-0518, HE 1319-1935, HE 1429-0551, HE 1447+0102, HE 1523-1155, HE 1528-0409, HE 2221-0453, HE 2228-0706 by Aoki et al. (2007). The main-sequence/turnoff star CS 29503-010 and the giant HE 0507-1653 by Aoki et al. (2007), with $[Fe/H] \sim -1.2$, have been discussed in Section 5.

A5.1 SDSS 0924+40, SDSS 1707+58, and SDSS 2047+00 (Figs. A10, A11, A11)

The three main-sequence/turnoff stars analysed by Aoki et al. (2008) are newly discovered CEMP-s stars: SDSS 0924+40 ($[Fe/H] = -2.51$; $T_{\text{eff}} = 6200$ K; $\log g = 4.0$), SDSS 1707+58 ($[Fe/H] = -2.52$; $T_{\text{eff}} = 6700$ K; $\log g = 4.2$), and SDSS

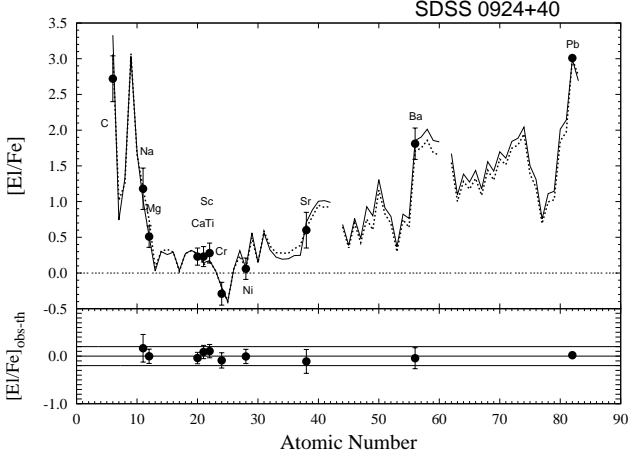


Figure A10. Spectroscopic $[El/Fe]$ abundances of the main-sequence star SDSS 0924+40 ($[Fe/H] = -2.51$; $T_{\text{eff}} = 6200$ K; $\log g = 4.0$) compared with AGB models of initial mass $M = 1.35$ and $2 M_{\odot}$, cases ST/9 and ST/5, dil $\sim 0.4 - 1.0$ dex, solid and dotted lines, respectively. Observations are from Aoki et al. (2008), who detected $[Ba/Sr] \sim [Pb/Ba] \sim 1.2$. The observed $[Mg/Fe]$ agrees better with the $M_{\text{ini}}^{\text{AGB}} = 1.35 M_{\odot}$ model as shown in the lower panel. An initial r -process enrichment of $[r/Fe]_{\text{ini}} = 0.5$ is adopted.

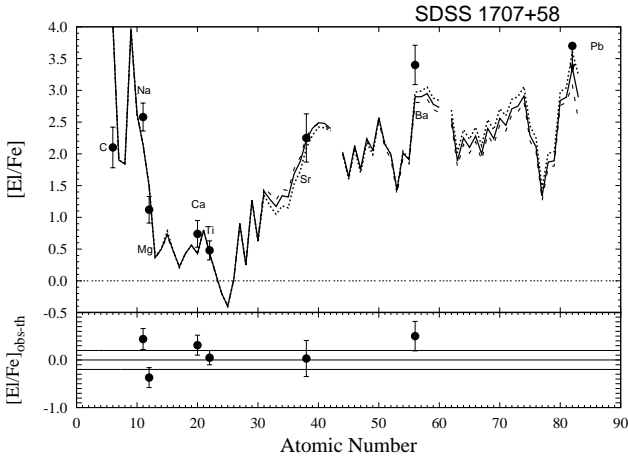


Figure A11. Spectroscopic $[El/Fe]$ abundances of the main-sequence star SDSS 1707+58 ($[Fe/H] = -2.52$; $T_{\text{eff}} = 6700$ K; $\log g = 4.2$) compared with AGB models of initial mass $M = 2 M_{\odot}$, cases ST/12 (dotted line), ST/18 (solid line), ST/24 (dashed line), and no dilution. Observations are from Aoki et al. (2008), who detected $[Ba/Sr] = 1.2$ and $[Pb/Ba] \leq 0.3$. Note that $[Na/Fe]$ has not been corrected with a 3D analysis based on NLTE calculations. An initial r -process enrichment of $[r/Fe]_{\text{ini}} = 0.5$ is adopted.

2047+00 ($[Fe/H] = -2.05$; $T_{\text{eff}} = 6600$ K; $\log g = 4.5$). For SDSS 0924+40 and SDSS 1707+58 only Sr (two lines) among the ls elements and Ba (five lines) among the hs elements have been detected. As well as Ba, SDSS 2047+00 has Y and Zr measurements (one line). Lead abundance is provided for SDSS 0924+40, while only an upper limit is available for SDSS 1707+58. The spectroscopic abundances of Aoki et al. (2008) were not corrected by a 3D analysis based on NLTE calculations.

SDSS 0924+40 needs AGB models with higher initial mass than $1.3 M_{\odot}$ due to the enhanced $[Na/Fe] \sim 1.2$ observed. Interpretations with AGB stellar models are shown in Fig. A10.

SDSS 1707+58 shows rapid radial velocity variations: according to Aoki et al. (2008) it belongs probably to a close binary system (similarly to HE 0024-2523 studied by Lucatello et al. 2003) or to a triple system (Preston et al. 2009). SDSS 1707+58 is a main-sequence star, with $T_{\text{eff}} = 6700$ K and $\log g = 4.2$ ($[Fe/H] = -2.52$). This star exhibits a very high s -process enhancement ($[Sr/Fe] = 2.25$ and $[Ba/Fe] = 3.4$; Aoki et al. 2008). At present, only an upper limit is measured for Pb, $[Pb/Fe] \leq 3.7$. A comparable s enhancement was found for CS 29528-028 by Aoki et al. (2007). In Fig. A11, we present possible solutions with AGB models of initial mass $M = 2 M_{\odot}$ and no dilution. In order to interpret the observed Pb upper limit, ^{13}C -pockets lower than case ST/12 are needed, but the observed $[Ba/Fe]$ is underestimated by about 0.4 dex. The observed $[Na/Fe]$ ratio is not corrected for a 3D analysis based on NLTE calculation, which may reduce this value (Aoki et al. 2007). $[C/Fe]_{\text{obs}}$ is about 2 dex higher than theoretical predictions. However, Aoki et al. (2008) specified that the C abundance is very uncertain in this star, because of the relatively low S/N of the spectrum.

For SDSS 2047+00, AGB models with initial masses in the range $M = 1.2 - 2 M_{\odot}$ may equally interpret the s -process elements. Possible solutions are shown in Fig. A12. The observed $[Na/Fe]$ ratio is overestimated by a $M_{\text{ini}}^{\text{AGB}} = 1.5 M_{\odot}$ model. We predict $[Pb/Fe]_{\text{th}}$ around 2 dex.

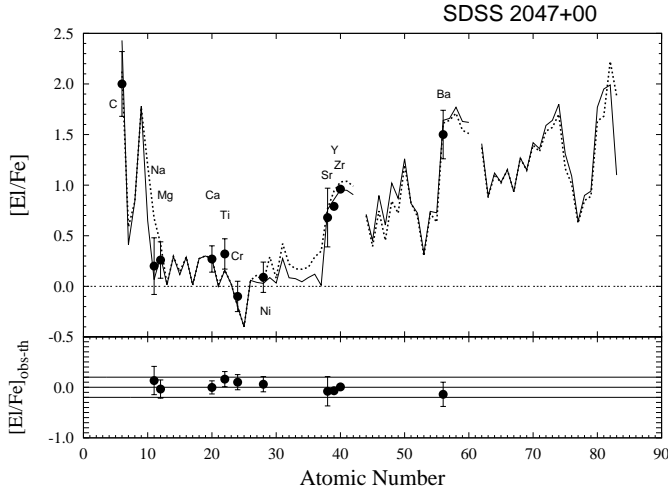


Figure A12. Spectroscopic $[El/Fe]$ abundances of the main-sequence star SDSS 2047+00 ($[Fe/H] = -2.05$; $T_{\text{eff}} = 6600$ K; $\log g = 4.5$) compared with AGB models of initial mass $M = 1.2$ and $1.5 M_{\odot}$, cases ST/12 and ST/5, $\text{dil} = 0.0 - 1.4$ dex, solid and dotted lines, respectively. Observations are from Aoki et al. (2008), who detected $[hs/ls] = 0.7$. The differences plotted in the lower panel refer to a $M_{\text{ini}}^{\text{AGB}} = 1.2 M_{\odot}$ model. We predict $[Pb/Fe]_{\text{th}} \sim 2$ dex. An initial r -process enrichment of $[r/Fe]_{\text{ini}} = 0.5$ is adopted.

A5.2 Ten CEMP-sII giants

Ten giants studied by Aoki et al. (2007) (HE 0206–1916, HE 0400–2030, HE 1157–0518, HE 1319–1935, HE 1429–0551, HE 1447+0102, HE 1523–1155, HE 1528–0409, HE 2221–0453, HE 2228–0706) are briefly discussed here. All stars have $[Fe/H] \leq -2.0$, with the exception of HE 0400–2030 ($[Fe/H] = -1.73$). Among the s -process elements only barium has been measured. Due to the barium uncertainty, a range higher than 1 dex may be predicted for the ls peak and for lead. The only indication about the AGB initial mass may come from Na. However, we underline the spectroscopic uncertainties which affects Na via NLTE and 3D corrections. As for similar cases, further studies are required because presently several AGB masses may equally fit the observations by changing the ^{13}C -pocket and the dilution. A constraint derives from the occurrence of the FDU, for which a dilution of about 1 dex is needed. All these stars are giants, with the exception of HE 0400–2030, for which the FDU is uncertain. Possible theoretical interpretations have been provided in Paper II, Table 11.

A6 CEMP-sI without Eu detection

Stars with a limited number of data may be classified in this group: six main-sequence/turnoff stars, HE 0012–1441 and HE 1410–0004 by Cohen et al. (2006), HE 2240–0412 by Barklem et al. (2005), CS 22956–28 by Masseron et al. (2010); Sneden et al. (2003b), CS 29509–027 by Sneden et al. (2003b), G 18–24 by Ishigaki et al. (2010), SDSS 0817+26 by Aoki et al. (2008), seven giants HE 1305+0132 by Schuler et al. (2007, 2008), HE 1443+0113 by Cohen et al. (2006), HE 2227–4044 by Barklem et al. (2005), CS 22960–053, HE 0441–0652, HE 1005–1439, HE 2330–0555 by Aoki et al. (2007).

A6.1 HE 0012–1441, HE 1410–0004 and HE 1443+0113

Cohen et al. (2006) reported 9 elements for HE 1410+0213 and 5 for HE 1443+0113. Oxygen is detected only for HE 1410–0004 ($[O/Fe] = 1.18$).

HE 1410–0004 is a mild s -process star with only Sr and Ba observed among the s -process elements. A very high upper limit is given for Pb ($[Pb/Fe] \leq 3$) and Eu. The only constraint comes from the low $[Na/Fe]$ observed that suggests solutions with AGB models of low initial mass. Further informations about the three s -peaks are needed for a deeper discussion.

Because of the limited number of elements analysed, all initial masses included in the range $1.3 \leq M/M_{\odot} \leq 2$ can equally interpret HE 1443+0113. The high Mg ($[Mg/Fe] = 0.9$, with 4 lines) observed in HE 0012–1441, a double lined spectroscopic binary, rules out solutions with models of $M_{\text{ini}}^{\text{AGB}} \leq 1.3 M_{\odot}$. Also for this star the spectroscopic data are too scarce for speculations about possible AGB solutions.

A6.2 CS 22956–028 (Fig. A13)

This main-sequence star has been analysed by Sneden et al. (2003b), Lucatello (2004) and recently by Masseron et al. (2010) ($[Fe/H] = -2.33$; $T_{\text{eff}} = 6700$ K; $\log g = 3.5$). It shows the lowest $[hs/ls]$ ratio of the sample, with ~ -0.6 . An upper limit is detected for Pb by Masseron et al. (2010). Theoretical AGB models with initial masses in the range $1.3 \leq M/M_{\odot} \leq 2$ predict negative $[hs/ls]$ values at $[Fe/H] \sim -2.3$ only if very low ^{13}C -pocket efficiencies are assumed. These models predict $[Pb/Fe]_{\text{th}} \sim 0.2 - 0.5$ dex. An example is shown in Fig. A13 with AGB models of $M_{\text{ini}}^{\text{AGB}} = 1.3 M_{\odot}$, cases ST/75, ST/80, ST/90, and $\text{dil} = 0.0$ dex.

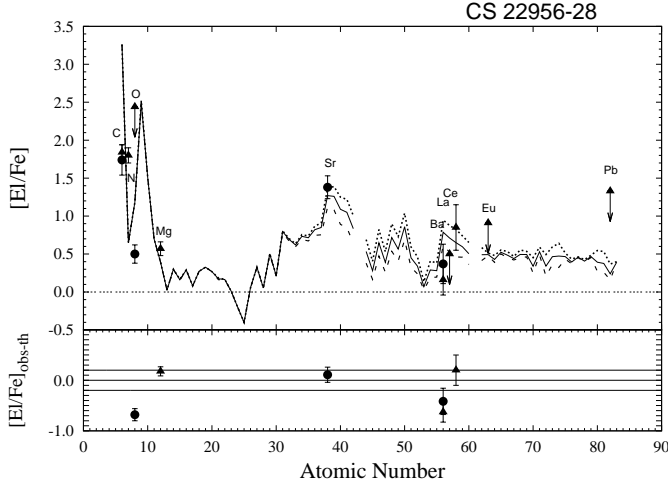


Figure A13. Spectroscopic $[El/Fe]$ abundances of the main-sequence/turnoff star CS 22956-28 ($[Fe/H] = -2.33$; $T_{\text{eff}} = 6700$ K; $\log g = 3.5$, Masseron et al. 2010) compared with AGB models of $M_{\text{ini}}^{\text{AGB}} = 1.3 M_{\odot}$, cases ST/75 (dotted line), ST/80 (solid line), ST/90 (dashed line), and no dilution. Observations are from Sneden et al. (2003b) (filled circles) and Masseron et al. (2010) (filled triangles), who reported $[hs/ls] \sim -1.0$ and $[Pb/hs] \leq 0.8$. An initial r -process enrichment of $[r/Fe]^{\text{ini}} = 0.5$ is adopted.

A6.3 CS 29509-027

The few data measured for this main-sequence star by Sneden et al. (2003b) (C, O, Sr and Ba) agree with all solutions with $M_{\text{ini}}^{\text{AGB}} = 1.2 - 2 M_{\odot}$. No constraints are provided by the limited number of spectroscopic data, in particular we can not provide an accurate $[Pb/Fe]$ prediction.

A6.4 G 18-24 (= BD 42° 2667)

The first spectroscopic observations for G 18-24 at high resolution by Stephens & Boesgaard (2002) provided $[Y/Fe] = 0.18 \pm 0.16$; $[Ba/Fe] = 0.36 \pm 0.46$ ($[Fe/H] = -1.4$). Recently, also Ishigaki et al. (2010) analysed this giant ($[Fe/H] = -1.62$; $T_{\text{eff}} = 6700$ K; $\log g = 3.5$): they found a mild enhancement in Y and Ba ($[Y/Fe] = 0.6 \pm 0.13$; $[Ba/Fe] = 1.2 \pm 0.17$). No informations about r -process elements are available.

We suggest to interpret this star with caution, because C and N have not been detected and no conclusive evidence of its binary nature has been found. Further investigations on this star would be desirable and any possible AGB contribution (e.g., Paper II, Table 11) needs to be confirmed by carbon and europium detections.

A6.5 Four CEMP-sI stars

Among the s -process elements only Ba is measured (Aoki et al. 2007) and no accurate theoretical predictions may be provided for these stars. In similar cases further studies are required, and at present all the AGB initial mass may equally fit the observations. Possible solutions for these star are listed in Paper II, Table 11, (CS 22960-053, HE 0441-0652, HE 1005-1439, HE 2330-0555).

A6.6 HE 2227-4044 and HE 2240-0412

For the subgiant HE 2227-4044 only the s -process elements Sr, Ba, and La were detected by Barklem et al. (2005). Similar spectroscopic data and a similar metallicity were reported for the subgiant HE 2240-0412. All AGB models in the range between $1.3 \leq M_{\text{ini}}^{\text{AGB}}/M_{\odot} \leq 2$ may equally interpret the observations, with dilutions of $\sim 0.8 - 1.7$ dex. We can give a lead estimation of $[Pb/Fe]_{\text{th}} \sim 2$, but this prediction is very uncertain. Similar spectroscopic data and metallicity are measured for another subgiant, HE 2240-0412. The same solutions can be adopted for both stars.

A6.7 HE 1305+0132

A preliminary discussion about this star has been provided by Gallino et al. (2010). This giant ($T_{\text{eff}} = 4462 \pm 100$ K; $\log g = 0.80 \pm 0.30$) was studied by Schuler et al. (2007, 2008). Discrepant metallicities ($[Fe/H] = -2.5 \pm 0.5$; $[Fe/H] = -1.9$ with higher resolution in 2008) were found by the authors. Probably the $[F/Fe] = 2.9$ detected by Schuler et al. (2007) is overestimated. No further investigations were provided ever since. As well as an overabundant $[Ba/Fe] = 0.9$ dex, no informations about the other s -process elements are available for this star.

A6.8 SDSS 0817+26

This main-sequence star has been analysed by Aoki et al. (2008). Unfortunately, a low signal-to-noise (S/N) spectra are detected with few iron lines available. Large errors have been estimated for the radial velocity and the difference between the values obtained from the SDSS spectrum and the HDS spectrum did not provide conclusive informations about the binarity of this object. The limited data do not permit to speculate about possible contributions from an AGB companion: an upper limit for carbon is detected, and only a solar Sr abundance ($[\text{Sr}/\text{Fe}] = 0.14 \pm 0.4$) and a slightly enhanced Ba have been measured ($[\text{Ba}/\text{Fe}] = 0.77 \pm 0.35$). No europium or lead lines are available. In SDSS 0817+26 no clear excess of carbon and neutron capture elements has been found and it is, therefore, excluded from the CEMP-*s* sample.

This paper has been typeset from a \TeX / \LaTeX file prepared by the author.